DISCRETE FOURIER TRANSFORM TECHNIQUES FOR POWER TRANSMISSION LINE PROTECTION

By

YOUSIF A. FAKHRO

Thesis submitted for the degree of Doctor of Philosophy
in the Faculty of Engineering of the University of London

Department of Electrical Engineering,
Imperial College of Science and Technology.
London, 1978.

ABSTRACT

During the last few years, the introduction has taken place of mini-computers in substations for carrying out tasks related to the steady-state monitoring of power systems. A natural development of the above would be to use such computer installations not only for the above purpose, but also for implementing and improving protection functions in power systems, functions that are currently catered for by analogue devices and methods.

The research work contained in this thesis is concerned with developing a scheme for the digital implementation of one such protection function, that of transmission line protection by means of fast fault detection or relaying. The scheme is necessarily required to exhibit an improvement over the existing analogue methods as far as fault detection time is concerned.

A fundamental approach to distance relaying by digital signal processing is based on the Fourier Transform. Indeed, this has been proposed from rather elementary considerations by Slemon et al [1], where a computation scheme resulting from numerical approximation of the Fourier Integral was suggested. However, modern digital signal processing techniques involving the powerful and analytically exact relationships of the Discrete Fourier Transform (DFT) are more appropriate for this kind of analysis. The first part of this research work, therefore, presents a study of the DFT leading to the initial adoption of a digital-analogue filter combination that forms the core of the distance relaying scheme. Then, improvements of this scheme involving original designs yielding simpler digital filtering algorithms that explore inherent symmetries in the DFT are developed, and their performance is critically assessed.

Finally, a complete protection scheme is arrived at which meets the paramount requirement of improved fault detection times.

To my mother and father

TABLE OF CONTENTS

ACKNOWLEDGEMENTS

The study presented in this thesis was carried out under the supervision of Dr. A.G. Constantinides of the Communication Laboratories of the Electrical Engineering Department, Imperial College. The author wishes to thank Dr. Constantinides for his thorough guidance, encouragement and advice during the course of the work. The help and counsel offered and provided by Dr. B.J. Cory, of the Power Systems Laboratories, is also deeply appreciated.

The author is grateful to the Central Electricity Generating Board Transmission Division for the supply of some test data and for the permission to publish analysis results.

Financial support extended by the University of London in the form of a Postgraduate Studentship is also very much appreciated.

Finally, to Mrs. Shelagh Murdock, who typed the text very conscientiously and with outstanding accuracy, and to Mr. R. Puddy for excellent drawings, the author owes many thanks.

LIST OF PRINCIPAL SYMBOLS AND ABBREVIATIONS

c.t.	current transformer
c.v.t.	capacitor voltage transformer
C	line capacitance per unit length
f_c	cutoff frequency of the analogue lowpass filter
f.i.a.	fault inception angle
FC	full cycle method
$F(\omega)$	continuous transform of analogue signal f(t)
$F(e^{j\omega T})$	continuous transform of discrete signal f(nT)
$F(r\Omega)$	coefficient of the Discrete Fourier Transform
$F_{hrn}(\Omega)$	fundamental coefficient of the DFT in the half-cycle negative repetition method
$F_{htp}(\Omega), F_{htn}(\Omega)$	fundamental coefficients of the DFT in the half-cycle positive and negative replication methods
$F_{qtt}(\Omega)$	the quarter-cycle method fundamental DFT coefficient
HC	half-cycle (negative repetition) method
$H_{lp}(j\omega)$	frequency response of the analogue lowpass filter
$H_{hp}(e^{j\omega T})$	frequency response of the digital highpass filter
$H_c(e^{j\omega T}), H_s(e^{j\omega T})$	frequency responses of the cosine and sine filters in the full cycle method
$H_{hc}(e^{j\omega T}), H_{hs}(e^{j\omega T})$	frequency responses of the cosine and sine filters in the half-cycle method
i	instantaneous line current
I_L	phasor line current
I_S	steady-state line current peak
k	discrete frequency variable
L	line inductance per unit length
L_L	line inductance
L_S	source inductance
n	discrete time variable
N	length of time sequence
r	discrete frequency variable
R	line resistance per unit length
R_L	line resistance
R_S	source resistance
R_f	fault resistance
s	Laplace transform variable
s/c	samples per cycle
T	sampling interval
v	instantaneous line voltage

V_L	phasor line voltage
V_S	steady-state line voltage peak
V_f	steady-state voltage peak at fault point
ω_o	fundamental radian frequency, 2π x 50 rad/sec. in the protection schemes
$\omega_o t'$	fault inception angle in relation to relaying point
Ω_s	sampling frequency
x_f	distance to fault
X_L	line reactance
Y	line shunt admittance per unit length
Y_o	line surge admittance
Z	line series impedance per unit length
Z_o	line surge impedance
Z_L	line impedance
Z_S	source impedance
Z_d	series impedance of full length of line
ϕ_f	fault inception angle in relation to fault point
ϕ_L	phase angle of I_L

CHAPTER 1

INTRODUCTION

Power systems are continually growing in size and complexity, in line with the ever-rising demand for electrical power. This is necessitating the development and utilisation of larger power generating and transmitting plant that, in turn, are requiring higher performance from protection systems.

In transmission systems, paramount importance is attached to highly reliable high speed protection. In the context of a high voltage grid system, elaborate and costly protective equipment is easily justified by the very high capital cost involved, and more so by the high costs incurred when line outages resulting from inadequate protection compel the running of low merit generating plant.

Protection systems for transmission lines utilising conventional electromagnetic and static relays have a good record of reliability. However, the rapid advances in, and the decreasing computational costs of, modern digital computers have brought forward the question of the feasibility of using mini-computers for implementing relaying functions. Mini-computer installations are beginning to appear in substations for carrying out tasks related to steady-state monitoring and switching, and it is certainly worthwhile investigating the possibility of exploiting the flexibility they offer through readily altered relaying functions and characteristics by the development and use of digital protection algorithms implementable on such class of computers.

The work presented in this thesis is an attempt at developing and analysing transmission line protection schemes viewed as digital signal processing methods. The schemes, based on digital filtering

through the Discrete Fourier Transform in a direct and a modified form, are to meet the requirements of faster fault detection and better fault discrimination than currently obtainable from analogue relays, and are also to be suitable for real-time implementation on a mini-computer.

A brief summary of the material in each chapter of the thesis is given as follows:

The remainder of this chapter gives an introduction to the problem of transmission line protection. Analogue relaying methods are outlined, and the particular practice of distance relaying, that is finding increasing application in long line protection, is reviewed. A short survey of previous work on computer methods for distance relaying is included.

Chapter 2 is devoted to a theoretical study of the Discrete Fourier Transform aimed at deriving the conditions for its optimum use in analysing transmission line signals both off-line and in real-time.

Chapter 3 firstly presents a simplified analytical study of high frequency signal generation on transmission lines during faults. The second part of the chapter deals with the off-line analysis of recorded real fault waveforms by the Discrete Fourier Transform. A comparison of the results of the theoretical study and the off-line analysis follows, through which the nature of the fault waveforms is established.

Chapter 4 is concerned with the description and analysis of a protection scheme based on the Discrete Fourier Transform. The filtering performance of the scheme is assessed, and limits to the fault detection times possible are estimated.

Chapter 5 outlines the development of a second protection scheme based on predictive methods in waveform filtering, and aimed at achieving faster filtering and fault detection times than those of the basic scheme of Chapter 4.

Chapter 6 deals with the analogue lowpass filter needed for band-limiting transmission line signals before digitally processing them in either of the two protection schemes of Chapter 4 and 5. The chapter discusses the derivation of the filtering performance of the two schemes when combined with their optimum analogue lowpass filters.

Chapter 7 concerns choosing a simple digital highpass filter, based on the results of Chapter 6, and greatly improving the filtering performance of the second proposed protection scheme of Chapter 5.

Chapter 8 describes the off-line tests carried out for proving the suggested protection schemes. The chapter also examines the problem of defining the digital relaying characteristic, in the impedance plane, in the context of exploiting the flexibility of digital methods in allowing the use of some highly discriminative characteristics.

The final conclusions are presented in Chapter 9, together with the original contributions of this work. The chapter gives also a few suggestions for possible future work in the development of further digital relaying algorithms based on signal processing methods.

1.1 ANALOGUE RELAYING OF TRANSMISSION LINES

Power transmission systems are subjected to varying kinds of faults caused by a reduction in the basic insulation strength between conductors under abnormal conditions. This reduction in insulation

results in a decrease in the impedance between conductors, or between conductors and earth, to a value below that of the lowest load impedance normal to a particular circuit, and can in some cases cause a flashover across the insulator string, producing in turn excess current or other detectable abnormalities [2] *.

Causes of faults are diverse. They range from deposited pollution in the form of soot, cement dust and even salts carried by wind-borne sea spray, to extreme weather conditions such as fog, lightning and ice and snow loading [2] . In fact, peculiar causes like birds and aircraft hitting lines are not unknown, along with the more conventional failures of insulators through breakage, puncture, and abnormal system loading.

Such diversity of causes serves to explain the relatively frequent occurrence of faults on overhead lines. The average rate of incidence of such faults on the Central Electricity Generating Board (CEGB) high voltage transmission system is two faults per 100 circuit-miles of lines per year [2] , amounting to a total of about 300 faults a year** on average, and rising to over one thousand faults in years with extremely severe winters.

The extreme severity of some faults owing to the tremendous amount of energy in a modern power system, necessitates prompt fault clearing if expensive damage is to be avoided. Clearance times currently obtained range from a low tenth of a second to one second or more, depending on the protective arrangements employed. However, with fault levels at the 400 kV highest supergrid transmission voltage

---

* Bracketed numbers are keyed to the References at the end of the thesis.

** For the period 1960/65.

ranging up to 35000 MVA with fault currents of the order of 60000 A for single-phase-to-earth faults, the need for lower fault clearance times arises. Very fast clearance will in fact be of paramount importance at the higher transmission voltages planned for the near future.

1.1.1 General Principles

A protection system isolates the faulty section of a line by the operation of some strategically located disconnecting devices known as circuit-breakers. Each of these circuit-breakers is controlled by a relay that is able to recognise abnormal conditions and cause the appropriate disconnecting devices to operate or trip.

Protection relays are of many diverse designs and are not exclusively electromagnetic in principle. Indeed, some are permadynamic, thermal or even solid-state devices. They all rely in their operation on line quantities that change during abnormalities, such as currents, voltages and impedances. Consequently, they are generally specified according to the duty they are required to perform: over-current relays for the measurement of excess current; impedance relays for the measurement of impedance and so on. A particular type of construction, based on a certain principle, can usually be used in relays with differing duties and applications. An attracted-armature relay, for example, is used for both over-current and over-voltage protection [3].

The change in the line's current and voltage during a fault can sometimes be accompanied by other abnormalities. The load current that under normal conditions follows a wholly metallic path with linear

impedance, is diverted to a partly new path through a power arc and the ground when a ground fault occurs. This path presents a nonlinear impedance that gives rise to a fault current containing harmonics. Such harmonics are detectable by electronic relays [4] that sound an alarm for faults not detected by normal relays.

The above principle, known as harmonic relaying, is not used for direct tripping because a reasonably accurate estimate of the magnitudes and frequencies of the harmonics likely to be encountered at a particular relaying point on a faulted line cannot be established beforehand. In fact, the line's transient response during a fault has been known to give rise to eigenfrequencies and an exponentially decaying dc component in the line's current. This phenomenon, which is treated in Chapter 3, impairs the accuracy of both harmonic and conventional relays and makes fast fault detection more difficult.

The requirement of any protection system of picking out and isolating only the faulty elements is referred to as discrimination. Most of the relays used in line protection discriminate to the location of fault, giving protection schemes based on two differing arrangements, known as unit and nonunit protection.

Unit protection systems detect and respond to abnormal conditions occurring only within the zones they are specifically intended to protect. Examples of such systems appear in the organisation tree of Figure 1.1. They are all characterised by the use of an end-to-end signalling channel, as is illustrated in Figure 1.2 which depicts one particular such system known as current-balance protection [2]. In this system, the magnitudes and phases of the currents entering and leaving the line are transmitted over the signalling

channel and tested for a difference that would indicate a fault. The high cost and complexity of the necessary signalling channel, however, make the use of this and all other unit systems unattractive for applications involving long lines.

Nonunit protection, on the other hand, employs no signalling channels. It can take the form of time-graded, current-graded or distance systems. In time-graded and current-graded systems, the circuit-breakers nearest to a fault are made to trip before all others by the respective use of time lag features and tapered relay current settings. Whilst such simple schemes are quite sufficient for the protection of radial feeders [2] and other simple transmission systems, more complicated and commonly encountered networks usually necessitate the application of the third form of nonunit protection, that of distance relaying.

1.1.2 Distance Relaying

Technical and economic considerations, it has been stated, often limit the choice of protection of long overhead lines to some form of distance relaying [2]. In this, the operation of the circuit-breakers is controlled by the distance from the relaying point to the fault. Such distance can be measured by making use of the fact that the length of a circuit for a given conductor diameter and spacing determines its fundamental impedance when the circuit is shorted at its end, and the relay therefore only has to measure the impedance, at 50 Hz, between the circuit-breaker location and the fault. The proportionality of the impedance of the circuit to its length is proven in Chapter 8.

A practical distance protection scheme is shown in Figure 1.3. The figure illustrates the important feature of back-up protection that a nonunit system offers, whereby a protective relay for one element of the system covers other elements too. The relay at A, for example, is intended to detect a fault in the section A to B, but is set to have a nominally instantaneous response only up to a distance Z_1 - about 80% of A to B - because of its limited precision. Faults occurring near or beyond the busbar at substation B, such as F_2 and F_3, would be cleared after a time lag of about 0.4 seconds and, in the case of F_3, only when the relay at B fails to trip instantaneously. The relay at A, therefore, acts as a back-up for that at B.

The current and voltage in a faulted line should not necessarily be directly compared to find the impedance. In fact, a distance relay, according to the type of element and connections employed, can be arranged to measure impedance, reactance or admittance. The line current I_L and voltage V_L are in general mixed in two measuring circuits, as in Figure 1.4, giving two phasor quantities S_1 and S_2 defined as:

$$S_1 = K_1 V_L + Z_{R1} I_L \qquad (1.1a)$$

and

$$S_2 = K_2 V_L + Z_{R2} I_L \qquad (1.1b)$$

where K_1 and K_2 are constants, and Z_{R1} and Z_{R2} are replica impedances. The relay then compares S_1 and S_2 in either magnitude or phase. In magnitude comparison the relay, then an amplitude comparator, operates when the scalar magnitude of one of the quantities S_1 or S_2 is larger than that of the other. A phase comparator, on the other hand, depends for its operation on the phase difference between S_1 and S_2, operating over a range of phase-angle differences and restraining over

the remaining portion of the full 2π circular arc. It has been shown [5] that there is no fundamental difference between these two principles of comparison, and it therefore suffices to consider phase comparators only. In these, the phase difference between S_1 and S_2 that causes operation of the relay is taken as anything between $+\pi/2$ through zero to $-\pi/2$. Thus, if the outputs of the measuring circuits are written as:

$$S_1 = a + jb = |S_1| \angle \alpha_1 \tag{1.2a}$$

and

$$S_2 = c + jd = |S_2| \angle \alpha_2 \tag{1.2b}$$

then the ratio of S_1 to S_2 would be:

$$\frac{S_1}{S_2} = \frac{a + jb}{c + jd} = \frac{ac + bd + j(bc - ad)}{c^2 + d^2} = \frac{|S_1|}{|S_2|}\angle \alpha_1 - \alpha_2 \tag{1.3}$$

and the phase difference α between S_1 and S_2 is:

$$\alpha = \alpha_1 - \alpha_2 = \cos^{-1} \frac{ac + bd}{\sqrt{(ac+bd)^2+(bc-ad)^2}} \tag{1.4}$$

which, with the criterion for operation taken as:

$$-\pi/2 < \alpha < +\pi/2, \quad \text{i.e.:} \quad \cos\alpha > 0 \tag{1.5}$$

gives the condition:

$$ac + bd > 0 \tag{1.6}$$

The line quantities, with the line voltage taken as the reference phasor, can be written as:

$$V_L = |V_L| \angle 0 \tag{1.7a}$$

$$I_L = |I_L| \angle -\phi_L = V_L/Z_L \tag{1.7b}$$

$$Z_{R1} = |Z_{R1}| \angle \theta_1 \tag{1.7c}$$

$$Z_{R2} = |Z_{R2}| \angle \theta_2 \tag{1.7d}$$

and when these are substituted into equations (1.1) that are then compared with equations (1.2), a, b, c and d are found and the inequality (1.6) becomes:

$$K_1K_2|Z_L|^2 + |Z_L| \cdot [K_1 \cdot |Z_{R2}| \cdot \cos(\theta_2-\phi_L) + K_2 \cdot |Z_{R1}| \cdot \cos(\theta_1-\phi_L)] + |Z_{R1}| \cdot |Z_{R2}| \cdot \cos(\theta_1-\theta_2) > 0 \qquad (1.8)$$

The above inequality is the general phase comparator characteristic. According to the connections employed in a specific relay element, the various constants in the inequality are determined and the relaying characteristic derived.

The three basic arrangements in distance relaying in use now are those measuring impedance, reactance and admittance.

a) The Impedance Relay

In this, the constants in the inequality (1.8) are chosen as:

$$|Z_{R1}| = |Z_{R2}| = |Z_R|,$$
$$\theta_1 = \theta_2 = \theta$$

and $K_1 = -K_2 = K,$

reducing the inequality to:

$$|Z_L|^2 < \frac{|Z_R|^2}{K^2}$$

which, on the X/R plane gives:

$$R_L^2 + X_L^2 < \frac{|Z_R|^2}{K^2} \qquad (1.9)$$

This is a circle with centre at origin and radius of $|Z_R|/K$, as shown in Figure 1.5(a). Operation of the relay occurs when the impedance locus traverses the circumference into the circle.

b) The Reactance Relay

The constants here are defined as:

$$|Z_{R1}| = |Z_{R2}| = |Z_R|,$$
$$\theta_1 = \theta_2 = \pi/2,$$

and $$K_1 = -K, - K_2 = 0,$$

giving the characteristic:

$$|Z_L|.\sin \phi_L < \frac{|Z_R|}{K}$$

or $$X_L < \frac{|Z_R|}{K} \qquad (1.10)$$

which is a line parallel to the R axis and distance $\frac{|Z_R|}{K}$ away from it. Relay operation occurs in the unshaded region below the line in Figure 1.5(b).

c) The Admittance (mho) Relay

This characteristic is derived by taking:

$$|Z_{R1}| = 0, \quad |Z_{R2}| = |Z_R|$$
$$\theta_1 = \theta_2 = \theta,$$

and $$K_1 = -K_2 = K,$$

which yields:

$$\left[R_L - \frac{|Z_R|}{2K}.\cos\theta\right]^2 + \left[X_L - \frac{|Z_R|}{2K}.\sin\theta\right]^2 < \frac{|Z_R|^2}{4K^2} \qquad (1.11)$$

or a circle of radius $\frac{|Z_R|}{2K}$ and passing through the origin, as in Figure 1.5(c).

Another characteristic that is of some significance and considerable application is that of the Directional Relay, wherein

operation occurs to the right of an inclined line in the X/R plane as shown in Figure 1.5(d). The inequality describing such operation is:

$$-\pi/2 + \theta_2 < \phi_L < \pi/2 + \theta_2 \qquad (1.12)$$

obtained from $\cos(\theta_2 - \phi_L) > 0$

which in itself is arrived at by substituting zeros for $|Z_{R1}|$ and K_2 in the general inequality of (1.8). Such directional feature is usually incorporated in impedance and reactance relaying of ring-mains and interconnected systems [2] , to guard against any relay operation that would otherwise be caused by faults occurring behind the relay protection zone and giving rise to fault currents flowing towards the busbar.

The four relaying characteristics outlined above can be implemented by several electromagnetic elements, the induction-cup and induction-disc being the most commonly used [3] . Static relaying elements, based on the block-average principle, are also used [4] .

The choice between reactance, impedance or admittance protection systems depends on such factors as the ratio of fault arc resistance to impedance to be measured, the operating time required, and the extent to which the protection system must be immune to power swings on the primary system. The simple impedance characteristic, and the reactance characteristic that is immune to the effect of fault resistance, are both liable to maloperation under power system swing conditions. Also, their operating times are relatively long because of the directional elements needed. Admittance relays are therefore normally specified where long lines are to be protected. Such relays have, in fact, largely superseded impedance and reactance relays on the Grid System in spite of their recent origin.

1.2 DIGITAL DISTANCE RELAYING

The principle underlying analogue distance relaying outlined above is equally applicable in relaying schemes employing digital processors. Samples of the voltage and current variations on a transmission line can be used, for example, to determine the impedance of the line to a fault point, and the location of this impedance on the Z plane can be taken as the key finding upon which a distance relaying program would base its decision. This is known as digital distance relaying, and is of prime interest here because of its potential in providing superior performance to that of conventional analogue electromagnetic, and even static, relaying.

One distinct advantage that digital relaying can offer is in the marked increase in the flexibility of the relaying characteristics obtainable, since the direct impedance determination involved makes possible any such characteristic. This could thus be tailored to provide maximum immunity from power swings and heavy system loadings, eliminating the need for directional elements in ring-mains and interconnected power systems.

A second advantage is the use of samples of the line's voltage and current in place of continuous quantities, thus making possible the application of digital signal processing techniques. Also, the VA requirements that the sampling circuits impose on the voltage and current transformers are negligible, compared to the burdens typically presented to these transformers by conventional relays' coils. These transducers are necessary for supplying the relays with the line quantities, and lower VA ratings make the design of more accurate types possible. Such types, in turn, will improve the performance of the protection system.

The most important advantage that digital relaying can probably offer, however, is that of faster fault detection. The possibility of this depends mainly on the powers and configurations of the processors used, and the impedance determination algorithms adopted. These two factors are next discussed.

1.2.1 Relay Implementation

A digital protection scheme can rely for its relaying functions on either suitably programmed mini- and micro-processors, or purposely built hardware units. When these are devoted to relaying, and are not assigned other substation functions, they can conveniently be referred to as digital relays, since the integrated installations they form would uniquely replace analogue electromagnetic or static relays.

Multi-task single computer installations were initially favoured for carrying out relaying functions and other requirements in a substation. Computer use in alarm monitoring, data logging, oscillography and supervisory control functions as well as relaying, it was argued, would help justify the expected high cost of the computer installation. Alas, it was soon realised that the reliability and integrity needs of the protection functions demended that back-up computers be available for certain prescribed modes of equipment failure. Also, a single minicomputer installation was later shown to be inadequate, in speed, for carrying out all the relaying and switching typically required in a substation.

A substation multi-computer system seemed the most obvious alternative. Such system, consisting of mini- and microprocessors connected in a network at the substation, would fulfil the security

and reliability needs. The economic viewpoint favours small low-cost processors or hardware for the relaying of each transmission line, with a central processor checking and monitoring all such relays in the substation. A more defined role of the central processor in back-up protection and monitoring in such a scheme is not obvious, but one possibility has been presented by Cory et al [6].

1.2.2 Survey of Previous Work

Methods and relaying algorithms that have been suggested and tested since interest in digital relaying began, are now outlined. Their claimed accuracies, when quoted, mostly apply to limited tests and are not to be taken as conclusive.

Implementation was, in most cases, on a minicomputer. While this allowed the evaluation and the examination of the merits of the various methods, it was understood that the use of smaller processors for the most efficient algorithms was to be eventually contemplated.

Some of the methods relied on the continual calculation of the line's fundamental impedance. Others initiated impedance calculation routines only after the detection of disturbances on the power system. The detection was often carried out by taking an integral number of samples of the voltages and current per cycle and comparing each sample as collected with the corresponding sample of the cycle before. When successive differences exceeded a specific tolerance, the algorithm would branch to begin an impedance calculation.

The methods can be broadly classified into two types, in accordance with the equations they adopt for relating the voltage and

current in the faulted line. The first of these equations involves phasors of voltage and current:

$$V_L = Z_L . I_L \qquad (1.13)$$

and the main effort in methods employing this is to determine the phasor representations of the voltage and current signals from sampled data of their instantaneous values. The second equation relates instantaneous values of the voltage and current:

$$v = R_L . i + L_L \frac{di}{dt} \qquad (1.14)$$

and provides, by the appropriate substitutions of sampled data and its differences, simultaneous equations in R and L that yield the faulted line impedance upon solving. This equation assumes that the line is resistive and inductive under fault conditions, such an assumption being valid even for a capacitive transmission line, as will be shown in Chapter 8.

In one of the earliest contributions to digital relaying, Mann and Morrison [7] presented a method based on phasor determination. It involved the predictive calculation of the peak voltage and peak current, and has since been referred to as the peak-determination method. The approach was entirely different from that used earlier on by Mann [8] in his table look-up procedure.

Mann and Morrison implemented their method without the use of analogue lowpass filters that should have preceded the analogue-to-digital conversion, or sampling. The relatively high sampling rate of 40 samples/cycle (s/c) helped dealing with high frequencies, but differentiation further accentuated those and was expected to result in gross errors. A rate of 40 s/c was chosen to minimise numerical errors,

but later on Ranjbar [9] , in his study of the frequency response of the method, showed the optimum rate to be 4 s/c.

The method's sensitivity to dc current offset was indirectly dealt with by suggesting the loading of the current transformer's secondary with specially chosen mimic impedances. This was based on the well known finding [10] that connecting an ideal current transformer's secondary circuit to a burden having the same X/R ratio as the primary circuit gives a purely sinusoidal voltage across the burden. It was recognised, however, that such compensation is limited because the primary system's quantities would differ from one fault to another, being dependent on the distance of the fault along the line.

The method was merited for its potential of very fast fault detection, since it required only the present and immediately preceding samples, thereby making possible the calculation of the waveform before its occurrence. This was made more feasible by the simplification of the stringent computer requirements that the same authors proposed in a later paper [11] . The processing of faulted information only, it was argued, was necessary, and working with healthy data in continual impedance calculation schemes was to be avoided.

An experimental system borrowing heavily from the mathematical and logical techniques of Mann and Morrison was tested and field-evaluated by Gilcrest, Rockefeller and Urden [12] . The system, functioning as one terminal of a transmission line fault protection, employed analogue lowpass filters and a lower, though asynchronous, sampling rate of about 12 s/c. First and second derivatives were used, in place of the value and first derivatives originally suggested by Mann and Morrison, to minimise errors from subharmonics and dc.

However, later examination [9] showed higher differences to be disadvantageous, since in reality they failed to improve the frequency response of the method, and instead resulted in greater high frequency amplification and increased numerical errors.

Slemon, Robertson and Ramamoorty [1] were the first to suggest using cosine and sine orthogonal functions, in a classical Fourier analysis form, for computing the fundamental frequency of the line's voltage and current from a set of samples over one full period of the system frequency. McLaren and Redfern [13] later implemented this method on a large off-line computer, using a high sampling rate of 128 s/c and no initial lowpass filters. The simulated waveforms employed were somewhat unrealistic in that they contained postfault constant amplitude noise signals, and the analysis of the method and derivation of its filtering characteristics were attempted in the continuous time domain, with no consideration given to the effect of sampling.

A generalised approach based on orthogonal function considerations was formalised by Hope and Umamaheswaran [14]. This included the Fourier series analysis, and a simplified alternative in which the cosine and sine functions were replaced with odd and even square waves. This gave a performance that was later investigated [9] and shown to be poorer than that of the Fourier series in dealing with the exponential dc offset and nonharmonics.

Direct impedance determination from instantaneous quantities, as in Equation (1.14), was probably first suggested by McInnes and Morrison [15]. It was recognised, however, that the use of the basic difference equation for obtaining the simultaneous equations in R and L was bound to give large numerical errors because of the high frequency

noise that the difference term would accentuate, as was observed in the Mann and Morrison method. Thus, McInnes and Morrison chose to integrate numerically the difference equation, making the creation of simultaneous equations possible through the substitution of sample values and numerical estimates of the integral over two intervals.

The significance of the length of the integration interval was not fully appreciated by McInnes and Morrison. They chose one quarter cycle, and based this on the speed of fault detection they were aiming at. However, it was later shown [9] that high and low frequency noise is best attenuated with respect to the fundamental with the integration interval being an odd multiple of half a cycle. Also, the choice of a relatively high sampling rate, probably influenced by the Mann and Morrison [7] approach of numerical error minimisation, was not optimum. These factors, combined with the fact that no analogue lowpass filters were used prior to sampling, explain why the performance of the method, as reported by the authors, was not up to expectations.

Ranjbar and Cory [16] presented another method based on the basic difference equation, Equation (1.14), and involving numerical integration. The suitable choice of the integration intervals and starting points, they argued, can eliminate any number of harmonics, and they consequently attempted the removal of the second, third and fifth harmonics, leaving only the seventh, eleventh and higher prime harmonics. The method involved more calculations than needed in the McInnes and Morrison method, but was thought to be superior from a filtering point of view.

In the same paper [16] Ranjbar and Cory also presented a mean square error minimisation method. This started with the integration

of the difference equation, assuming it to be an inequality because of the presence of an error. The mean of the square of this error over a second interval was minimised by equating its partial derivatives with respect to R and L to zero. This in turn gave two simultaneous equations for R and L. The method can be seen to be relatively complicated, and was later discarded despite its improved accuracy.

Luckett, Munday and Murray [17] had, at about the same time as Ranjbar and Cory, suggested another method based on least squares. Curve fitting, through finding least square fits of samples to a sine wave containing harmonics and dc, led to the derivation of some complicated weighting functions, the coefficients of which were calculated off-line. Best estimates for the voltage and current phasors were then obtained by the on-line substitution of samples in those weighting functions. The initial knowledge of the exponential dc time constant was assumed, though, and this constituted a serious drawback, since such time constant is known to vary for differing faults and is indeterminate beforehand.

Least square polynomial fits were adopted by Phadke, Hlibka and Ibrahim [18] for data smoothing applied before determining the voltage and current phasors. Polynomials, with orders less than the number of data samples employed, were chosen, and smoothed voltage and current sample values and their derivatives were obtained by direct substitution of samples in discrete weighting functions derived from the least square fitting. The smoothed values and derivatives were then used to find voltage and current phasors by the peak-determination method of Mann and Morrison [7]. The technique was applied with a high sampling rate and a narrow data window, and the marked improvement it showed on the Mann and Morrison method was expected since the main source of error in the latter was the high frequencies that unsmoothed data contained.

Some of the methods outlined above relied on the extraction of the fundamental waveforms through indirect and direct filtering. The rest attempted the direct determination of the fundamental impedance. A number of other, less consistent, approaches have also been reported in various literature. A team in the University of Missouri-Columbia [19], for example, attempted fault detection employing the high frequency components that faults generate. The first and largest such component in the fault transient, it was postulated, was dependent on the type and location of fault. A hardware fault detector unit capable of detecting the high frequency components was developed and was to be interfaced to a substation computer. The practicability of this method is questionable, since it is based on a somewhat simplified relation between the high frequency transients and fault type and location. In fact, the first systematic and solid investigation of the high frequency transients and their dependence on fault configuration in a section of an interconnected power system has only recently appeared [20], and its results suggest a more complicated correlation between the transients and the fault, because of the possible appearance of some significantly large line-transducer resonance components that the method does not take into consideration. The method also requires the knowledge of circuit constants, which would impair the versatility of any relay adopting it.

Laycock [21] presented a number of methods based on differing approaches. He started with the analogue, and then digital, filtering of the voltages and currents before using them in a block-average comparator. He then replaced the static comparator with a digital sampling comparator program that was to derive the impedance loci on the X/R plane in a digital manner. In another scheme, half cycles of

voltages and currents were digitally correlated with reference sinusoids with varying phases, and best matches that indicated the phase were found, leading to the determination of the line's impedance. The sinusoids were later replaced by square waves, making on-line implementation possible. A further simplification that led to polarity-coincidence correlation was also introduced, and was later used by McLaren and Redfern [22] in their hybrid phase comparator that applied the correlation concept in phase determination involved in a comparator implementation. This technique was very interesting and showed favourable results, but it lacked the flexibility and ready compatability that only those schemes that directly determined the line's impedance offered.

Many of the schemes described above did not exploit their underlying principles to the full. It is felt that the careful choice of the relevant parameters, and the inclusion of modifications when necessary, will improve their performance in general. The basic principle of one of those schemes, that of the Fourier analysis, is thus next examined in the hope that the development of an optimum version of that scheme will become possible.

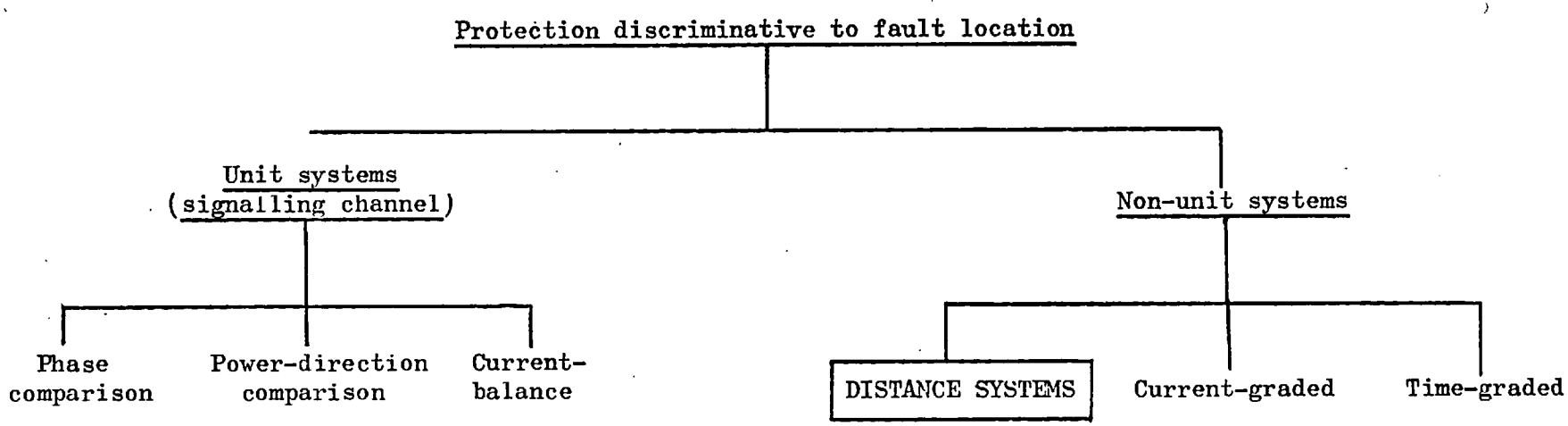

Fig. 1·1 Classification of transmission line protection schemes.

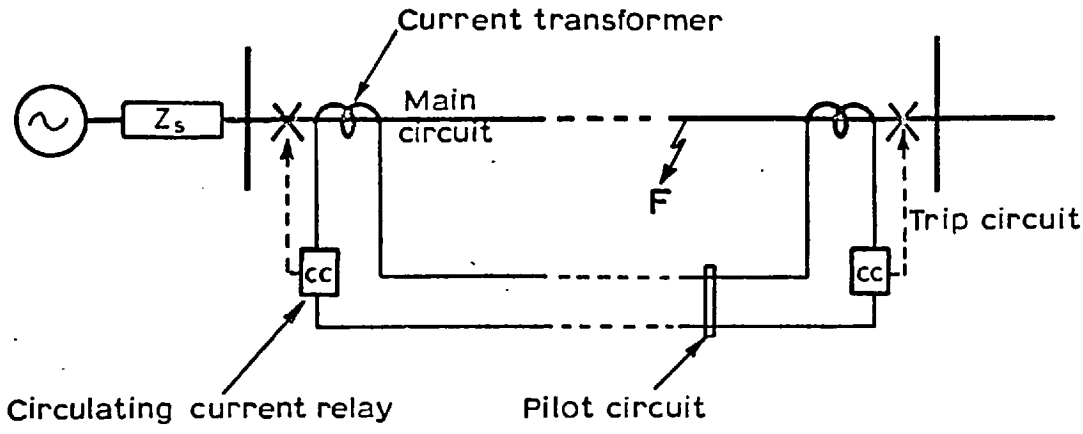

Fig. 1·2 Current-balance system using circulating current principle : unit protection.

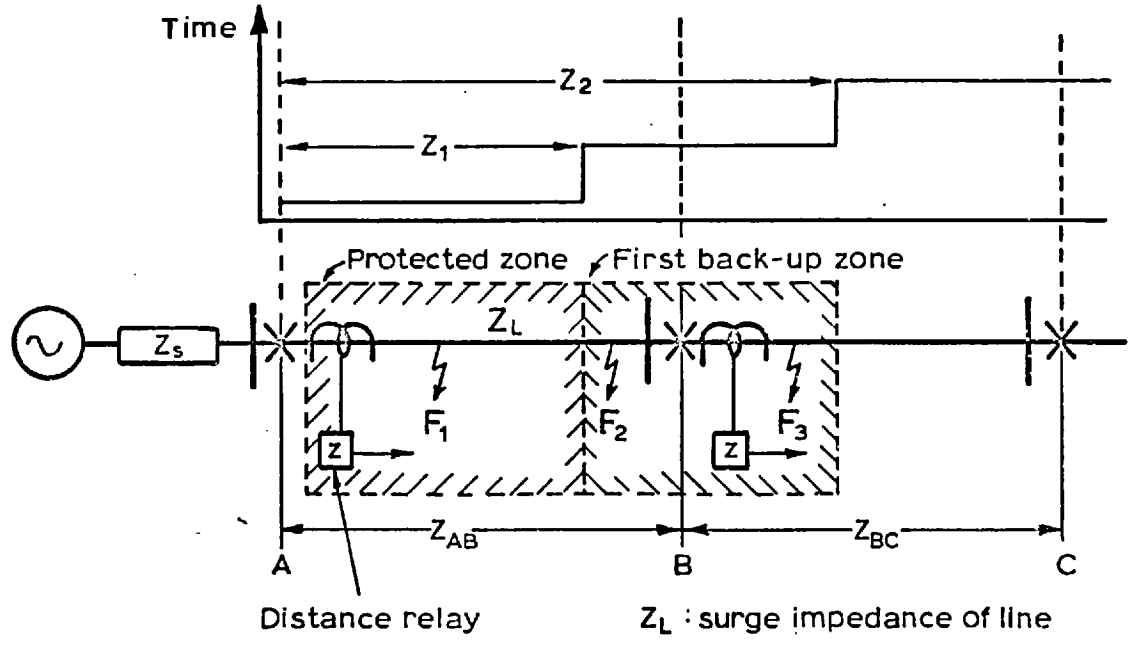

Fig. 1·3 Distance system with time features : non-unit protection.

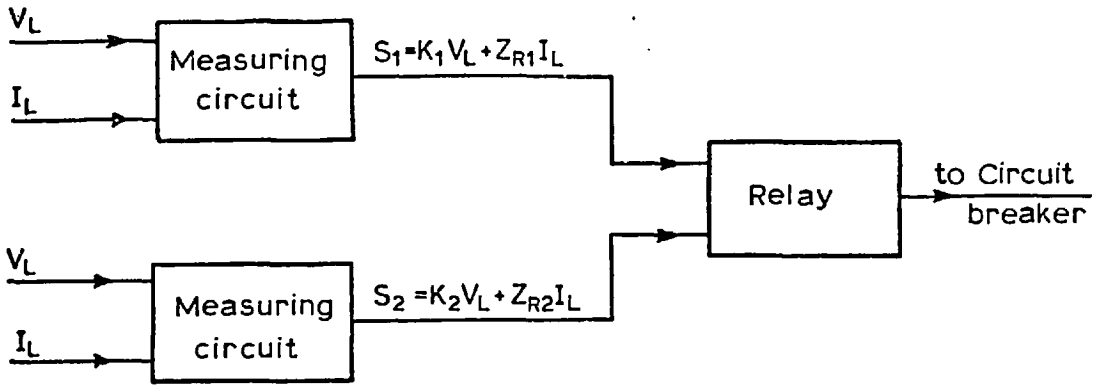

Fig. 1·4 Block diagram of a comparator relay.

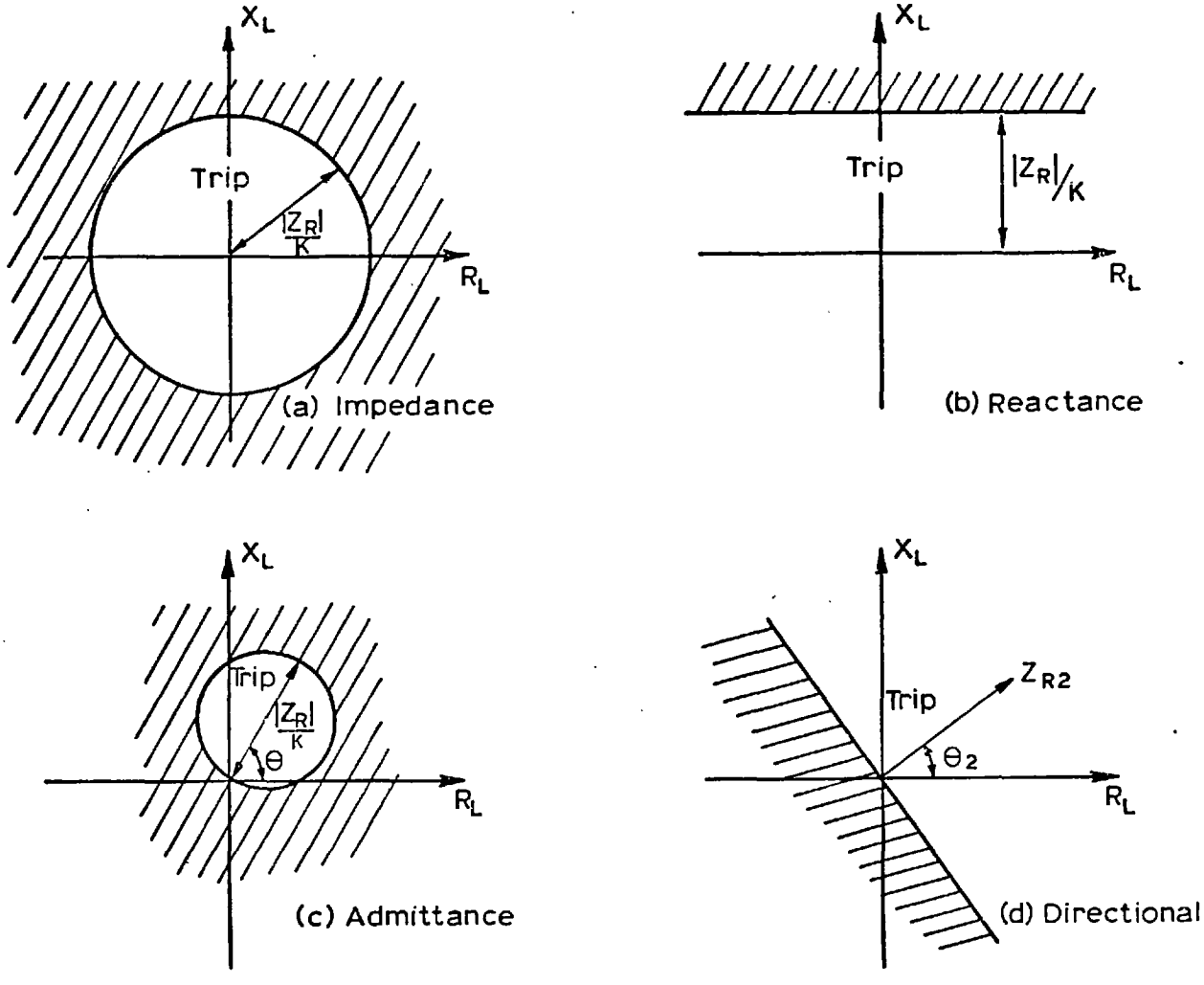

Fig. 1·5 Distance relaying characteristics.

CHAPTER 2

THE DISCRETE FOURIER TRANSFORM

The Fourier transform has for long been known for providing exact quantitative spectral analysis of signals. A time signal f(t), defined over the entire time domain, gives, when transformed into the frequency domain, a spectral density defined by [23] :

$$F(\omega) = \int_{-\infty}^{\infty} f(t).\exp(-j\omega t)\, dt \qquad (2.1a)$$

with this density giving the same time function when mapped back into the time domain by the complementary inverse transform:

$$f(t) = \frac{1}{2\pi} \int_{-\infty}^{\infty} F(\omega).\exp(j\omega t)\, d\omega \qquad (2.1b)$$

The pair of integrals appearing above is derived from the basic complex Fourier series identities [23] that define a periodic waveform in terms of complex exponential variations with complex coefficients:

$$g_p(t) = \sum_{k=-\infty}^{\infty} g_k.\exp(jk\,\omega_o t) \qquad (2.2a)$$

where $$g_k = \frac{1}{\tau} \int_0^{\tau} g(t).\exp(-jk\,\omega_o t)\, dt \qquad (2.2b)$$

ω_o being the fundamental radian frequency of the waveform, and τ the period:

$$\omega_o = \frac{2\pi}{\tau} \qquad (2.2c)$$

and the coefficients g_k constitute the amplitude distribution of the line spectrum, corresponding to a spectral density given by [24] :

$$F(\omega) = \sum_{k=-\infty}^{\infty} g_k.2\pi.\delta(\omega - k\omega_o) \qquad (2.2d)$$

While the applicability of the Fourier series is restricted to periodic signals only, it is still much more frequently used than the continuous transform, since the latter requires the evaluation of integrals between infinite limits in the time domain. Such evaluation is seldom possible in practice, and approximating signals to periodic variations that can be handled by the series is often adopted as a compromise.

The desirability for totally numerical procedures in spectral analysis led to the derivation of the Discrete Fourier Transform (DFT). This extension of the Fourier series maps a sequence of samples f(nT) of length N into another sequence of the same length [25] :

$$F(r\Omega) = \sum_{n=0}^{N-1} f(nT).\exp(-jr\Omega nT), \quad 0 \leqslant r < N \tag{2.3a}$$

with an inverse (IDFT) that maps $F(r\Omega)$ back into f(nT):

$$f(nT) = \frac{1}{N} \sum_{r=0}^{N-1} F(r\Omega).\exp(jr\Omega nT) \tag{2.3b}$$

$F(r\Omega)$ constitutes a finite line spectrum, with the frequency increment Ω defined in terms of the sampling interval T in the time domain as:

$$\Omega = \frac{2\pi}{NT} \tag{2.3c}$$

thereby ensuring that the period $N\Omega$ of the spectrum [26,27,28] equals the sampling frequency $\frac{2\pi}{T}$.

2.1 INTERPRETATION OF THE DFT

The DFT will be shown to give a true description of a time signal only when such signal is periodic, bandlimited and correctly sampled. The interpretation of the DFT of signals in general is thus of interest, such interpretation not being obvious.

There exists a well-formulated theory [29] that relates the DFT to the desired continuous spectrum of the time signal. However, this theory involves explanations that are far from straightforward. A simpler approach has therefore been developed, and is given below together with the classical theory referred to above. The new approach gives complete insight into the mechanism of the DFT, from which the appropriate choice of the relevant parameters (T, N and Ω) readily follows. Also, the effects and benefits of employing windows for data in the time domain become apparent, making a decision on the use of such windows, based on sound criteria, possible.

2.1.1 The Classical Approach

The problem, as stated above, is the determination of the continuous transform $F(\omega)$ of a bandlimited time signal $f(t)$ from the DFT of a finite sequence of samples $f(nT)$ of the time signal. Classically, this is made possible through the complex Fourier series expansion of $g_p(t)$, a periodic version of a function $g(t)$ that is formed by the truncation of the initial waveform $f(t)$ over a period covering the whole of the sequence of samples $f(nT)$.

As is well known [30], the continuous transform $G(\omega)$ of $g(t)$ is in fact specified at discrete frequencies by the complex Fourier series coefficients g_k of $g_p(t)$. This is evident in Figure 2.1(c) and (d),

and is easily proved by comparing the coefficients g_k to the transform $G(\omega)$. For, expanding $g(t)$ in a Fourier series in the interval $(0, \tau)$, as in Equations (2.2), yields:

$$g_p(t) = \sum_{k=-\infty}^{\infty} g_k . \exp(jk\omega_o t) \tag{2.4a}$$

with the coefficients g_k given by:

$$g_k = \frac{1}{\tau} \int_0^{\tau} g(t) . \exp(-jk\omega_o t)\, dt \tag{2.4b}$$

and comparing this to the transform $G(\omega)$ of $g(t)$:

$$G(\omega) = \int_0^{\tau} g(t) . \exp(-j\omega t)\, dt \tag{2.5}$$

we have:

$$g_k = \frac{G(k\omega_o)}{\tau}, \qquad -\infty \leqslant k \leqslant \infty \tag{2.6}$$

When the sequence $f(nT)$ is used in place of the truncated function $g(t)$ in Equation (2.4b) above, the integral reduces to a summation and the coefficients g_k become:

$$g'_k = \frac{1}{N} \sum_{n=0}^{N-1} f(nT) . \exp(jk\omega_o nT) \tag{2.7}$$

giving a periodic line spectrum that repeats itself every N points. If $g(t)$, and therefore $g_p(t)$, are bandlimited with:

$$g_k = 0, \qquad |k| > \frac{N-1}{2} \tag{2.8}$$

then g_k and g'_k would be equal over a range of k [31] :

$$g_k = g'_k = \frac{1}{N} \sum_{n=0}^{N-1} f(nT) . \exp(jk\omega_o nT), \quad 0 \leqslant k \leqslant \frac{N-1}{2} \tag{2.9}$$

Comparing the above expression for g_k to that for the DFT in Equation (2.3a), it can be seen that they are the same except for a factor N, and r and k both bounded:

$$\frac{F(r\Omega)}{N} = g_k, \qquad 0 \leqslant r=k \leqslant \frac{N-1}{2} \tag{2.10}$$

The coefficients g_k, however, have been shown in Equation (2.6) to specify $G(\omega)$, and we thus have:

$$g_k = \frac{F(k\Omega)}{N} = \frac{G(k\omega_o)}{\tau}, \qquad 0 \leqslant k \leqslant \frac{N-1}{2} \tag{2.11}$$

from which it is seen that the DFT values are the same as the sampled values of the continuous transform, except for some scaling, and with $\Omega = \omega_o$. Examination of the definitions of Ω and ω_o as in Equations (2.3c) and (2.2c) respectively shows that they are in fact equal.

It was assumed in Equation (2.8) in the foregoing analysis that g(t) was bandlimited and that the sampling rate used in obtaining f(nT) was high enough to account for all the constituent frequencies of g(t). A truncated time function, however, can never be bandlimited [28], and therefore in practice aliasing is invariably introduced. As a consequence, the DFT values will differ from the Fourier series coefficients, as is depicted in Figure 2.1(d) and (e), with the exact relation now given by [31]:

$$F(k\Omega) = N. \sum_{m=-\infty}^{\infty} g_{mN+k}, \qquad 0 < k < N \tag{2.12}$$

It must also be remembered that, even with aliasing, the transform $G(\omega)$ which the DFT values specify is in fact the convolution [32] of the desired continuous transform $F(\omega)$ of the original signal f(t) with the transform of the rectangular truncation window, the

latter being of the $\frac{\sin x}{x}$ form:

$$G(\omega) = \tau . \int_{-\infty}^{\infty} F(\theta) . \exp\left[-j(\omega-\theta).\frac{\tau}{2}\right] . \frac{\sin\left[(\omega-\theta).\frac{\tau}{2}\right]}{(\omega-\theta) . \frac{\tau}{2}} . d\theta \qquad (2.13)$$

$G(\omega)$ will be a smeared version of $F(\omega)$, as in Figure 2.1(a) and (c), and the degree of resemblance between the two cannot be perceived off-hand. It is obvious, however, that resemblance increases with the duration τ of the window, with the $\frac{\sin x}{x}$ function becoming a delta function in the limit as $\tau \longrightarrow \infty$, and making $G(\omega)$ and $F(\omega)$ identical.

The above suggests that the DFT of general composite waveforms may be difficult to relate to the continuous transform. For this reason, the analysis of the DFT performing as a digital harmonic analyser is now studied from a viewpoint that will shed more light on its mechanism.

2.1.2 A Novel Approach

The finite sequence $f(nT)$ has so far been obtained by truncating, repeating and sampling the continuous waveform $f(t)$. The sequence could in fact be directly obtained by multiplying $f(t)$ by the discrete rectangular window $w_R(nT)$ as in Figure 2.2.

Thus, in the frequency domain, $F(\omega)$ is convolved with the spectrum of the discrete window given by [33] :

$$W_R(e^{j\omega T}) = \exp\left[-j\omega\left(\frac{N-1}{2}\right)T\right] . \frac{\sin\left(\frac{\omega NT}{2}\right)}{\sin\left(\frac{\omega T}{2}\right)} \qquad (2.14)$$

giving a spectrum the samples of which at discrete frequencies are specified by the DFT values, as in Figure 2.2(c) and (d). If a single cosinusoid is therefore to appear as one component only in the DFT, its radian frequency must be a multiple of $\frac{2\pi}{NT}$, as only then would the

continuous transform be sampled at the peak of the $\frac{\sin Nx}{\sin x}$ function, giving $\frac{N}{2}$, and sampled at the zeros located between the sidelobes elsewhere.

This leads to the fundamental result that correct DFT application is only when the frequencies making up the waveform being analysed are all multiples of a fundamental the period of which is defined by the duration NT of the window. The highest frequency allowed would still be restricted by the sampling rate being employed. Such a waveform will be periodic, and is thus characterised by a harmonic spectrum [24].

To illustrate this for a simple waveform consisting of one frequency only, consider:

$$f(t) = A_m.\cos(m\omega_o t) + B_m.\sin(m\omega_o t) \qquad (2.15)$$

When this waveform is expanded in a Fourier series over a period τ, equalling $\frac{2\pi}{\omega_o}$, the coefficients g_k of the series will all be zero, except for g_m and g_{-m}, and these, being complex conjugates, combine to give the real cosine and sine coefficients of Figure 2.3(a). Sampling f(t) every T seconds, with $T = \frac{2\pi}{N\omega_o}$, gives the sequence f(nT), and the DFT of this will consist of one component with a real and an imaginary part that are N/2 times the cosine and sine coefficients of the series respectively, as is shown in Figure 2.3(b). Thus:

$$\begin{aligned} F(m\Omega) &= F_c(m\Omega) + j.F_s(m\Omega) \\ &= N.g_m \\ &= \frac{N}{2}(A_m - jB_m) \end{aligned} \qquad (2.16)$$

and the cosine, rather than the sine, therefore appears as possessing no phase in the DFT. From this, it would be more logical to take the cosine as the reference waveform, and this will be the case in the rest of this thesis except when otherwise stated.

2.2 DETERMINATION OF THE DFT PARAMETERS

The use of the DFT for the analysis of waveforms generated on faulted transmission lines is now examined. The 50 Hz fundamental that is predominant under both steady-state and fault conditions is taken as the frequency increment of the DFT, and as has been established, the analysis will be exact only when all other frequencies present stand in simple multiple proportion to one another and to the fundamental. The likely presence of nonharmonics and subharmonics of the fundamental, and of exponentially decaying dc offset, is for the moment ignored.

2.2.1 Off-Line Analysis

The spectrum of the signal is to be specified up to a high frequency in this analysis. This necessitates the calculation of a long DFT that is carried out on a large computer.

The spectrum is assumed to be of interest up to the 100^{th} harmonic, or 5000 Hz,with any frequency above that being too small to justify initial analogue filtering. The corresponding sampling rate that would equal or exceed the Nyquist rate [26,27] would be anything above 10000 Hz, giving a sampling interval T that is equal to or less than 100 μsec. With a frequency interval Ω of 2π x 50 radians/second (rad/sec), the number of samples N needed is calculated from Equation (2.3c) to be 200, covering the 20 msec. duration of the 50 Hz fundamental as expected. However, the computationally efficient Fast Fourier Transform (FFT) algorithms [25,34] could be used for the fast calculation of DFTs with lengths that are powers of 2, and N is accordingly chosen as the next higher value above 200 that is a power of 2, i.e. 256, giving 78.125 μsec. for T, with Ω still at 2π x 50 rad/sec.

When a record of the fault waveform is not available, for one reason or another, over the entire 20 msec. immediately succeeding the fault incidence, the problem of completing the time sequence arises. One solution is to take all the undefined samples as zeros, giving a DFT resembling the DFT that would be obtained with all the sequence defined. Examining Figure 2.4(a) and (b) shows that the alternative use of the uncompleted sequence as it is gives a less accurate frequency representation, as well as upsetting the agreed choice of parameters, since the number of samples available now is less than N.

Sequence completion by other methods has also been suggested. One method [34] postulates the partial repetition of the defined portion of the sequence over the undefined portion. Another recommends switching to a higher sampling rate [35]. Both these methods, however, can be shown to be unsatisfactory for the application considered here.

2.2.2 Real-Time Schemes

The calculation of one or more spectral components of the DFT is to be carried out in real-time, and on a small processor or a minicomputer, in these schemes. Low sampling rates, giving short sequences, are employed because of the limited power of the processors, with the duration of the data window kept at 20 msec. Consequently, low order harmonics only are allowed, and an analogue lowpass filter is to precede sampling. This and all other aspects of real-time schemes are discussed in more detail in Chapters 4, 5 and 6.

2.3 DATA TAPERING IN THE TIME DOMAIN

A continuous time function can only be observed over a finite length of time, or through a time window. In the frequency domain, the spectrum of the window convolves with the spectrum of the signal and smears it, or spreads it out. The phenomenon, known as leakage, is illustrated in Figure 2.1(a), (b) and (c) for the standard rectangular window. Other windows have been devised with spectra in which side-lobes are suppressed at the expense of wider main lobes, and the use of such windows reduces leakage in the spectrum of the signal being observed. In the time domain, these windows aim at rounding off potential discontinuities at each end of the finite time function being analysed.

With discrete time functions, the standard discrete rectangular window of Figure 2.2(b) is replaced by other discrete windows for leakage reduction in the DFT. This, however, involves some intermediate changes in the interpretation approach described in subsection 2.1.2, and it would be easier to introduce the desired window by finally multiplying the finite sequence of time samples of Figure 2.2(d) by the appropriate weighting coefficients, thereby retaining the rectangular window as an intermediate step. Such multiplication of time sequences corresponds to the convolution of the repeated DFTs of the original time sequence and the window, and this convolution in turn reduces to the periodic discrete convolution of the two DFTs. The mathematical proof of this result is of no particular interest here and can be found elsewhere [25,33]. The result itself can be restated to mean that the effect of employing a discrete window on a finite time sequence can be investigated by cyclically convolving the DFT of the sequence with that of the window.

A discrete hanning window, the coefficients of which are arrived at by sampling the well-known continuous hanning window [25], will be used here. The DFT of this discrete window is readily obtained by expanding its continuous version in a Fourier series, and is in fact no more than a fundamental component and a dc component, the latter having a magnitude which is twice that of the former.

The effects and merits of windowing will now be studied. The component of prime interest in the DFT is the fundamental, and the fidelity in its reproduction is to be used as a criterion. A 64-point DFT is employed, this being a compromise between the long 256-point DFT decided upon for the use in off-line analysis, and the short 8 or probably 16-point DFT expected to appear in real-time schemes. The relevant parameters are chosen in a manner similar to that outlined in Section 2.2.

2.3.1 Signals with Harmonic Spectra

Figure 2.5 shows the DFT of a 150 Hz cosinusoid, together with a smaller 500 Hz component and a dc component. Both cosinusoids are faithfully reproduced in magnitude and phase, and it is expected that the fundamental itself and all its other permissible harmonics (50, 100, 150, 200,...,1550 Hz) will also be correctly reproduced. The phases cover the full circular arc of 2π, and the restriction imposed by the principal value of the tangent being $-\pi/2$ to $\pi/2$ is corrected for by the examination of the real and imaginary parts of the transform and the subsequent addition of $\pm\pi$ to the arctangent when necessary.

The dc component always appears as real, with its magnitude being twice what is expected, since it is the only component with no

image in the spectrum. A cosinusoid of 1.0 amplitude and 180° phase, for example, appears as a component with a magnitude of 32 ($= \frac{N}{2}$), and when its frequency tends to zero, transforming it into a negative dc of 1.0, the spectrum will show a dc component of magnitude 64.

The effect of the application of the hanning window is seen in Figure 2.6. The wide main lobe in the spectrum of the window, manifesting itself in a fundamental component in its DFT, explains the relative distribution, though only local, of the spectrum now. The phases, however, remain correct at the component frequencies.

2.3.2 Nonharmonics and the Exponential dc Offset

The exponential dc offset encountered in voltage and current signals on transmission lines is known to have a time constant that covers several cycles of the 50 Hz fundamental [3,9] . Its DFT would thus be very much like that of a proper dc, and only differing in the small contributions that would now appear at low harmonics.

Figure 2.7 shows one such exponential dc, with a time constant of 100 msec., superimposed on a 50 Hz cosinusoid. Both components appear accurately in the DFT, with the phase of the fundamental also correct. The error contributions to the fundamental from the exponential dc could subtract, through negative real and imaginary parts, from the fundamental component, which explains why this latter component now appears slightly smaller than 32.

Windowing an exponential dc is not admissible, since the wide main lobe of the window's spectrum creates, when convolved with the dc component in the DFT, a fundamental that is in fact not present

as in Figure 2.8. Such a fundamental also appears when the second harmonic is windowed.

Nonharmonics, in the absence of a fundamental, result in a small apparent component at 50 Hz. This component becomes negligible when the nonharmonic giving rise to it is either close in frequency to a harmonic, or is considerably higher than the fundamental. The use of a window is thus not contemplated here, with the total absence of the fundamental being unlikely in the first place.

2.3.3 The Combined Presence of Harmonics and Nonharmonics

When nonharmonics appear together with the fundamental and harmonics, the DFT gives a fairly good reproduction of the fundamental in both phase and magnitude, this being more so when the frequencies of the nonharmonics in question are considerably higher than 50 Hz. Figure 2.9 shows one such case. The use of a window here only slightly improves the amplitude distribution in the DFT, reducing leakage due to nonharmonics, but more significantly it also halves the magnitude of the fundamental, as can be seen by comparing Figures 2.9 and 2.10.

2.4 CONCLUSION

The Discrete Fourier Transform can be used for the accurate spectral analysis of a periodic bandlimited signal, with its parameters depending on the period and bandwidth of such signal.

The presence of nonharmonics introduces some errors in the analysis, and, although at first it may seem that such errors can be reduced by windowing data, further consideration shows that the

advantages gained by using windows are in fact limited. A window would halve the magnitude of the fundamental component when such component is originally present. More importantly, a large apparent component would appear at the fundamental frequency by windowing a dc or a second harmonic component, when the fundamental is in reality absent. It is thus decided against the use of data windows for all the applications of the DFT that are considered in this thesis.

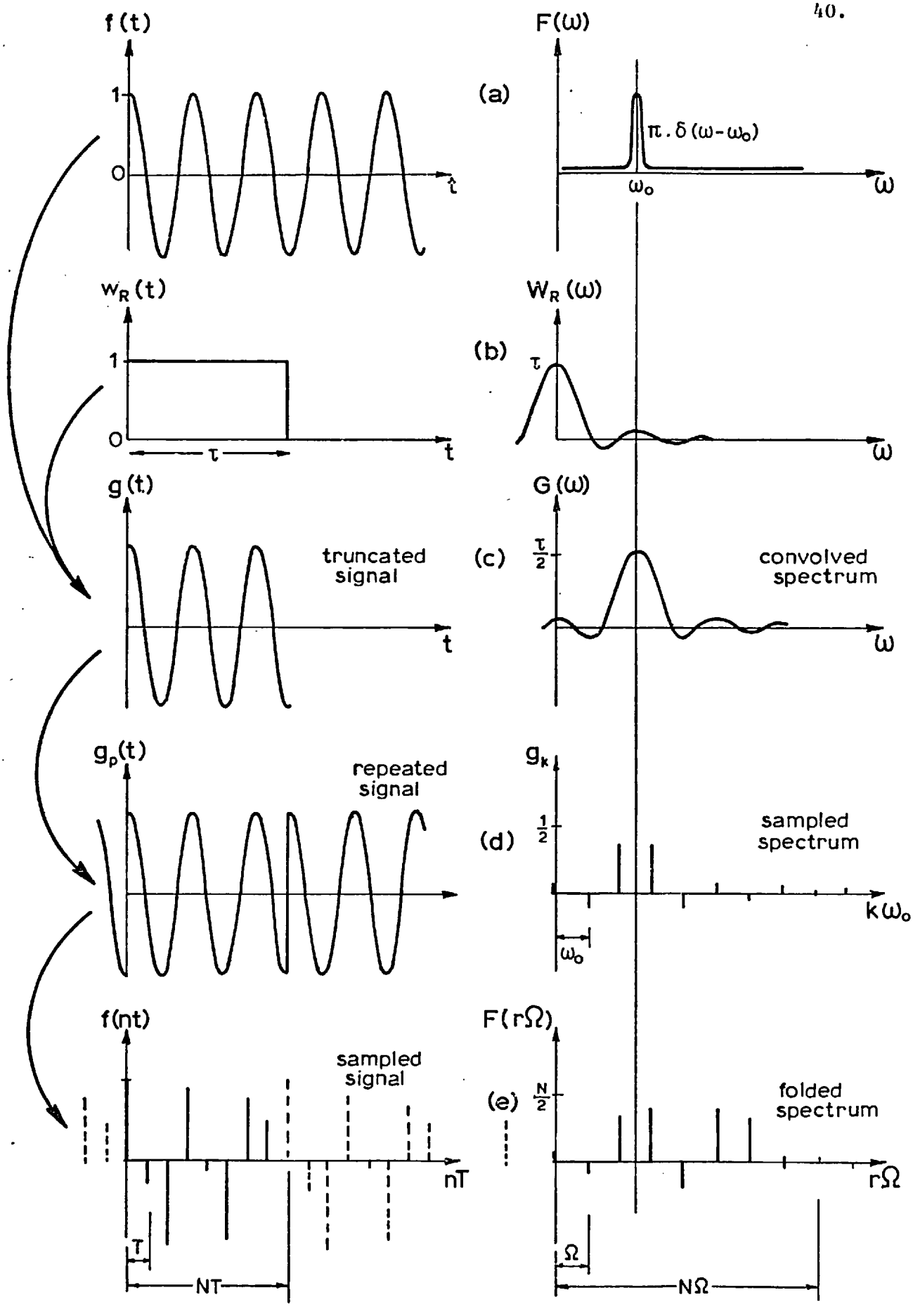

Fig. 2·1 Formation of a finite time sequence by truncation, repetition and sampling – The Classical Approach.

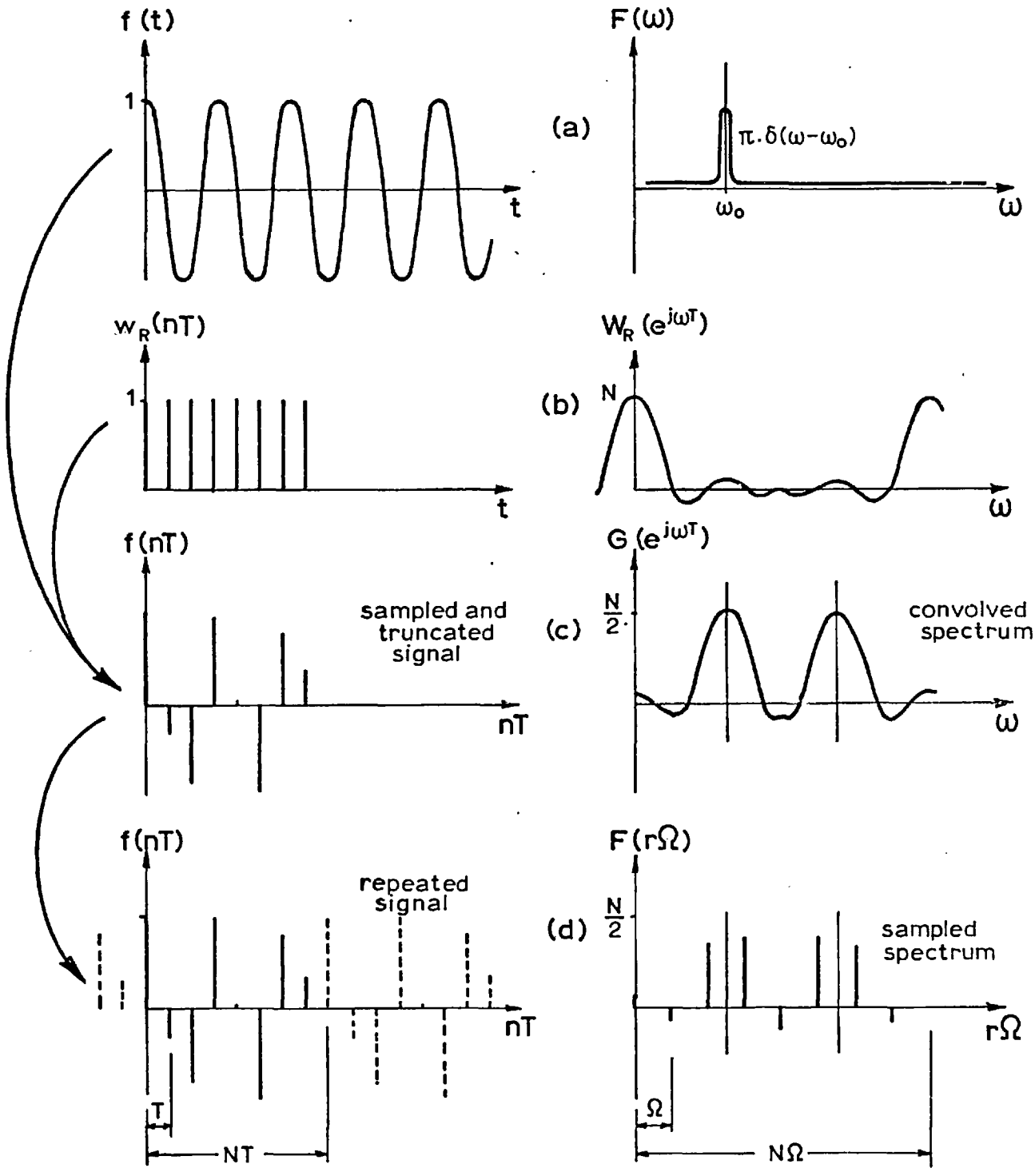

Fig. 2·2 Formation of a finite time sequence by sampling, truncation and repetition – An Alternative Approach.

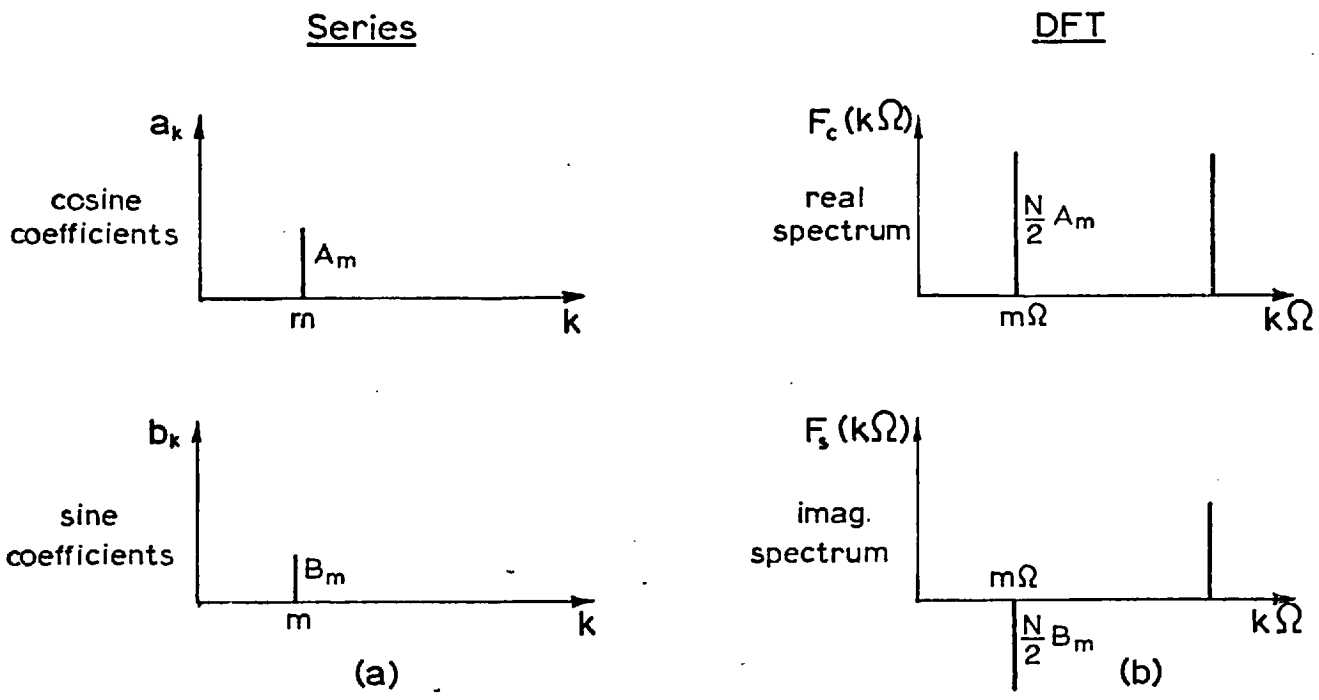

Fig. 2·3 Analysis of a shifted cosine with the Fourier series and the DFT.

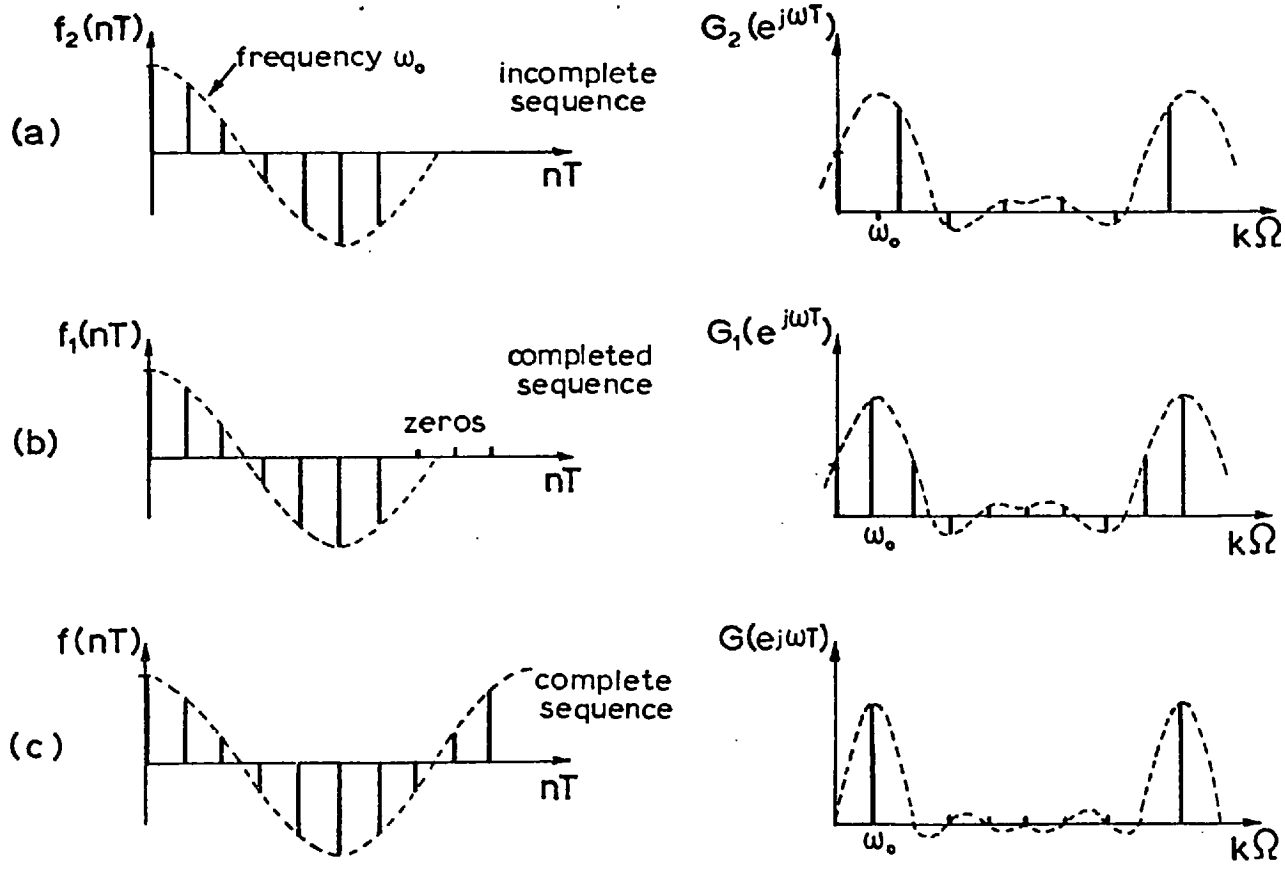

Fig. 2·4 Completion of a sequence by the addition of zeros.

A 64-POINT DFT WITH A RECTANGULAR WINDOW

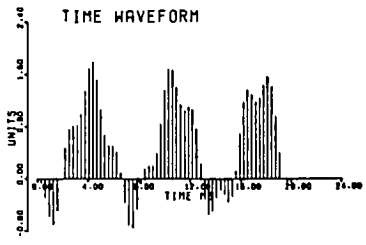

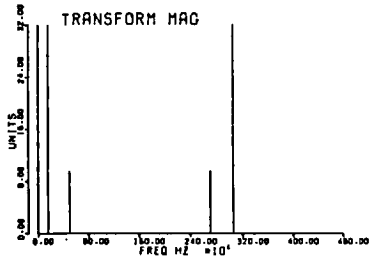

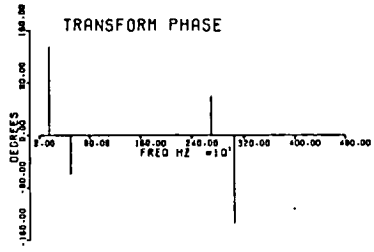

FREQUENCY RESOLUTION = 50.0 HZ
THEREFORE SAMPLING INTERVAL = 0.3125 MS
AND HIGHEST FREQ. ALLOWED = 1.60 KHZ

NO EXPONENTIAL ENVELOPE

NO EXPONENTIAL OFFSET

FREQS USED(HZ)	MAG	PHASE
0.0	0.5	0.0
150.0	1.0	135.0
500.0	0.3	-60.0

Fig. 2·5

A 64-POINT DFT WITH A HANNING WINDOW

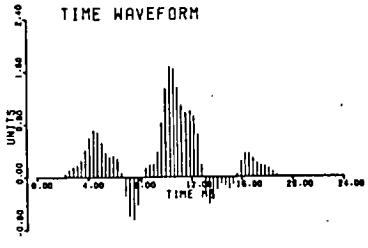

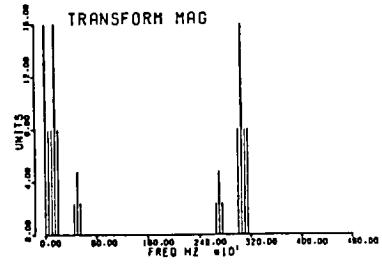

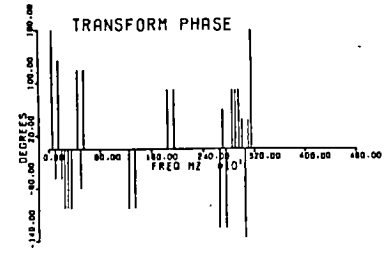

FREQUENCY RESOLUTION = 50.0 HZ
THEREFORE SAMPLING INTERVAL = 0.3125 MS
AND HIGHEST FREQ. ALLOWED = 1.60 KHZ

NO EXPONENTIAL ENVELOPE

NO EXPONENTIAL OFFSET

FREQS USED(HZ)	MAG	PHASE
0.0	0.5	0.0
150.0	1.0	135.0
500.0	0.3	-60.0

Fig. 2·6

A 64-POINT DFT WITH A RECTANGULAR WINDOW

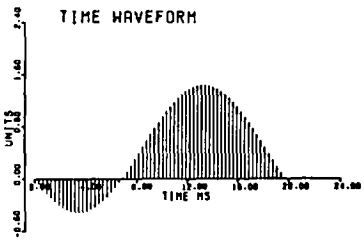

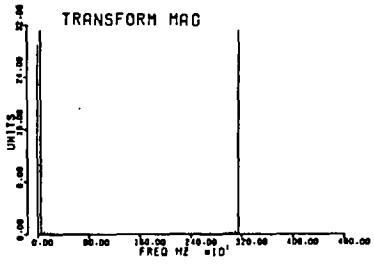

FREQUENCY RESOLUTION = 50.0 HZ
THEREFORE SAMPLING INTERVAL = 0.3125 MS
AND HIGHEST FREQ. ALLOWED = 1.60 KHZ

NO EXPONENTIAL ENVELOPE

EXP OFST	INIT VAL	TIME CONST MS
	0.5	100.0

FREQS USED(HZ)	MAG	PHASE
50.0	1.0	120.0

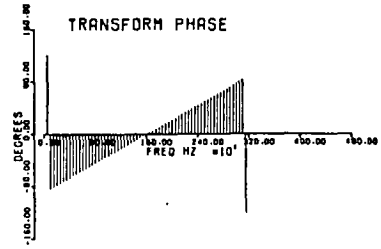

Fig. 2·7

A 64-POINT DFT WITH A HANNING WINDOW

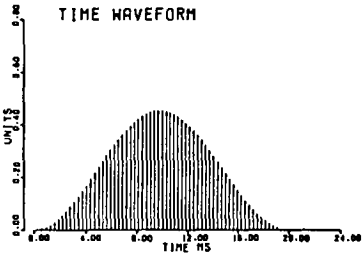

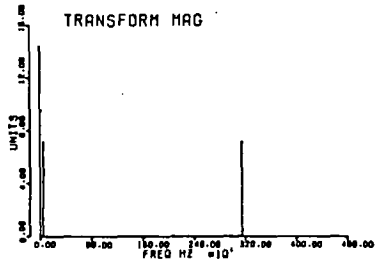

FREQUENCY RESOLUTION = 50.0 HZ
THEREFORE SAMPLING INTERVAL = 0.3125 MS
AND HIGHEST FREQ. ALLOWED = 1.60 KHZ

NO EXPONENTIAL ENVELOPE

EXP OFST	INIT VAL	TIME CONST MS
	0.5	100.0

FREQS USED(HZ)	MAG	PHASE
0.0	0.0	0.0

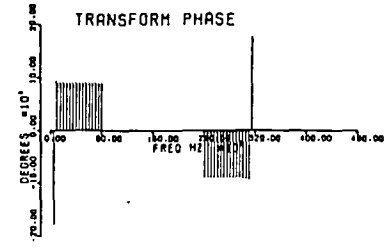

Fig. 2·8

A 64-POINT DFT WITH A RECTANGULAR WINDOW

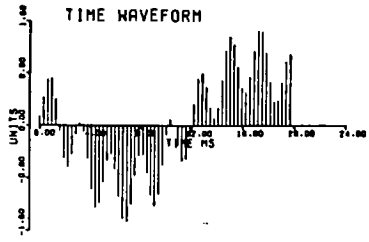

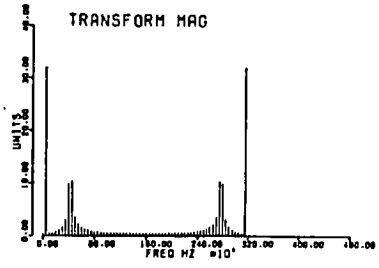

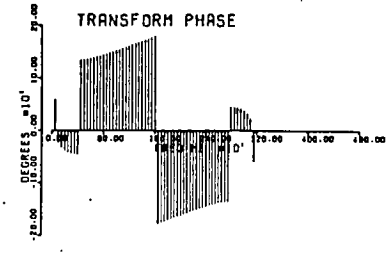

FREQUENCY RESOLUTION = 50.0 HZ
THEREFORE SAMPLING INTERVAL = 0.3125 MS
AND HIGHEST FREQ. ALLOWED = 1.60 KHZ

NO EXPONENTIAL ENVELOPE

NO EXPONENTIAL OFFSET

FREQS USED(HZ)	MAG	PHASE
50.0	1.0	60.0
425.0	0.5	-135.0

Fig. 2·9

A 64-POINT DFT WITH A HANNING WINDOW

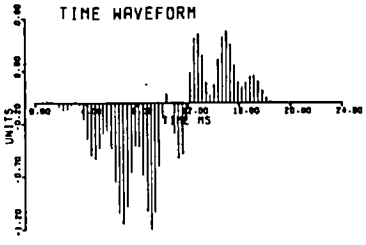

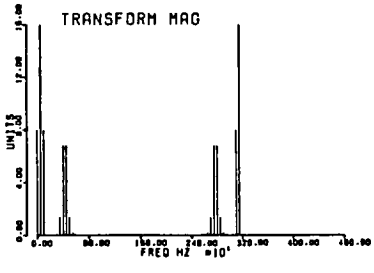

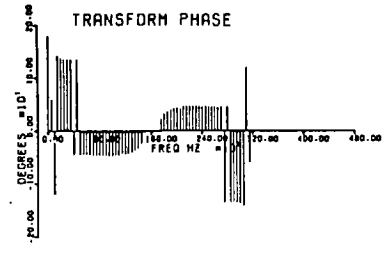

FREQUENCY RESOLUTION = 50.0 HZ
THEREFORE SAMPLING INTERVAL = 0.3125 MS
AND HIGHEST FREQ. ALLOWED = 1.60 KHZ

NO EXPONENTIAL ENVELOPE

NO EXPONENTIAL OFFSET

FREQS USED(HZ)	MAG	PHASE
50.0	1.0	60.0
425.0	0.5	-135.0

Fig. 2·10

CHAPTER 3

TRANSMISSION LINE FAULT TRANSIENTS

Transmission lines are linear networks, with parameters such as inductance and capacitance that can be regarded as frequency independent. However, the lossy nature of some lines introduces frequency and delay distortions [36] whereby different frequencies travelling along the line undergo varying attenuations and propogation delays. Thus, abrupt changes in voltage and current caused by faults or switching would travel distorted along lossy lines, giving rise to what is known as transient distortion.

In the recently introduced domain of computer protection, the acceptance of proposed digital relays is governed by reliability considerations that are known to impose searching and stringent tests [2] on conventional relays. Such considerations necessitate the knowledge of the nature and composition of fault transients, that in turn makes possible the simulation of fault waveforms and their use for proving the algorithms employed in the digital relays.

Power system switching and energisation transients [37] , that are in some aspects similar to fault transients, have recently been shown some increased interest. This is because the extremely high transmission voltage levels being used nowadays mean that the design of insulation which, in the past, was mainly determined by lightning discharge causing overvoltage phenomena [37,38] , is now more determined by the behaviour of the system under switching conditions. Thus, conditions under which transient voltages might develop had to be known for the reliable operation of power systems, and methods for the analysis of switching transients were consequently developed.

In this chapter we present a simplified analytical study of fault transients, employing a method that has been suggested elsewhere [37,39,40] for determining switching transients. Also presented are the results of off-line analysis, of some actual fault waveforms, obtained by the technique described in Section 2.2. We finally attempt to arrive at a basic description of fault transients based on the analytical study and the numerical analysis.

3.1 THE TRANSMISSION LINE EQUATIONS

The partial differential equations that give the variation of the voltage v and current i on a transmission line, with respect to both time and distance, are well known [36] . They are derived by considering voltages and currents in an incremental length δx of a transmission line, accounting for the distributed character of the line, as in Figure 3.1. The use of a distributed-parameter model automatically takes into consideration the wavelike propogation of voltages and currents, giving rise to the finite travelling time on the line, which is necessary for the study of transients.

The equations themselves are simultaneous partial differential equations:

$$-\frac{\partial}{\partial x} v(x,t) = R.i(x,t) + L.\frac{\partial}{\partial t} i(x,t) \qquad (3.1)$$

and

$$-\frac{\partial}{\partial x} i(x,t) = G.v(x,t) + C.\frac{\partial}{\partial t} v(x,t) \qquad (3.2a)$$

where R, L, G and C are the line constants per unit length. The conductance G can be taken for most practical purposes to be zero, giving:

$$-\frac{\partial}{\partial x} i(x,t) = C \cdot \frac{\partial}{\partial t} v(x,t) \qquad (3.2b)$$

and Equations (3.1) and (3.2b) are the telegraph equations, which reduce to the lossless wave equations for R = 0.

3.1.1 Analytical and Numerical Solutions

The analytical solution of the partial differential equations above is simple only in single mode propagation, and then only with simple initial and boundary conditions [39,40] . The mathematical complexity increases rapidly with the complexity of the network to be analysed. Recognising this in the study of switching and line-energisation transients [39,40,41] , mathematical treatments which were based on iterative methods were adopted for the solution of the differential equations.

The partial differential equations are reduced to ordinary differential equations by various methods. One such method [39] is based on a digital computer adaptation of the traditional transient analyser, which is used for setting up a scale model of the system being analysed. The ordinary differential equations resulting from replacing distributed-parameter elements, such as lines, by lumped π or T sections, are then solved digitally on the digital computer by a Runge-Kutta type of numerical integration routine. However, such use of lumped constants for representing lines introduces errors, since the representation behaves in the same way as the actual line for one particular frequency only, with an associated bandwidth. Wideband transients consequently have their high frequency components attenuated in the solution. This was demonstrated by Slemon et al [1] in their investigation of the inaccuracies in the simulation of fault transients by models utilising lumped-parameter elements, together with

the effects of these inaccuracies on the performance of high speed static relays. From this, the use of several π sections for each line was suggested as an improvement, and this has formed the basis of the majority of fault waveform simulation programs that have appeared up to data.

In another approach [40], the partial differential equations are transformed into partial differential equations in only the space variable x, or ordinary differential equations, by the Laplace transform. Expressions for the voltage and current transforms are then obtained by digitally solving the ordinary differential equations through a transformation of coordinates and the application of time delay functions. Finally, the inverse transforms of these expressions are formed, giving the voltage and current at any point on the line at any time.

The Fourier transform also has been used [41] for reducing partial differential equations to ordinary differential equations. In its usual form, however, this transform yields divergent integrals when applied to some functions that are normally encountered in transient studies, such as step and ramp functions, and consequently a modified Fourier transform was chosen which included an attenuation factor in the time domain. The voltage and current transforms were obtained, by solving the ordinary differential equations, in terms of hyperbolic distance variations and operational impedances. The inverse transforms were then formed by numerical integration, and gave the voltages and currents.

Away from differential equations, another method [39] was proposed that required the calculation of the system response over a range of frequencies by the Fourier transform. This response was then

multiplied by the frequency description of a step input, giving the frequency response of the line to the step. The response in the time domain was then calculated by applying the inverse transform, solved numerically on a digital computer since analytical solutions could not be found in most cases.

The Bewley lattice diagrams also formed the basis of one method [39] , that was more accurate and more suited to the calculation of transmission line energisation transients. The line was specified by its surge impedance and surge travel times, and the reflected and refracted voltages and currents at junctions and terminations were calculated by the use of reflection and refraction coefficients as in a lattice diagram.

The above numerical solution methods are each applicable to one test condition at a time. None would give an indication of what transient compositions to be expected in general, and some assume simplified models that may not be accurate enough for transient studies. It was thus decided to try and develop analytical expressions for voltages and currents in simple networks in terms of line parameters, as these would provide a general description of transient compositions, and would enable computations of transients on different lines to be carried out.

3.2 A SIMPLIFIED ANALYTICAL STUDY OF FAULT TRANSIENTS

An analytical solution to the fault problem sought is limited to very simple network configurations, as has already been discussed. The network chosen here is that of a single feeder connecting a generation node to an infinite bus, or the grid, as shown in Figure 3.2.

This choice is based on the fact that voltage magnitude, real power and limits to reactive power are usually all specified for a generation node in load flow problems [42] . This makes possible the determination of current flowing from the node which, when used together with the node voltage as boundary conditions in the steady-state solution of the line equations, gives a simple solution, as will be seen in subsection 3.2.2 below.

As a further simplification, only one phase is considered, narrowing the range of faults possible to open-conductor faults and conductor-to-earth faults. The former are of no appreciable significance in fast relaying, since the low currents, if any at all, associated with them can cause no damage to plant. Earth, or ground, faults, however, are of interest and will be investigated. Such faults will be treated as short-circuits or solid earth faults where the resistance between the conductor and ground drops to a very low value [2] , usually a few ohms.

The most common ground fault, however, is that in which a flashover occurs between a conductor and a tower [38] , with the resulting fault resistance comprising the arc resistance and the tower resistance, as well as the resistance between the tower footing and true earth. The tower resistance is negligible, but the arc resistance is appreciable, unless, of course, an arc does not form, as in the case of a fallen conductor [2] , for example. The tower footing resistance, too, is appreciable, and is known to range from a few ohms to a few hundred ohms, depending on the moisture content of the soil and on provisions taken for ensuring good earth footing [38] .

Fault resistance cannot therefore be neglected, as it can be comparable to the reactance of the line from the relaying point to the

fault. In what follows, however, the line equations are solved for a solid earth fault, and a fault resistance is not introduced until Chapter 8, where fault transients are simulated.

3.2.1 Fault Simulation: the Principle of Superposition [43]

The Laplace transform technique is now to be used for solving Equations (3.1) and (3.2b) for the line voltage and current during a fault. The knowledge of these quantities at the sending end of the line is sought.

A solid earth fault reduces the voltage at the fault point to zero, as in Figure 3.3(a). The complete transient solution of the line equations, with such voltage as a boundary condition, is intractable, and will, at any rate, involve the steady-state solution as a means of relating the voltage at the fault point to that at the generation node at the instant of fault incidence. The knowledge of such a relation is important because the performance of a relay is usually assessed in terms of the state of the voltage at the sending end of the line when the fault occurs.

The inevitable need for the steady-state solution makes it more logical to combine this solution with a much simpler transient solution, for obtaining the complete transient solution. The linearity of the line allows such superpositioning, whereby the disturbance by the fault is viewed as the sudden application of a fictitious voltage source to the fault point while the system is at rest, and with the original voltage source e(s) removed, as in Figure 3.4. This fictitious voltage, together with the steady-state voltage, now gives the short-circuit condition as in Figures 3.3(b), (c) and (a).

The fictitious source must be equal in magnitude and 180^{o} out of phase to the voltage at fault point. The steady-state solution of the original source, and the transient solution of this fictitious source, are now discussed.

3.2.2 The Steady-State Solution

As mentioned earlier, the choice of a feeder for the network meant that the voltage and current at the generation node, or the sending end, are known and could be used as boundary conditions. With a sinusoidal excitation voltage e(t), they are simple harmonic functions of time:

$$v(0,t) = V_S.\sin(\omega_o t) \tag{3.3}$$

and

$$i(0,t) = I_S.\sin(\omega_o t - \phi_S) \tag{3.4}$$

with V_S and I_S real constants. Now, the voltage and current along the line will also exhibit this harmonic variation, since the line is linear, and therefore a symbolic solution [36,44] of the equations that will employ time independent functions is:

$$v(x,t) = \mathrm{Im}\left[V_x(x).\exp(j\omega_o t)\right] \tag{3.5}$$

and

$$i(x,t) = \mathrm{Im}\left[I_x(x).\exp(j\omega_o t)\right] \tag{3.6}$$

$V_x(x)$ and $I_x(x)$ being both complex functions of x. Substituting Equations (3.5) and (3.6) in the line equations, Equations (3.1) and (3.2b), gives:

$$-\frac{dV_x}{dx} = (R + j\omega_o L).I_x = Z.I_x \tag{3.7}$$

and

$$-\frac{dI_x}{dx} = (j\omega_o C).V_x = Y.V_x \tag{3.8}$$

Z and Y being the series impedance and shunt admittance per unit length. Eliminating I_x and V_x respectively from the above equations gives:

$$\frac{d^2V_x}{dx^2} = \gamma^2.V_x \qquad (3.9)$$

and

$$\frac{d^2I_x}{dx^2} = \gamma^2.I_x \qquad (3.10)$$

and the general solution of the voltage function $V_x(x)$ and the current function $I_x(x)$ from either Equation (3.9) or Equation (3.10) above, together with Equation (3.7) or Equation (3.8), is:

$$V_x(x) = A.\exp(-\gamma x) + B.\exp(\gamma x) \qquad (3.11)$$

and

$$I_x(x) = \frac{A}{Z_o}.\exp(-\gamma x) - \frac{B}{Z_o}.\exp(\gamma x) \qquad (3.12)$$

and both $V_x(x)$ and $I_x(x)$ thus consist of wavelike disturbances moving in opposite directions, since γ, the propogation constant, is complex and is defined in terms of the attenuation constant α and the wavelength constant β as:

$$\gamma = \alpha + j\beta = \sqrt{ZY}$$
$$= \sqrt{(R + j\omega_o L).j\omega_o C} \qquad (3.13)$$

where both α and β are functions of ω_o since the line is with losses [36]. A and B are complex constants, and the surge impedance Z_o is defined as:

$$Z_o = \frac{1}{Y_o} = |Z_o|.\theta_{Z_o}$$

$$= \sqrt{\frac{Z}{Y}}$$

$$= \sqrt{\frac{R + j\omega_o L}{j\omega_o C}} \qquad (3.14)$$

Using the boundary conditions of Equations (3.3) and (3.4) in Equations (3.11) and (3.12), together with Equations (3.5) and (3.6), determines the complex constants A and B, which, when substituted back into Equations (3.11) and (3.12), and in turn in Equations (3.5) and (3.6), give for the line current and voltage the well known hyperbolic functions solution:

$$v(x,t) = \mathrm{Im}\left[V_S.\exp(j\omega_o t).\cosh(\gamma x) - Z_o.I_S.\exp(j(\omega_o t-\phi_S)).\sinh(\gamma x)\right] \tag{3.15}$$

and

$$i(x,t) = \mathrm{Im}\left[I_S.\exp(j(\omega_o t-\phi_S)).\cosh(\gamma x) - Y_o V_S.\exp(j\omega_o t).\sinh(\gamma x)\right] \tag{3.16}$$

The above equations can be rearranged to give the line quantities in terms of real sinusoidal variations as:

$$v(x,t) = C.\exp(-\alpha x).\sin(\omega_o t - \beta x + \theta_C) + D.\exp(\alpha x).\sin(\omega_o t + \beta x + \theta_D) \tag{3.17}$$

and

$$i(x,t) = C.|Y_o|.\exp(-\alpha x).\sin(\omega_o t - \beta x + \theta_C - \theta_{Z_o}) - D.|Y_o|.\exp(\alpha x).\sin(\omega_o t + \beta x + \theta_D - \theta_{Z_o}) \tag{3.18a}$$

with the real constants C and D, and angles θ_C and θ_D, defined by:

$$C.\exp(j\theta_C) = \frac{1}{2}\left[V_S + |Z_o|.I_S.\exp(j(\theta_{Z_o} - \phi_S))\right] \tag{3.18b}$$

and

$$D.\exp(j\theta_D) = \frac{1}{2}\left[V_S - |Z_o|.I_S.\exp(j(\theta_{Z_o} - \phi_S))\right] \tag{3.18c}$$

Equations (3.17) and (3.18) describe standing waves for the voltage and current. The variation of either quantity with time, on a particular point along the line, is thus sinusoidal. The difference between the amplitudes and phases of these sinusoidal oscillations at various points on the line is small, since, assuming a velocity of propogation equalling that of light, the distance that the corresponding

travelling waves cover in one cycle would be 3720 miles, which is much greater than the length of the transmission line, that seldom exceeds 100 miles and only accommodates a small portion of the complete cycle of the standing wave pattern. However, the space variation cannot be neglected altogether, and Equation (3.17) will in fact be used to determine the fault point voltage for a particular sending end voltage.

3.2.3 The Transient Solution

The Laplace transform is now used for reducing the partial differential equations, Equations (3.1) and (3.2b), to ordinary differential equations that are then solved for the voltage and current transforms in the transient solution of the initially quiescent line. The steady-state voltage at the fault point P at the moment of fault occurrence determines the fictitious source voltage, and its magnitude V_f and phase ϕ_f are found for a particular sending end voltage $V_S.\sin(\omega_o t')$ by the use of the fault inception angle $\omega_o t'$, together with the fault distance x_f, in Equation (3.17). The instant t' corresponds to the time $t = 0$ in the transient solution, and we thus have:

$$v(x_f,t') = V_f.\sin(\phi_f) \qquad (3.19a)$$

where ϕ_f, which is the phase angle of the fault point voltage at the instant of fault occurrence, is now measured with the sine wave, rather than the cosine wave, as a reference. This is a convention that also applies to the fault inception angle, and is noted here because it contradicts the convention adopted in the Fourier transform studies, where the cosine wave was taken as the reference.

The fictitious source voltage is now given by:

$$e_f(t) = -V_f.\sin(\omega_o t + \phi_f) \qquad (3.19b)$$

and this forms one boundary condition, the other being:

$$v(0,t) = -R_S.i(0,t) - L_S.\frac{d}{dt} i(0,t) \qquad (3.20)$$

where R_S and L_S are the resistance and inductance respectively of tne source impedance Z_S.

Taking the Laplace transform of the line equations, Equations (3.1) and (3.2b), yields the time independent relations:

$$-\frac{\partial}{\partial x} V(x,s) = R.I(x,s) + L\left[s.I(x,s) - i(x,0)\right] \qquad (3.21)$$

and

$$-\frac{\partial}{\partial x} I(x,s) = C.\left[s.V(x,s) - v(x,0)\right] \qquad (3.22)$$

which, with the initial conditions $i(x,0) = v(x,0) = 0$ for an initially quiescent line, gave after the elimination of $I(x,s)$ and $V(x,s)$ respectively:

$$\frac{\partial^2}{\partial x^2} V(x,s) = (R + sL).sC.V(x,s) \qquad (3.23)$$

and

$$\frac{\partial^2}{\partial x^2} I(x,s) = sC.(R + sL).I(x,s) \qquad (3.24)$$

and the solution of any of the above equations consists of a complementary function and no particular integral. For the voltage transform:

$$V(x,s) = E(s).\exp(-\gamma_s x) + F(s).\exp(\gamma_s x) \qquad (3.25)$$

where E and F are functions of s, and γ_s is defined by:

$$\gamma_s^2 = sC.(R + sL) \qquad (3.26)$$

The current transform is found from Equation (3.21) to be:

$$I(x,s) = \frac{E(s)}{Z_{os}}.\exp(-\gamma_s x) - \frac{F(s)}{Z_{os}}.\exp(\gamma_s x) \qquad (3.27)$$

with Z_{os} given by:

$$Z_{os} = \frac{1}{Y_{os}} = \sqrt{\frac{R + sL}{sC}} \qquad (3.28)$$

The use of the Laplace transforms of the boundary conditions of Equations (3.19b) and (3.20) makes it possible to determine the functions E(s) and F(s), which, when substituted back into Equations (3.25) and (3.27), give:

$$V(x,s) = -V_f.\frac{\omega_o.\cos(\phi_f)+s.\sin(\phi_f)}{s^2+\omega_o^2}.\frac{\exp(+\gamma_s x)-\Gamma(s).\exp(-\gamma_s x)}{\exp(+\gamma_s x_f)-\Gamma(s).\exp(-\gamma_s x_f)} \qquad (3.29)$$

and

$$I(x,s) = +V_f.Y_{os}.\frac{\omega_o.\cos(\phi_f)+s.\sin(\phi_f)}{s^2+\omega_o^2}.\frac{\exp(+\gamma_s x) + \Gamma(s).\exp(-\gamma_s x)}{\exp(+\gamma_s x_f)+ \Gamma(s).\exp(-\gamma_s x_f)} \qquad (3.30)$$

where $\Gamma(s)$, the reflection coefficient at the sending end, is defined as:

$$\Gamma(s) = \frac{Z_{os} - Z_{Ss}}{Z_{Ss} + Z_{os}} \qquad (3.31)$$

with the direction of travel from the sending end to the fault taken as reference, and with Z_{Ss} given by:

$$Z_{Ss} = R_S + sL_S \qquad (3.32)$$

Inversion of the transforms in Equations (3.29) and (3.30) is much simplified with the reflection coefficient $\Gamma(s)$ taken as +1. The source e(t) is thus assumed ideal, with zero impedance. This gives for the current transform I(x,s):

$$I(x,s) = +V_f.Y_{os}.\frac{\omega_o.\cos(\phi_f) + s.\sin(\phi_f)}{s^2+\omega_o^2}.\frac{\cosh(\gamma_s x)}{\sinh(\gamma_s x)} \qquad (3.33)$$

The voltage transform, however, is now reduced to zero, and the sending end voltage is probably best estimated by the substitution

of the sending end current in Equation (3.20). The sending end current itself is obtained by taking the inverse transform of Equation (3.33) with x = 0:

$$I(0,s) = +V_f.Y_{os}.\frac{\omega_o\cos(\phi_f) + s.\sin(\phi_f)}{s^2+\omega_o^2}.\frac{1}{\sinh(\gamma_s x_f)} \qquad (3.34)$$

which, with poles at $s = \pm j\omega_o$, gives a sinusoidal component:

$$i_1(0,t) = \frac{+V_f.|Y_o|}{H}.\sin(\omega_o t + \phi_f - \theta_{Z_o} - \theta_H) \qquad (3.35a)$$

where $$H.\exp(j\theta_H) = \sin h(\gamma x_f) \qquad (3.35b)$$

and, with other poles given by the solution of $Z_{os}.\sinh(\gamma_s x_f) = 0$, yields an exponentially decaying dc component for $s = -\frac{R}{L}$:

$$i_2(0,t) = \frac{+V_f}{x_f.\sqrt{R^2+\omega_o^2L^2}}.\sin(\theta_D-\phi_f).\exp(-\frac{R}{L}.t) \qquad (3.36a)$$

where $$\theta_{Z_d} = \arctan(\frac{\omega_o L}{R}) \qquad (3.36b)$$

and an infinite number of high frequency components for $s = -\frac{R}{2L} \pm j\omega_n\sqrt{1-\varepsilon_n^2}$:

$$i_3(0,t) = \sum_{n=1}^{\infty}(-1)^n.k_n.\exp(-\frac{R}{2L}.t).\sin(\omega_n\sqrt{1-\varepsilon_n^2}.t + \theta_n) \qquad (3.37a)$$

where $$\omega_n = \frac{n\pi}{T} \qquad (3.37b)$$

$$T = x_f\sqrt{LC} \qquad (3.37c)$$

$$\varepsilon_n = \frac{RT}{2\pi Ln} \qquad (3.37d)$$

$$k_n = \frac{+2V_f.k_{1n}.\sqrt{\frac{C}{L}}}{k_{2n}.T.\sqrt{1-\varepsilon_n^2}} \qquad (3.37e)$$

$$\theta_n = \theta_{k_{1n}} - \theta_{k_{2n}} - \arctan(\frac{\sqrt{1-\varepsilon_n^2}}{\varepsilon_n}) \qquad (3.37f)$$

$$k_{1n}.\exp(j\theta_{k_{1n}}) = \omega_o.\cos(\phi_f) - \varepsilon_n.\omega_n.\sin(\phi_f) + j\omega_n\sqrt{1-\varepsilon_n^2}.\sin(\phi_f) \quad (3.37g)$$

and $$k_{2n}.\exp(j\theta_{k_{2n}}) = \omega_n^2(1 - 2\varepsilon_n^2) - \omega_o^2 + 2j.\varepsilon_n.\omega_n^2\sqrt{1-\varepsilon_n^2} \quad (3.37h)$$

The complete current solution is not obtained by adding the steady-state component $i(0,t)$ of Equation (3.4), to the transient components i_1, i_2 and $i_3(0,t)$ of Equations (3.35a), (3.36a) and (3.37a). The fault inception angle $\omega_o t'$ is introduced as a phase in the steady-state current, transforming its time origin to the instant of fault incidence, as with the transient components. The steady-state current is thus written as:

$$i(0,t) = I_S.\sin(\omega_o t + \phi_{ss}) \quad (3.38a)$$

where $$\phi_{ss} = \omega_o t' - \phi_S \quad (3.38b)$$

An estimate of the magnitudes of the steady-state and exponentially decaying dc currents of Equations (3.35a) and (3.36a), shows that these currents are comparable to the prefault steady-state current in the network. The initial value of the dc offset depends on the fault point voltage phase ϕ_f, which combines with the impedance angle θ_{Z_d} of the line. The latter is nearly $\pi/2$ for high voltage lines, which means that a small fault inception angle, giving in turn a small ϕ_f, would result in a large dc offset, while a fault inception angle of $\pi/2$ would reduce the dc to zero. Such variation of the dc offset is substantiated by observations that have been reported elsewhere [3,9].

The damped high frequency current components of Equation (3.37a) are also influenced by the angle ϕ_f, but in the opposite manner. The coefficient k_n can be seen to be roughly proportional to $\sin(\phi_f)$,

meaning that a zero fault inception angle gives no high frequency components. The significance of these high frequency currents, even with ϕ_f equalling $\pi/2$, is, however, questionable. This is because of the presence of the relatively large surge impedance term in the denominator of the expression of Equation (3.37e) for the coefficient k_n.

The complete solution of the voltage, obtained by adding the steady-state solution to the transient solution that is found from the transient current solution and the source impedance, will also contain a steady-state component, an exponential dc offset and an infinite number of high frequencies. The exponential dc, however, is now much smaller than the steady-state value, mainly because the source's inductance, as obtained from the subtransient reactance of the generator, is usually not large enough to produce an appreciable voltage from the exponential current of Equation (3.36a).

The high frequency components, on the other hand, are expected to be more significant in the voltage, and mainly because their frequencies, being much higher than the fundamental, would result in a larger source reactance than for the steady-state component. The frequency of the lowest of these frequencies is roughly inversely proportional to the distance of the fault from the sending end, Equation (3.37b), and is about 900 Hz for a 400 kV line and a fault distance of 100 miles. For a closer fault, say 10 miles, the frequency goes up to 9000 Hz. Such dependence on the travel time T along the line justifies referring to these high frequency components as the eigen frequencies of the network.

The generation of the high frequency transients on a faulted line is attributed to the discharge of capacitive energy through the

line's inductance [9] . It has been recognised for some time, and has in fact formed the basis of some protection schemes. The team at the University of Missouri-Columbia [19] , that attempted the detection of these frequencies, arrived at a relation describing their dependence on the fault distance, to which the relation envisaged above is similar.

The time constant of the dc current offset is governed by the series impedance of the line, and is typically over 50 msec. This explains using time constants of 100 msec for the dc offset analysed by the DFT in Chapter 2. The high frequencies considered then were, however, only a few hundred Hz, such being significantly lower than the eigen frequencies predicted by the analytical study. This is because the eigen freqiencies, together with some even higher frequencies generated by scattered switching operations, are all expected to be removed by the analogue lowpass filter that is to precede the analogue to digital convertor (ADC) of any digital processor. The relatively low frequencies chosen were, on the other hand, used because it is known that such frequencies can sometimes appear as ringing, or resonance, between the line capacitance and the leakage reactance of the transducers [21] , that are used for voltage measurements, and that the model line employed so far does not consider. The capacitor voltage transformer (c.v.t.) is one such transducer that is most commonly used, and is shown schematically in Figure 3.5. The existence of these resonance frequencies will now be demonstrated through the spectral analysis of a few actual fault transients.

3.3 THE ANALYSIS OF REAL FAULT WAVEFORMS

The complexity of the average interconnected power system makes simulation studies possible only when simplifications are introduced. As was seen in Section 3.2, the analytical study of a simple model of one transmission line still required further simplifications, simplifications that made the validity of the results of the study questionable.

The composition of the fault transients, as arrived at so far, has thus to be substantiated, or more probably complemented, by studies utilising actual fault waveforms. This is of importance at this stage because the design of the digital relay, that is to be next considered, would largely depend on the frequency contents of the waveforms that the relay will be expected to process.

3.3.1 Data Acquisition: Test Conditions

The waveforms used were obtained from magnetic tape recordings of fault voltages and currents on the Sundon end of the Sundon-Cowley 400 kV three-phase circuit, which forms a part of the CEGB Supergrid. The first fault, fault A, was a phase-to-earth fault, obtained by fixing a fine steel wire between the blue phase conductor and earth at a point 33.5 miles from Sundon, as in Figure 3.5, with the circuit-breaker CB1 open. The oscillograms of Figures 3.6(a) and (b) show the blue phase current and the yellow phase voltage after the circuit-breaker CB1 was closed. The yellow phase voltage is used in the analysis because the blue phase voltage was almost zero.

Fault B was a blue phase short-circuit close to the Sundon end of the circuit, and immediately following the c.v.t., as shown in Figure 3.5. An earthing lead was now used in place of the steel fuse-wire, and the circuit-breakers switching sequence adopted was the same as that for fault A. Oscillograms of the blue phase current and yellow phase voltage are shown in Figures 3.6(c) and (d).

High fidelity recordings of the fault currents and voltages, produced on a precision tape recorder with a 10 kHz bandwidth, were made available to us. It was decided to sample these at a rate of 12.8 kHz, and feed the samples into a large computer (CDC 6400) for carrying out off-line analysis. 256 samples, covering the cycle of the 50 Hz that immediately followed fault incidence, were analysed, in accordance with the procedure developed in subsection 2.2.1. The analysis results are shown in Figure 3.7.

3.3.2 Results of Spectral Analysis

The fault inception angle was zero in both faults. Large exponentially decaying currents are thus expected, and they do in fact clearly manifest themselves in the spectra of Figures 3.7(a) and (c). The absence of the eigen frequencies from the voltages is also consistent with the one-phase model studied, where a zero fault inception angle gave no eigen frequencies.

However, the spectrum of the voltage of fault B, Figure 3.7(d), also shows a significant component at and around 250 Hz. This is also evident in the oscillogram of Figure 3.6(d), and is presumably the resonance components that the analytical study does not predict, and that is accounted for by the presence of the c.v.t.'s. As well as this

resonance, c.v.t.'s have been shown [45] to introduce enough errors in transient voltages to degrade the performance of conventional relays in speed and stability. Further considerations of the effects of the c.v.t.'s are, however, outside the scope of this thesis.

The dominance of the resonance components has recently been pointed out by Thorp et al [20], in their attempt at establishing the dependence of these components on the prevailing structure of the power system. From a systematic study that involved a very large number of faults simulated on a laboratory model of a line, and covering various system configurations and types and locations of faults, Thorp et al observed that both voltage and current waveforms contained significant components of frequencies ranging between 250 Hz and 550 Hz. The composition of the postfault waveforms was reported to be mostly dependent on the system configuration, and almost independent of the fault type and location.

Fault resistance, that the analytical model took as zero, can come about in a few forms. In test A, which looked like a short-circuit, the fuse-wire started an arc that must have had a relatively high resistance, assuming that no metallic vapour was emitted. Arc resistance is known to be nonlinear, and this explains the distortion in the voltage during the first few milliseconds after the incidence of fault A, as in Figure 3.6(b). In fact, initial waveform distortion is to be expected even in faults involving conductors falling to the ground, as then numerous small arcs between conducting particles in the ground would contribute to an overall nonlinear fault resistance [4].

The likelihood of an appreciable fault resistance in all phase-to-earth faults reduces the possibility of the appearance of the eigen frequencies with significant amplitudes. The damping that these frequencies undergo is increased by a fault resistance, and they are thus expected to appear for only a few milliseconds, if at all.

3.4 CONCLUSION

The results of a simplified analytical study of a fault, combined with the analysis results of actual fault transients, and a number of other considerations and observations reported in various literature, suggest a composition of fault transients.

Fault currents, it is concluded, can have some appreciable exponentially decaying dc offsets, as proved by the analytical study presented. Fault voltages, on the other hand, can contain some very high eigen frequencies of the faulted line and, more predominantly, resonance components of a few hundred Hz, caused by resonance between the lines and the capacitor voltage transformers. The possible existence of these resonance components was demonstrated by the DFT analysis carried out.

Consideration of a few possible fault configurations showed that the fault resistance is not to be neglected. It is expected to result in high attenuation rates for the eigen frequencies, and its nonlinearity is expected to produce distortion in voltages and currents immediately following fault incidence.

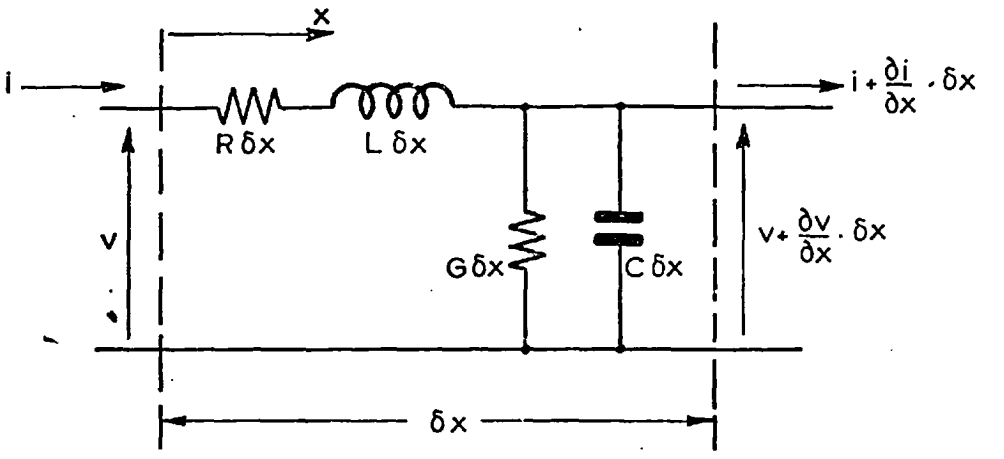

Fig.3·1 Incremental length of a transmission line.

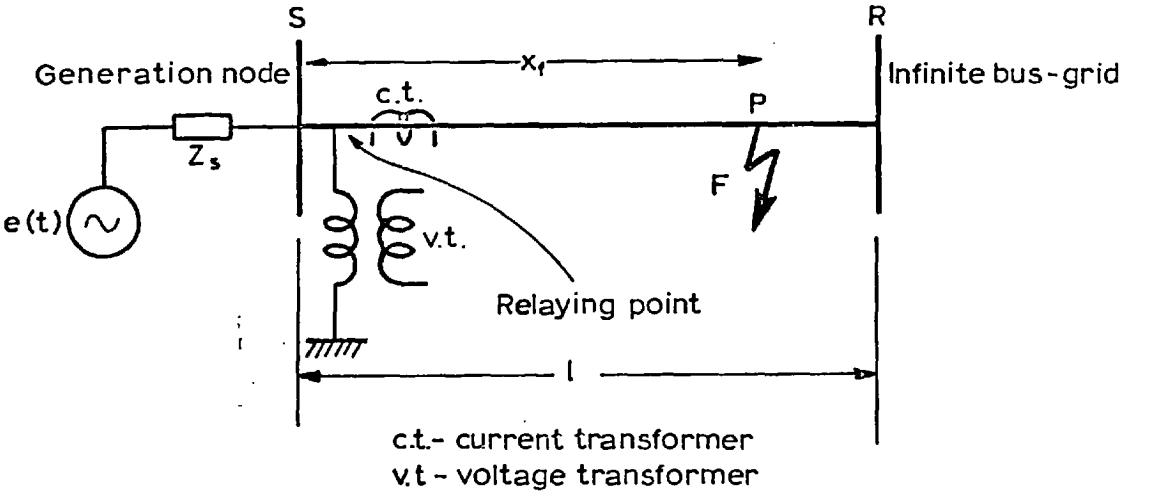

Fig. 3·2 Model of a faulted feeder.

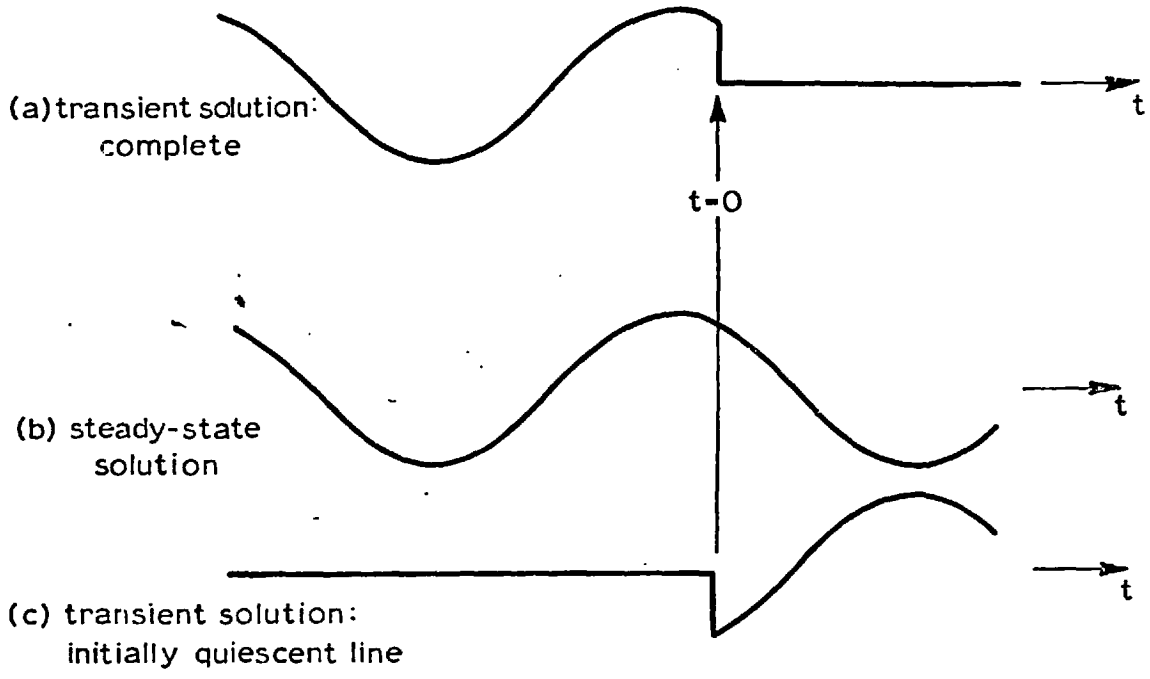

Fig. 33 Voltage at fault point - the superposition of solutions.

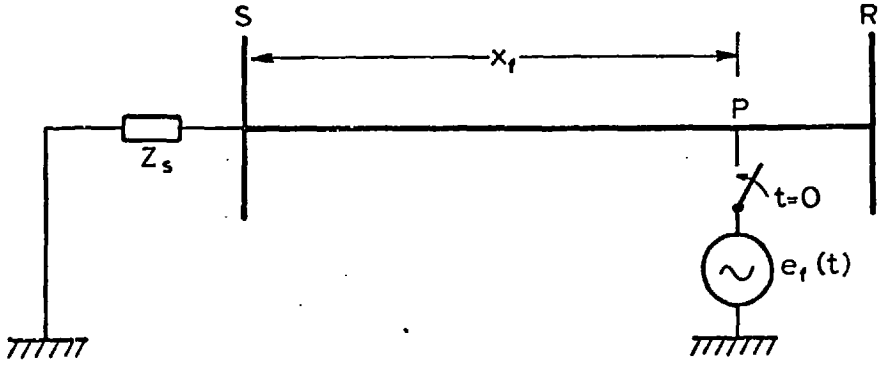

Fig. 3·4 Application of a fictitious source at fault point.

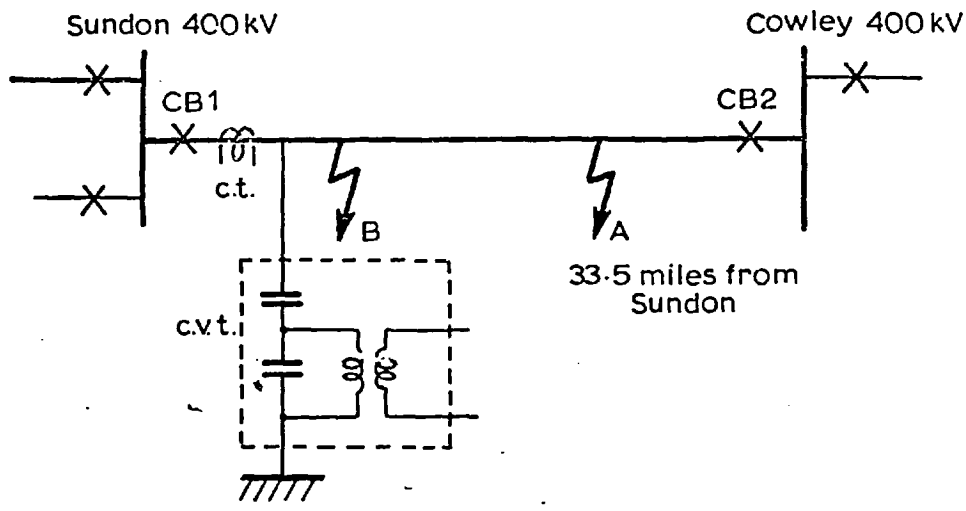

Fig. 3·5 The Sundon-Cowley test circuit.

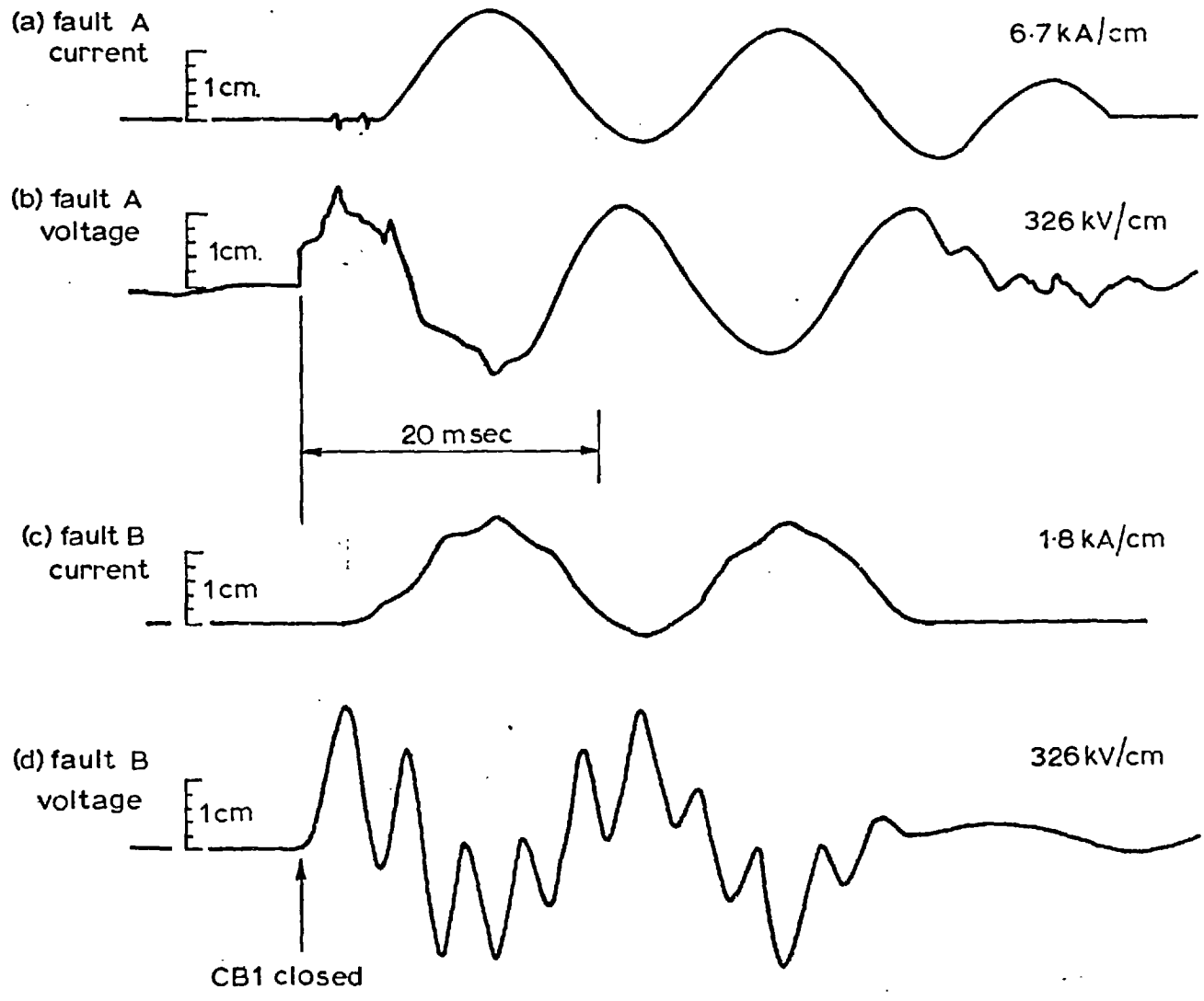

Fig. 3·6 Reproduced field oscillograms of fault currents and voltages.

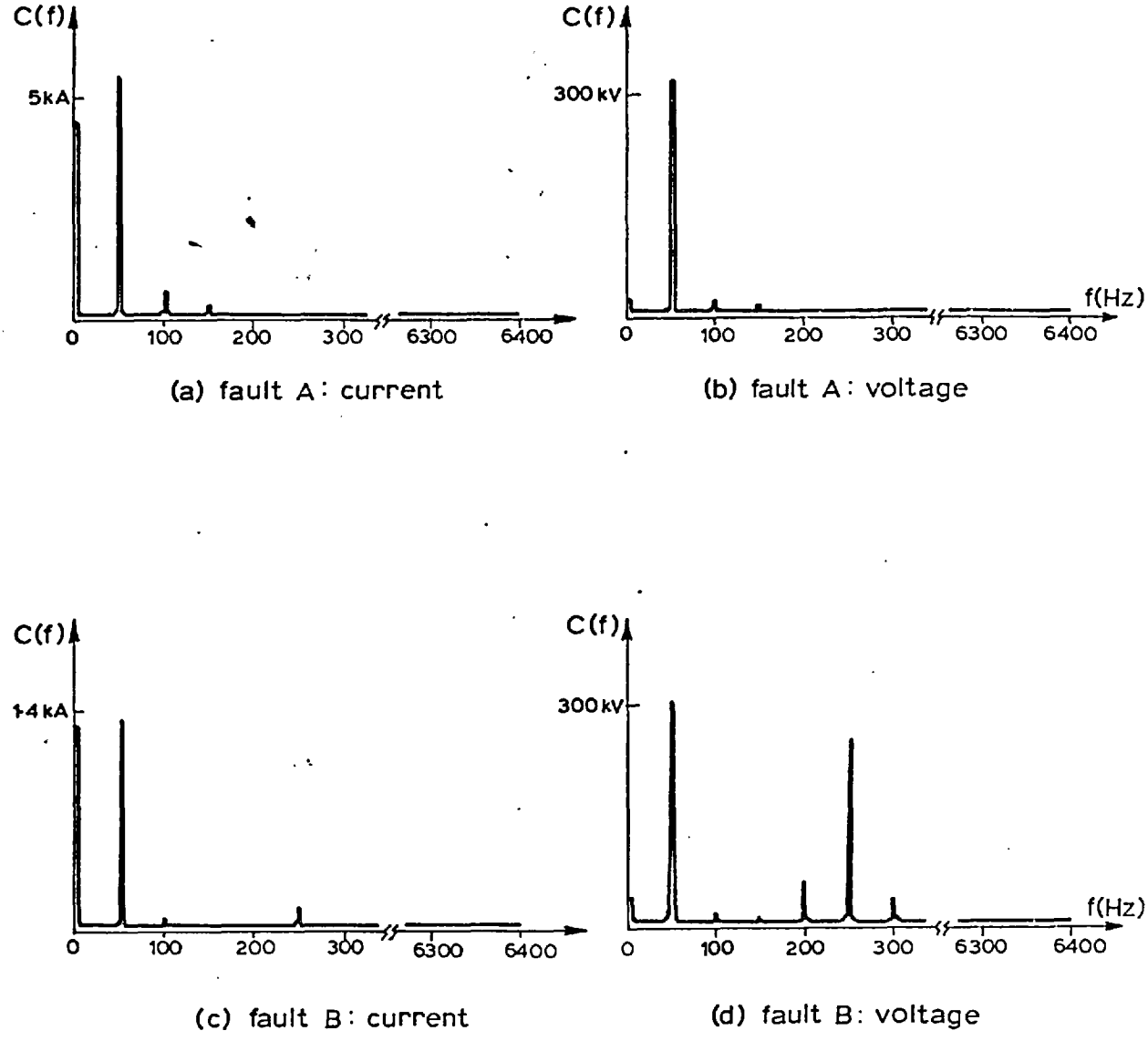

(a) fault A: current

(b) fault A: voltage

(c) fault B: current

(d) fault B: voltage

Fig. 3·7 Amplitude distributions of spectra of test waveforms.

CHAPTER 4

THE FULL CYCLE METHOD: PROTECTION SCHEME I

In Chapter 1 it was shown that most of the known digital relaying methods were based on distance relaying, whereby the line impedance, and hence distance, to the fault was employed. One of the two categories of the protection schemes discussed had as its main effort the determination of the phasor representations of voltage and current signals from sampled data of their instantaneous values, with the line impedance then obtained from the ratio of such phasors.

The Discrete Fourier Transform is one algorithm that is capable of determining a phasor representation from data samples. Its frequency selectivity properties were demonstrated in Chapter 2, and this chapter presents a study of a scheme based on its real-time adaptation. The scheme is referred to as the full cycle method because it requires data that cover one full cycle of the fundamental 50 Hz. Here, the filtering performance of the scheme is examined, and its suitability assessed in relation to the frequency description of fault transients as obtained in Chapter 3. Estimation of some typical fault detection times are finally given.

4.1 PHASOR REPRESENTATION

The phasor representation desired is that of the fundamental 50 Hz. component, and consequently the duration of data required is 20 msec, as justified in Chapter 2. A real-time scheme is concerned with the continuous determination of the voltage and current phasors, using data incorporating the latest samples of these quantities. For one quantity, then, N samples covering one cycle are stored in a shift

register, as in Fig. 4.1. Every sampling interval, a new sample is loaded in the left-most location of the shift register, and all previous samples are shifted one place to the right, with the originally right-most sample discarded.

The fundamental component is calculated from the stored samples as:

$$F(\Omega) = \sum_{n=0}^{N-1} f(nT).\exp(-j\Omega nT) \qquad (4.1)$$

which can be rewritten in a non-recursive digital filter form [46] as:

$$F_m(\Omega) = \sum_{n=0}^{N-1} f((m-N+1+n)T).\exp(-j\Omega(n+q)T) \qquad (4.2a)$$

The current output F_m is now calculated from the current input $f(mT)$ and $(N-1)$ past inputs: $f((m-1)T)$ to $f((m-N+1)T)$, while the phase ΩqT is introduced to change the reference point of the orthogonal cosine and sine waveforms that make up the complex exponential. The original reference point corresponding to the oldest input sample $f(0)$, as in Equation (4.1), is to be shifted by $\Omega(N-1)T$ to the current instant in time mT. Such negative shift can be replaced by a complementary positive shift of ΩT, since $\Omega NT = 2\pi$. We thus take q as 1, and the change of variable $p = (N-1)-n$ in Equation (4.2a) now gives:

$$F_m(\Omega) = \sum_{p=0}^{N-1} f((m-p)T).\exp(j\Omega(p+\ell)T) \qquad (4.2b)$$

where the phase $\Omega\ell T$ is added for a possible improvement in the filtering performance of the scheme.

Equation (4.2b) can be implemented as two transversal digital filters [46] utilising one common delay line, as shown in Figure 4.2. The two filters, non-recursive, are defined by:

$$A(mT) = \sum_{p=0}^{N-1} f((m-p)T).\cos(\Omega(p+\ell)T) \qquad (4.3)$$

and

$$B(mT) = \sum_{p=0}^{N-1} f((m-p)T).\sin(\Omega(p+\ell)T) \qquad (4.4)$$

This digital filter representation lends itself easily to the concept of the filtering performance, or frequency response, of the scheme. However, the processor-algorithm implementation of Figure 4.1 is the one contemplated and will consequently be used for the study of all other aspects of the scheme, notably the fault detection times.

In the processor-algorithm implementation, the line resistance and reactance are determined directly from the components of the voltage and current phasors, without the need for forming their quotient. In terms of V_L and I_L, given by:

$$V_L = A_v + j.B_v \qquad (4.5a)$$

and

$$I_L = A_i + j.B_i \qquad (4.5b)$$

the impedance, Z_L, can be written as:

$$Z_L = \frac{V_L}{I_L} = R_L + j.X_L$$

$$= \frac{A_v.A_i + B_v.B_i}{A_i^2 + B_i^2} + j.\frac{A_i.B_v - A_v.B_i}{A_i^2 + B_i^2} \qquad (4.6)$$

and this form presents savings in the computations it requires since it avoids phasor division which involves square roots and trigonometric functions.

4.1.1 The Sampling Rate

The lowest permissible sampling rate [26,27,28] for a 50 Hz phasor representation must be greater than 100 Hz. Starting at 150 Hz, the rate must go up in steps of 50 Hz to ensure synchronous sampling. The corresponding number of samples per cycle, N, would start at 3 and increase in steps of 1.

The time needed for calculating the DFT coefficient is determined by the number of multiplications involved, this in itself being a function of the length, N, of the data sequence. Interestingly, the rotating phasor $\exp(j\Omega pT)$ exhibits some symmetry that makes it possible to replace some of the required multiplications by additions. In Figure 4.3, with N = 5, symmetry about the axis AB is apparent. This results in a reduction in the number of multiplications needed for calculating the real, or imaginary, part of the coefficient from N to $\frac{(N-1)}{2}$. A further reduction is possible with even values of N, where additional symmetry would exist about CD, and likewise about EF when N is a multiple of 4. The total coefficient calculation time therefore increases in an irregular manner with N, since additions require typically only one-tenth as much time as multiplications.

The variation of the coefficient calculation time, normalised at N = 4, is shown in Figure 4.4. It is evident from the figure that values of N that are multiples of 4 offer the distinct advantage of minimal total time to sequence length ratio. The calculation of the coefficient with N = 8, for example, would require a time shorter than, or as long as, that needed for N = 5, 6 or 7. We opt for N = 8, since this allows higher order harmonics in the time waveform, thereby reducing the stringent requirements on the initial analogue lowpass

filtering, the need for which is explained in Chapter 6. The choice will also be justified by the study of Section 4.2 of the frequency response of the method, which will reveal that non-harmonic suppression slightly improves in general as N increases.

Of all the multiples of 4, those that are also powers of 2 are preferred: 4, 8, 16 and 32. This is because the corresponding sampling rates stand in geometric progression, and would consequently give spectra, or frequency responses, of the scheme that are consecutively expanded by factors of 2. Spectrum expansion by any smaller factor is considered too small for a significant change to emerge in the response. Finally, values of N that are larger than 32 are not considered because the real-time calculation of the DFT coefficients that they involve is not feasible.

4.1.2 The Processing Cycle

The protection algorithm is to continually determine the voltage and current phasors and line impedance, and decide on the presence of a fault. A processing cycle that comprises all these duties will require about 0.5 msec. for impedance determination, as from Equation (4.6), and another 0.5 msec. for executing the logic involved in relaying criteria that utilise digital relaying characteristics.

The total duration of a processing cycle, however, will depend on N since it must include the time taken for the phasor determination, or DFT coefficient calculation. On a pdp-15 minicomputer with a multiplication time of 25 μsec, this total amounts to 1.01 msec. for 4 s/c, 1.15 msec. for 8 s/c, 1.43 msec. for 16 s/c and 1.99 msec. for 32 s/c.

4.1.3 Continuous and Fault-initiated Processing

The sampling interval with 4 and 8 s/c is longer than the duration of a processing cycle. This makes possible continuous processing, whereby a processing cycle is initiated immediately after the arrival of each new sample. However, with 16 and 32 s/c, the cycle duration exceeds the sampling interval, making it necessary to employ an additional shift register for storing incoming samples as a processing cycle is being executed. The stored samples are then loaded into the main shift register, and another processing cycle initiated.

Complications arising from the introduction of the additional shift register, with 16 and 32 s/c, can be avoided by employing an alternative sequence whereby the line impedance is calculated only when a disturbance is detected in the voltage or current. This fault-initiated processing relies for the initial disturbance detection on comparing voltage samples to corresponding samples in the preceding cycle, and searching for cases when successive comparisons reveal differences that are in excess of a tolerance [11,12] .

The high degree of stability needed in the disturbance detection logic, together with the lack of continuous impedance monitoring, render fault-initiated processing more suitable for fault classification and location algorithms [43] . Its adaptation in digital hardware or small processor relays, totally devoted to relaying one end of a line, offers no overall advantage over continuous processing, even at 16 and 32 s/c when the latter form of processing requires an additional shift register.

4.2 THE DISCRETE FOURIER TRANSFORM FILTER

The frequency response of the scheme is now examined by the study of the digital filter implementation. In Figure 4.2, the outputs of the two non-recursive structures with orthogonal impulse responses are combined to form the phasor representation of the 50 Hz component. The analysis of each structure on its own can present no difficulty, and is easily obtained by employing the Z-transform [25,34]. However, the combined structure cannot be described in an equally simple manner, and will require extending the Z-transform approach.

4.2.1 The Cosine and Sine Filters

The first of the two filters defined by Equations (4.3) and (4.4) has coefficients that are equal to the samples of a cosinusoid covering one cycle of its variation, with its frequency being that of the 50 Hz fundamental. This filter is thus referred to as the cosine filter. Similarly, the structure of Equation (4.4) with its coefficients given by samples of a sinusoid of the same fundamental frequency, is referred to as the sine filter.

The frequency responses of the linear time-invariant cosine and sine filters are found through the formation of their transfer functions, such functions being identical to the Z-transforms of the impulse responses [46]. For the cosine filter, thus, taking the Z-transform of both sides of Equation (4.3) gives:

$$\sum_{m=0}^{\infty} A(mT).z^{-m} = \sum_{n=0}^{\infty}\left(\sum_{p=0}^{N-1} f((m-p)T).\cos(\Omega(p+\ell)T)\right).z^{-m}$$

$$= \sum_{p=0}^{N-1} \cos(\Omega(p+\ell)T).\sum_{m=0}^{\infty} f((m-p)T).z^{-m}$$

or $$A(z) = \sum_{p=0}^{N-1} \cos(\Omega(p+\ell)T).F(z).z^{-p} \qquad (4.7)$$

which, when expressed as the ratio of the transform of the output to that of the input, becomes:

$$H_c(z) = \sum_{p=0}^{N-1} \cos(\Omega(p+\ell)T).z^{-p}$$

$$= \frac{(1-z^{-N})(\cos\gamma - z^{-1}.\cos(\gamma - x))}{1 - 2.z^{-1}.\cos x + z^{-2}} \qquad (4.8a)$$

$$= \frac{(1-z^{-N})}{2}\left(\frac{\exp(j\gamma)}{1-z^{-1}.\exp(jx)} + \frac{\exp(-j\gamma)}{1-z^{-1}.\exp(-jx)}\right) \qquad (4.8b)$$

where $$x = \Omega T \qquad (4.8c)$$

and $$\gamma = \Omega\ell T \qquad (4.8d)$$

Similarly, the transfer function of the sine filter is:

$$H_s(z) = \frac{(1-z^{-N})(\sin\gamma - z^{-1}.\sin(\gamma - x))}{1 - 2z^{-1}.\cos x + z^{-2}} \qquad (4.9a)$$

$$= \frac{(1-z^{-N})}{2j}\left(\frac{\exp(j\gamma)}{1-z^{-1}.\exp(jx)} - \frac{\exp(-j\gamma)}{1-z^{-1}.\exp(-jx)}\right) \qquad (4.9b)$$

The substitution $\exp(-j\omega T)$ for z^{-1} is now used in the transfer functions. For the cosine filter, this gives:

$$|H_c(e^{j\omega T})| = \frac{\left|\sin(\frac{\omega NT}{2})\right|}{|\cos(\omega T)-\cos x|}\sqrt{(\cos\gamma - \cos(\omega T).\cos(\gamma - x))^2 + (\sin(\omega T).\cos(\gamma - x))^2} \qquad (4.10a)$$

and $$\theta_c(\omega) = -\omega T\left(\frac{N}{2} - 1\right) + \frac{\pi}{2} + \arctan\left(\frac{\sin(\omega T).\cos(\gamma - x)}{\cos\gamma - \cos(\omega T).\cos(\gamma - x)}\right) \qquad (4.10b)$$

where $$H_c(e^{j\omega T}) = \pm\left|H_c(e^{j\omega T})\right|.\exp(j.\theta_c(\omega)) \qquad (4.10c)$$

and, for the sine filter:

$$|H_s(e^{j\omega T})| = \frac{|\sin(\frac{\omega NT}{2})|}{|\cos(\omega T)-\cos x|}\sqrt{(\sin\gamma-\cos(\omega T).\sin(\gamma-x))^2+(\sin(\omega T).\sin(\gamma-x))^2} \qquad (4.11a)$$

and

$$\theta_s(\omega) = -\omega T(\frac{N}{2}-1)+\frac{\pi}{2}+\arctan(\frac{\sin(\omega T).\sin(\gamma-x)}{\sin\gamma-\cos(\omega T).\sin(\gamma-x)}) \qquad (4.11b)$$

Inspection of Equations (4.10a) and (4.11a) above reveals that both frequency responses contain a $\frac{\sin(\frac{N\alpha}{2})}{\cos\alpha-K}$ term. This is accounted for by the presence, in the transfer functions, of a comb filter $(1-z^{-N})$ and two conjugate complex digital resonators $\frac{\exp(j\gamma)}{1-z^{-1}.\exp(jx)}$ and $\frac{\exp(j\gamma)}{1-z^{-1}.\exp(-jx)}$. These resonators combine to form a real cosine or sine resonator, which, together with the comb filter, produce the cosine and sine filters that are in fact no more than an elemental frequency sampling filter [46].

Recursive realisations of the cosine and sine filters are therefore possible. A cosine resonator, for example, can either be realised as two parallel recursive conjugate first order complex resonators [34], or as two cascaded sections as in Figure 4.5. This recursive realisation may seem advantageous in the reduction it offers in the number of multipliers that would otherwise be needed for the non-recursive realisation of Figure 4.2. However, this is achieved at the expense of a few extra delays, and will only be of significant importance for very large values of N, where a large number of multiplications would still be needed in the algorithm even after the symmetry of the impulse response is exploited along the lines explored in Section 4.1.

It is also known that stability considerations in resonators impose the use of damping constants [46], in the resonator loops, to

prevent errors of various constants from giving rise to instability. This brings to light the significant fact that a stray pulse in the resonator input can give rise to an infinitely long cosinusoidal or sinusoidal error component. This component can only be made to decay, and relatively slowly, by critical damping. These factors combined make recursive realisation unattractive.

A sketch of the frequency responses of the cosine and sine filters is shown in Figure 4.6(b). The comb filter has N zeros that are uniformly spaced along the unit circle in the z-plane, as in Figure 4.6(a). Two of these zeros are coincident with the poles of the real resonator, and are thus cancelled. This gives a non-zero magnitude of N/2 for the frequency response at these points.

The effect of γ, the additional phase in the impulse responses, is now examined. The filters should ideally transmit 50 Hz signals only, and have zero gains at all other frequencies. Differentiation of the magnitudes of the frequency responses shows that there exists a value of γ, for each filter, that minimises the magnitude of its response for all frequencies below 50 Hz. This value would seem optimum, since it results in the highest possible suppression of the dc and subharmonics, except that it also simultaneously maximises the response below 50 Hz for the other filter, and the response above 50 Hz for the filter itself. As for the areas under the responses, the value of γ that minimises such area for one filter maximises it for the other. Thus, no optimum value of γ emerges, and it is taken as zero.

The magnitudes of the frequency responses, $|H_c(e^{j\omega T})|$ and $|H_s(e^{j\omega T})|$, are now plotted with 4, 8, 16 and 32 s/c. Figures 4.7 to 4.10 depict these responses, normalised at 50 Hz, and with a 5 Hz

frequency increment. They are all characterised by total dc and harmonic suppression up to their respective folding frequencies, and they all exhibit suppression of non-harmonics to an extent that increases with the sampling rate.

4.2.2 The Combined Filter

The linearity and time-invariance that characterised the cosine and sine filters no longer apply when these two filters are combined to form the DFT filter. The magnitude and phase of the fundamental component are now directly outputted, as shown in the model system of Figure 4.11. This model will be used to examine the filtering operation that each signal, voltage and current, undergoes. While it was pointed out in Section 4.1 that the outputs of the individual cosine and sine filters could directly determine the impedance, analysis along these lines is avoided because of the complexity involved.

The DFT filter is linear insofar as the principle of superposition is applicable. The cosine and sine filters' outputs, resulting from various frequencies in the input, would in fact be the sums of the individual outputs for one of the input frequencies at a time. When one frequency is present at the input, an increase in its amplitude will give a proportional increase in the magnitude output of the filter.

The presence of a non-harmonic, however, gives a contribution at the output that is interpreted as a fundamental component. In this respect, nonlinearity comes into being. More importantly, the magnitude output for a non-harmonic input depends on both the amplitude and phase of such input, and the filter is thus time varying. This is

illustrated in Figure 4.12, where the normalised magnitude of the fundamental component in an 8-point DFT is seen to vary with the phase of the 70 Hz signal used.

A conventional frequency description of the DFT filter cannot therefore be formulated. However, since all inputs are interpreted as fundamental components in the magnitude output, and since the faithful reproduction of the 50 Hz in a composite input would be ideal, then the error associated with such reproduction, and introduced by the non-harmonics in the input, could be used as a criterion. We therefore aim at a frequency plot that would display the levels of attenuation that non-harmonics undergo before appearing as contributions to the fundamental component in the magnitude output.

The time-varying nature of the filter means that for each non-harmonic input there will exist a phase shift giving rise to the worst case of least attenuation, or highest transmission. Such phase and transmission could be found through the direct differentiation of the magnitude of the DFT fundamental component for a particular non-harmonic, as obtained from Equations (4.3) and (4.4). However, an alternative approach based on the cosine and sine filters frequency responses, as already obtained, is opted for.

Remembering that the cosine and sine filters are both linear, and time-invariant, their individual outputs for a cosinusoidal input with a phase, $A.\cos(\omega_o nT + \phi)$, would in fact be cosinusoids of the same frequency ω_o and with additional phase shift:

$$O_c(nT) = A.\left|H_c(e^{j\omega_o T})\right|.\cos(\omega_o nT + \phi + \theta_c(\omega_o)) \qquad (4.12)$$

and

$$O_s(nT) = A.\left|H_s(e^{j\omega_o T})\right|.\cos(\omega_o nT + \phi + \theta_s(\omega_o)) \qquad (4.13)$$

which, when combined for a magnitude, yield:

$$\sqrt{[0_c(nT)]^2 + [0_s(nT)]^2} =$$

$$= A.\sqrt{|H_c(e^{j\omega_o T})|^2.\cos^2(\omega_o nT+\phi+\theta_c(\omega_o))+|H_s(e^{j\omega_o T})|^2.\cos^2(\omega_o nT+\phi+\theta_s(\omega_o))} \quad (4.14)$$

This magnitude is now divided by the amplitude A, of the input signal, to give the transmission:

$$|H_{cs}(e^{j\omega_o T})| =$$

$$= \sqrt{|H_c(e^{j\omega_o T})|^2.\cos^2(\omega_o nT+\phi+\theta_c(\omega_o))+|H_s(e^{j\omega_o T})|^2.\cos^2(\omega_o nT+\phi+\theta_s(\omega_o))} \quad (4.15)$$

The first derivative with respect to $(\omega_o nT + \phi)$ of the transmission of Equation (4.15) above can now be formed and equated to zero. One of the two resulting total phases gives the maximum transmission when substituted back into Equation (4.15). The procedure is identical to that when an input signal of the form $A.\cos(\omega_o t)$ is chosen, but the argument $(\omega_o nT + \phi)$ is used to illustrate the fact that the phase corresponding to maximum transmission should not necessarily be an integer multiple of $\omega_o T$ simply because a sampled data system is at hand.

Maximum transmissions, calculated at frequency intervals of 5 Hz, are shown labelled as 'worst combined responses' in Figures 4.7 to 4.10 for 4, 8, 16 and 32 s/c respectively. They are seen to be quite similar to the cosine and sine responses, except in the immediate vicinities of 50 Hz, where their normalised magnitudes are greater than unity as a result of non-linearity.

At the fundamental and all the harmonics the DFT filter exhibits linearity and time-invariance. This is explained by the phases

and magnitudes of the frequency responses of the cosine and sine filters at these frequencies. For the fundamental, for example, we have from Equations (4.10) and (4.11):

$$H_c(e^{j\Omega T}) = \frac{N}{2}.\exp(j.0) \qquad (4.16a)$$

and

$$H_s(e^{j\Omega T}) = \frac{N}{2}.\exp(-j.\frac{\pi}{2}) \qquad (4.16b)$$

giving a transmission:

$$\left|H_{cs}(e^{j\Omega T})\right| = \sqrt{(N/2)^2.\cos^2(\Omega nT+\phi)+(N/2)^2.\cos^2(\Omega nT+\phi-\pi/2)}$$
$$= N/2 \qquad (4.17)$$

which is independent of the input phase. Also, transmission at all the harmonics can be proved to be zero, and this is all in accordance with the properties of the DFT as discussed in Chapter 2.

Formulation of the frequency response of the DFT filter through the conventional Z-transform approach would not be valid. It may be argued that the system of Figure 4.11 could be represented by a complex Z-transform with its real and imaginary parts defined by the transfer functions of the cosine and sine filters respectively, and with the frequency response then obtained by substituting $\exp(-j\omega T)$ for z^{-1}. However, it is to be remembered that an imaginary transfer function can only describe an imaginary system with an imaginary impulse response, and that such impulse response is employed in the calculation of the output of the DFT filter, as in Equation (4.2b), merely because this calculation is simplified when complex arithmetics are used. In the real Fourier series, for example, both the cosine and sine components are real, and the appearance of the operator j in the time domain in the DFT is not to be confused with j that describes quadrature in the frequency domain.

The worst combined responses for different sampling rates all seem to have zero transmission at dc. This is significant in view of the likelihood of the presence of dc components in fault transients, as discussed in Chapter 3. However, the attenuation of the non-harmonics is unacceptably low, at least with 4 and 8 s/c. This cannot be further discussed at this stage, as the introduction of an initial analogue lowpass filter is expected to modify the frequency responses in a manner that will warrant a separate study, and this is left to Chapter 6.

4.3 TIME DOMAIN PERFORMANCE

The abrupt change in the line impedance that accompanies a fault takes some time to manifest itself as changes in the voltage and current phasor representations obtained from the filters. Fault detection times therefore depend on the speed at which these changes are transmitted through the filters, and the time performance of the protection scheme is now roughly assessed with such concept as a criterion.

4.3.1 Transient Delay

A transient change in the input of a non-recursive digital filter, with (N-1) delays, is not fully felt in its output until NT seconds later, after the first post-transient sample has travelled along the whole of the transversal structure. Some effect, however, would be transmitted to the output immediately after the transient change occurs, and would increase with time as more post-transient data appear in the delay line, as in Figure 4.13.

It is thus taken that the transient delay of the filter be defined as NT/2 seconds, this being the time that elapses before the midpoint of the output charge is reached. This approach, which only applies to non-recursive filters, borrows from passive analogue filter theory, where the step delay is defined as the time required for the output to reach half its steady-state value, with a unit step input [47].

4.3.2 Estimation of Fault Detection Times

The time that elapses between fault incidence and its detection is equal to the transient delay of the filters which the protection scheme employs, plus a processing cycle. To this can also be added one sampling interval, to account for the case when a sampling instant falls immediately before the occurrence of the fault. The total is therefore slightly over the transient delay value of 10 msec., since the processing cycle and sampling interval amount to no more than a few milliseconds, at least with 8, 16 and 32 s/c.

For faults near the receiving end of the line, however, the impedance trajectory, as calculated from the voltage and current phasors, will not cross the relaying characteristic until probably all the contents of the shift register are postfault. The exact time required will in fact depend on both the position of the fault on the line and on the prefault load impedance Z_R, this being very nearly the impedance that the relay initially sees, as will be proved in Chapter 8.

A practical case, where the load impedance Z_R is three times as large as the series impedance Z_d of the full length of the line, is shown in Figure 4.14. With the impedance trajectory assumed to be travelling at a constant rate from Z_R to Z_L, crossing the relaying

characteristic on, or in the vicinity of, its top boundary, the fault detection time can range from 13 to 20 msec., depending on the position of the fault on the line.

4.4 CONCLUSION

A protection scheme based on a real-time adaptation of the DFT was described. The scheme involved the separate filtering of the line voltage and current signals, and this filtering action was analysed and shown to be favourable in view of the frequency composition of the signals it is intended to handle.

Estimations of fault detection times revealed, however, that such times could run into the fundamental cycle duration mark, thereby reducing the competitiveness of the scheme against the very fast relaying target aimed at.

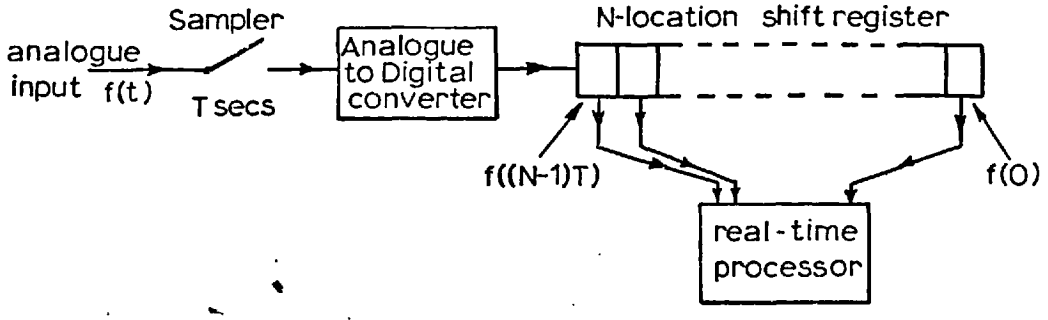

Fig. 4·1 Processor implementation of DFT coefficient calculator

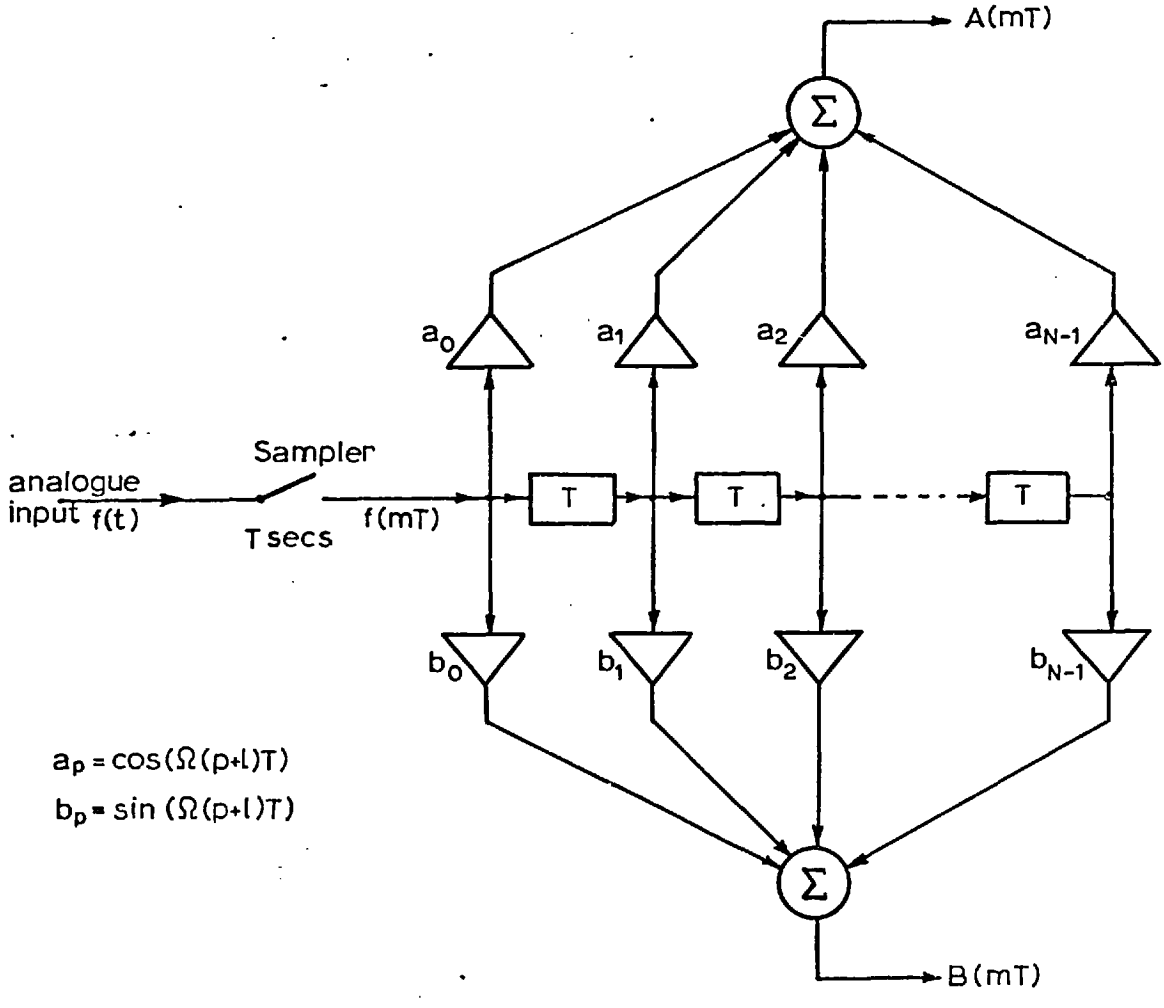

Fig. 4·2 Nonrecursive digital filter implementation

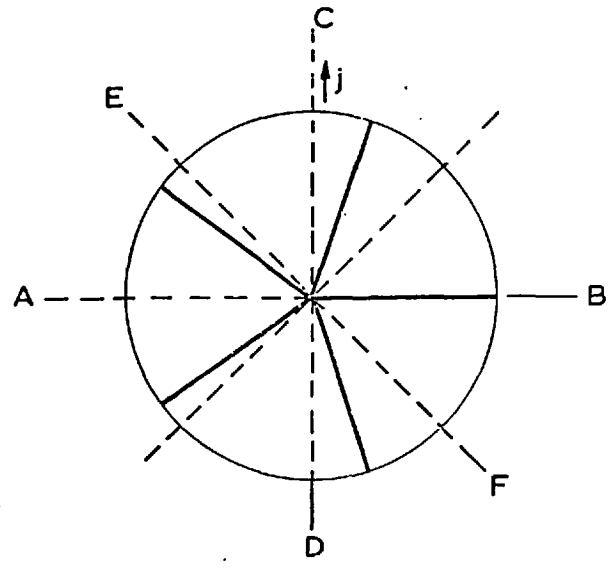

Fig. 4·3 Possible values of the rotating phasor exp (jΩpT) with N=5

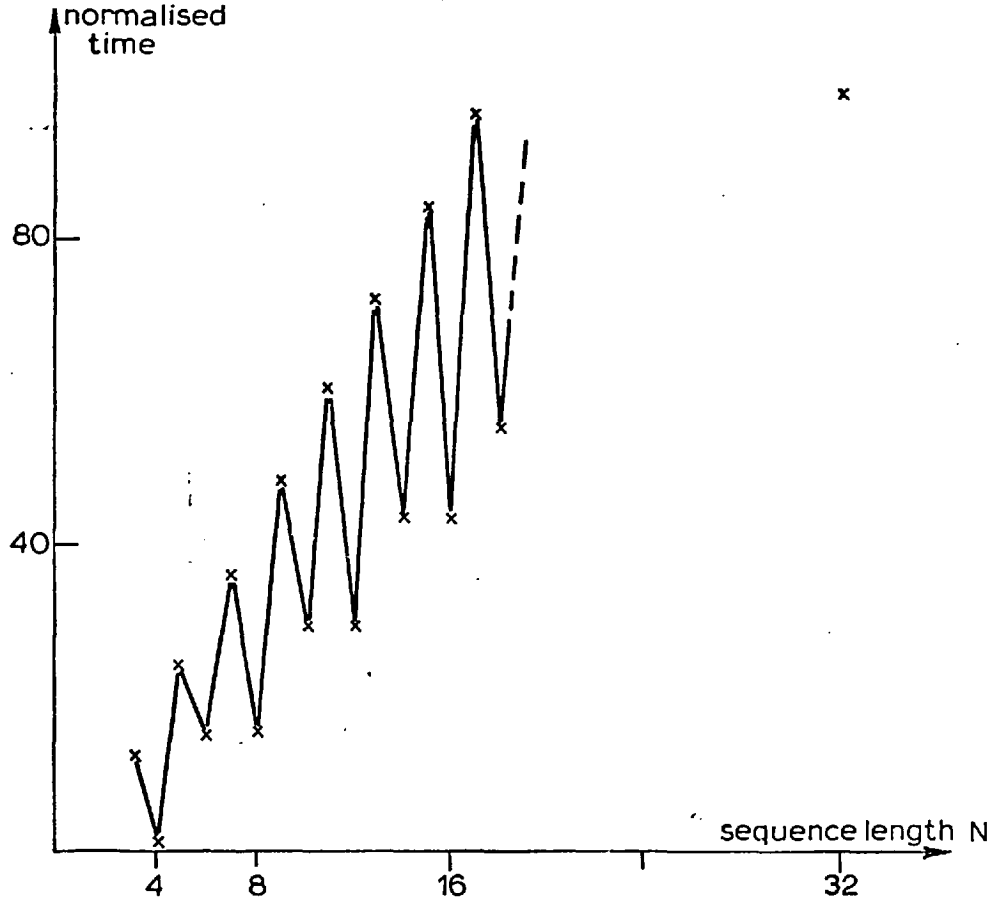

Fig. 4·4 Variation of coefficient calculation time with sequence length

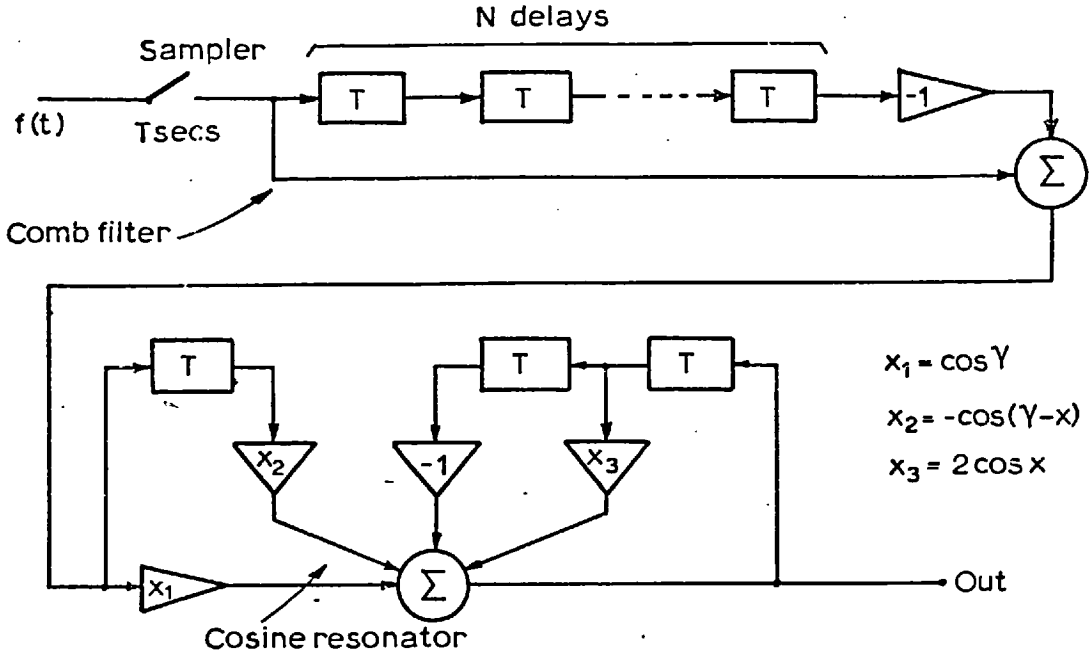

Fig. 4·5 Cascade realisation of the comb filter and the recursive cosine resonator

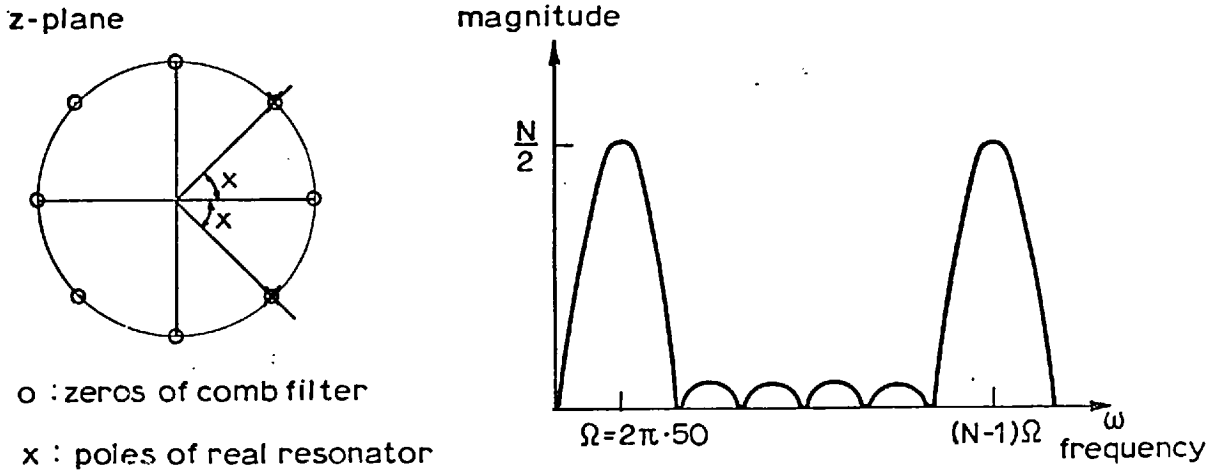

(a) Pole-zero interpretation for N=8

(b) Sketch of amplitude response

Fig. 4·6 The pole-zero pattern and a sketch of the frequency response of the cosine and sine filters.

FULL CYCLE METHOD
4 SAMPLES PER CYCLE

AMPLITUDES OF FREQUENCY RESPONSES

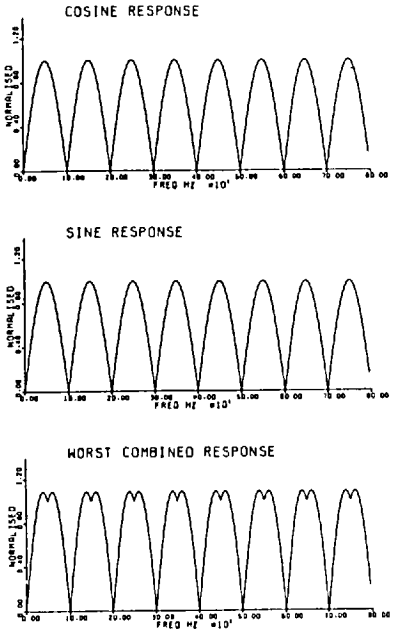

Fig. 4·7

FULL CYCLE METHOD
8 SAMPLES PER CYCLE

AMPLITUDES OF FREQUENCY RESPONSES

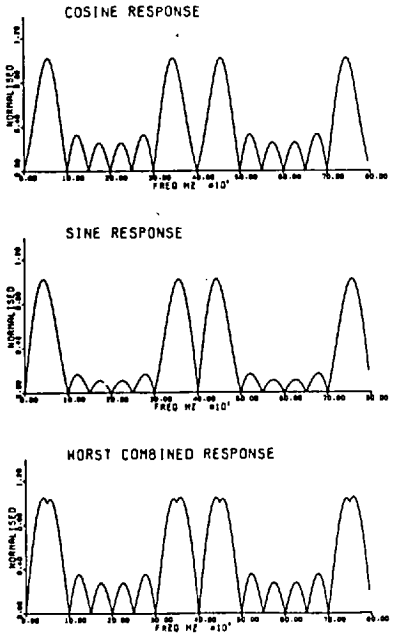

Fig. 4·8

FULL CYCLE METHOD
16 SAMPLES PER CYCLE

AMPLITUDES OF FREQUENCY RESPONSES

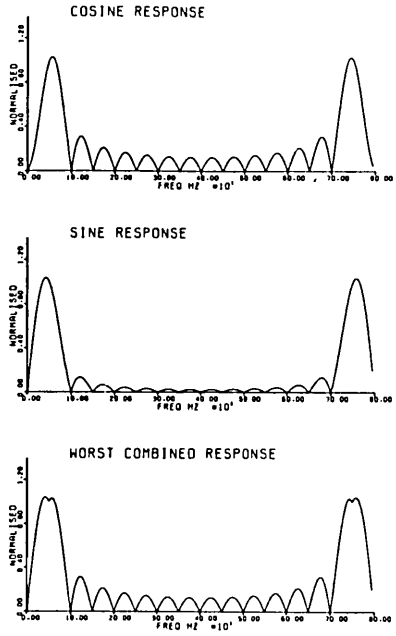

Fig. 4·9

FULL CYCLE METHOD
32 SAMPLES PER CYCLE

AMPLITUDES OF FREQUENCY RESPONSES

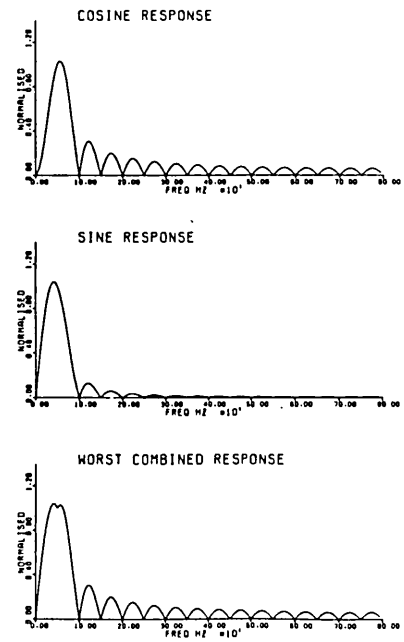

Fig. 4·10

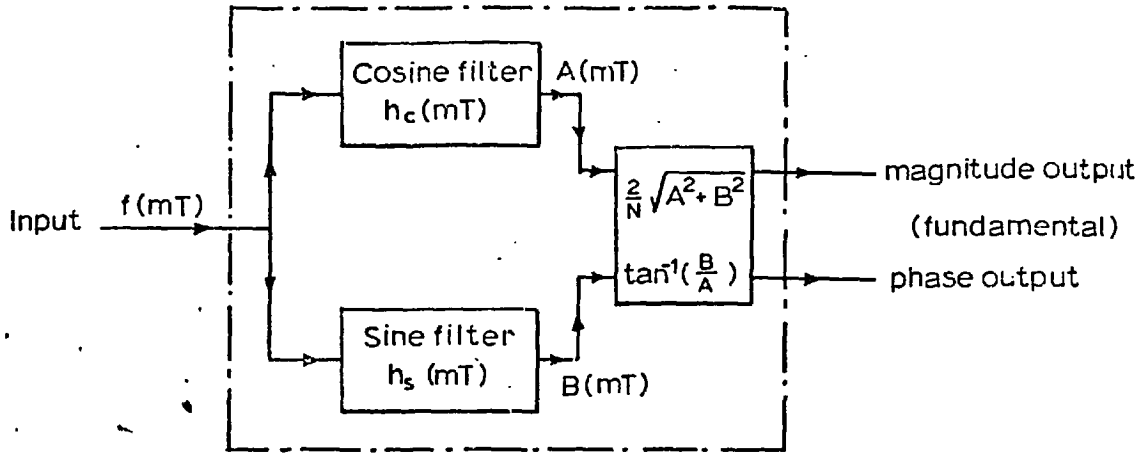

Fig. 4·11 The combined (DFT) filter

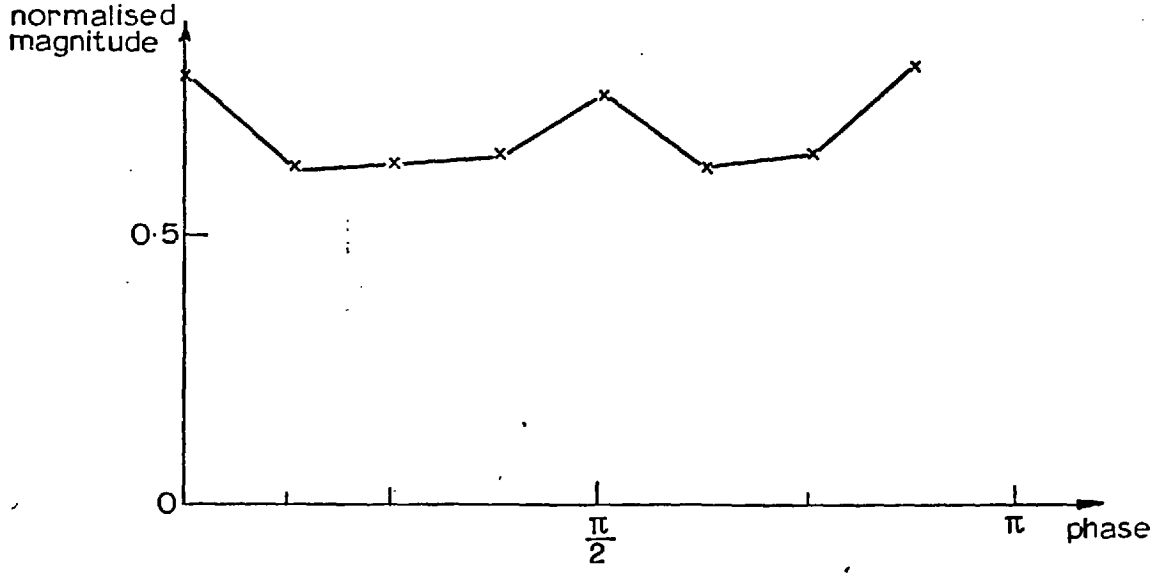

Fig. 4·12 Variation of fundamental component in the DFT of a 70 Hz waveform with phase.

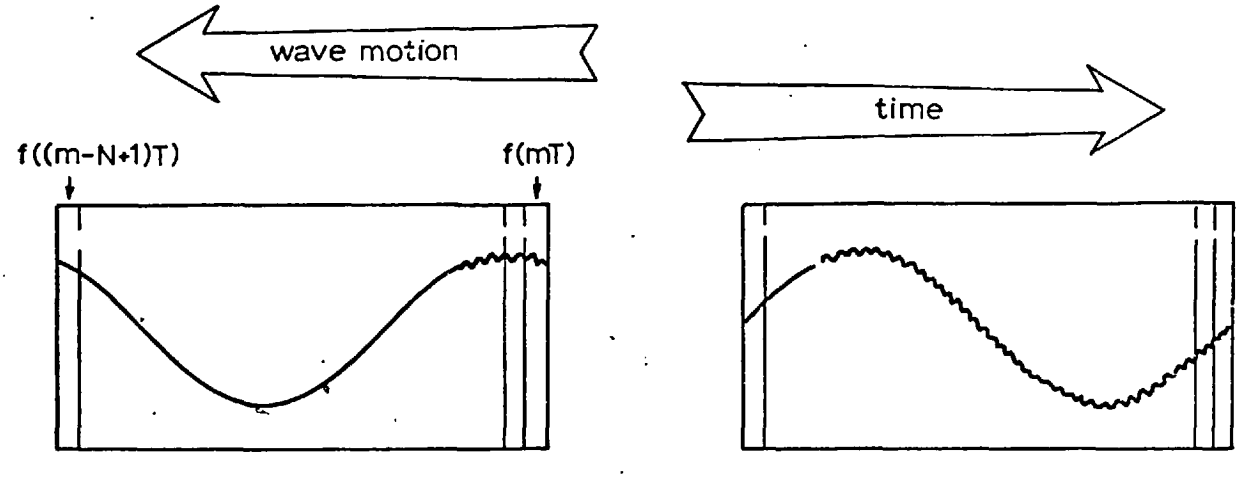

(a) A few milliseconds after fault (b) Almost 20 msec after fault

Post fault data shown zigzagged

Fig. 4·13 Contents of delay line after fault incidence

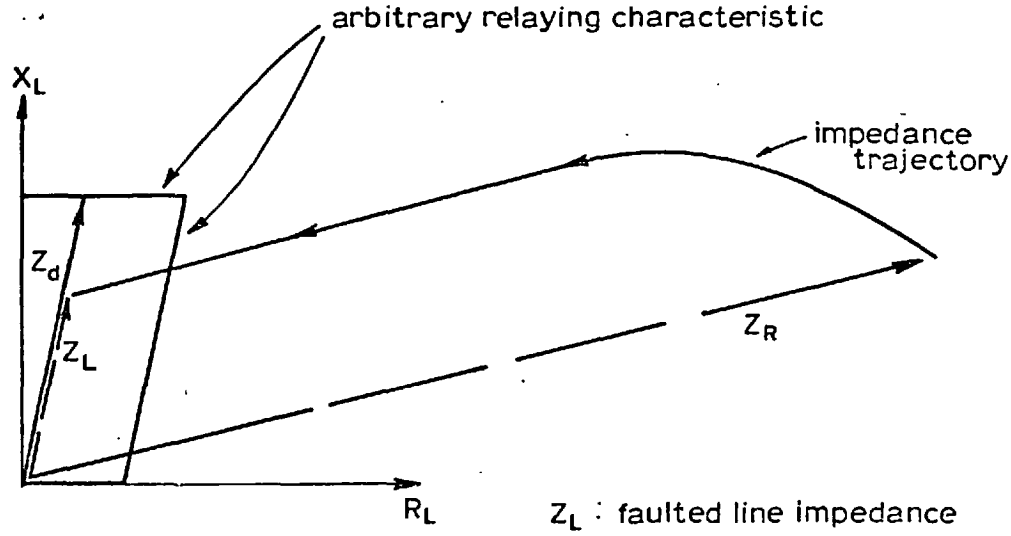

Z_L : faulted line impedance

Z_d : series impedance of full length of line

Z_R : load impedance

Fig. 4·14 Faulted line impedance trajectory in relation to the relaying characteristic

CHAPTER 5

PREDICTIVE METHODS: PROTECTION SCHEME II

A real-time protection scheme based on the Discrete Fourier Transform was described in Chapter 4. The scheme was shown to be capable of satisfactorily filtering the 50 Hz component from the transmission line fault voltages and currents by utilising samples of these quantities covering 20 msec. However, this meant that faults near the receiving end of the line would probably not be detected by the scheme until about 20 msec. after fault incidence, since detection in such cases required wholly postfault data.

A search for a phasor determination algorithm that requires less postfault data was therefore instigated. This led to the development of a few methods that are described in here and that require shorter data sequences than those needed in the full cycle method. The methods all involve the prediction of the full cycle data sequence from the knowledge of only a few of its samples, and they consequently result in modifications in the DFT.

This chapter first presents a simple study of some intrinsic geometric properties of the sampled cosinusoidal oscillation. The study reveals that the complete definition of the oscillation over its entire period can be formed from a number of its samples covering only a fraction of the period. This is then followed by the design of the predictive methods, and the derivation of their modified DFT's. The method most suitable for a protection scheme is then determined, and its frequency response and fault detection times are finally obtained and assessed.

5.1 DATA SEQUENCES WITH REDUNCANCIES

Phasor determination in the full cycle method of Chapter 4 involved N data samples that covered one fundamental cycle duration. With healthy voltages and currents, containing no other frequency than the 50 Hz, some of this data can be shown to be redundant,

This involves sequence completion operations that must first be defined.

5.1.1 Repetition and Replication

The data sequence lengths that correspond to the sampling rates adopted in the protection scheme of Chapter 4 are 4, 8, 16 and 32. In the definitions that follow, therefore, N is assumed even, with the discrete variable n that specifies the samples f(nT) ranging from 0 to (N-1).

A sequence of length N defined over its first half, or its first N/2 samples only, can be completed by positively repeating this first half, thereby giving a second half defined by:

$$f(nT) = f((n - \frac{N}{2})T), \qquad \frac{N}{2} \leqslant n \leqslant N-1 \tag{5.1}$$

or, alternatively, it can be compleyed by negatively repeating the first half according to:

$$f(nT) = -f((n - \frac{N}{2})T), \qquad \frac{N}{2} \leqslant n \leqslant N-1 \tag{5.2}$$

When the $(\frac{N}{2} + 1)^{th}$ sample of the incomplete sequence is also known, there become possible two other completion procedures. The defined portion of the sequence is of length $(\frac{N}{2} + 1)$ now, and it can

be positively replicated, or mirror-imaged, to form an even completed sequence of length N with its last $(\frac{N}{2} - 1)$ samples given by:

$$f(nT) = f((N-n)T), \qquad \frac{N}{2} < n \leq N-1 \qquad (5.3)$$

or, it can be negatively replicated forming an odd sequence according to:

$$f(nT) = -f((N-n)T), \qquad \frac{N}{2} < n \leq N-1 \qquad (5.4a)$$

The point about which the sequence is replicated thus corresponds to the $(\frac{N}{2} + 1)^{th}$ sample, this sample being the first in the second half of the sequence. This leaves the first sample f(0) unreplicated, and the infinite repetition of the completed sequence is therefore non-overlapping, as is required in the sample representation of a periodic signal.

A set of conditions emerges for odd sequences from the definition of Equation (5.4a), since for $n = \frac{N}{2}$ we have:

$$f(\tfrac{N}{2}T) = -f(\tfrac{N}{2}T)$$

and consequently,

$$f(\tfrac{N}{2}T) = 0 \qquad (5.4b)$$

Similarly, for n = 0, and with the requirement of the periodic repetition of the completed sequence being odd about the first sample in the sequence, we have:

$$f(0) = 0 \qquad (5.4c)$$

Examples of repeated and replicated sequences are shown in Figure 5.1. The given first half of the sequence of Figure 5.1(a) is

negatively repeated after its last sample S_ℓ, while the completed sequence of Figure 5.1(b) is formed by positively replicating the first half about the sample S_h. The first half itself is seen to be the result of negatively replicating the first quarter about the sample S_q, with the first and fifth samples consequently taken to be zero as required by Equations (5.4b) and (5.4c). This illustrates that more than one replication operation is possible for each sequence completion, with the whole completed sequence being even or odd depending on the sign of the replication that is carried out about the $(\frac{N}{2}+1)^{th}$ sample.

5.1.2 Defining the Fundamental Cosinusoid

A cosinusoid can in theory be defined over one full cycle from the knowledge of its variation over the first quarter of the cycle only. This quarter can then be negatively replicated to form the first half, which in turn produces the full cycle when either positively replicated or negatively repeated. With a sampled cosinusoid, the validity of such completion requires that sampling be synchronised in the peaks and zeros of the variation.

The set of the first few samples of a cosinusoid that is shifted in phase, however, will only contain all the samples of the desired quarter-cycle variation if the samples of this set cover a time interval that is longer, by a specific amount, than quarter of the period of the cosinusoid. This time interval, referred to as the width of the minimum defining window, will depend on the initial phase shift ϕ_{cv} of the cosinusoid, as is illustrated in Figure 5.2. The dependence is in fact cyclic, and is shown in Figure 5.3 for the full 2π phase range.

The limits of the minimum defining window widths are thus quarter of and half the period. These limits form the bases of the data completion procedures that will now be employed in a number of phasor determination algorithms.

5.2 THE MODIFIED DISCRETE FOURIER TRANSFORMS

The sequence completion procedures discussed in Section 5.1 are now used, in a manner suggested by the observations of the cosinusoid recorded above, to obtain completed sequences for the input of the DFT. The use of such sequences will in fact result in a number of modified DFT calculation algorithms.

A few phasor determination methods are discussed below, each corresponding to a particular sequence completion philosophy. It will be shown that there exist some limitations as to the validity of each method, mainly because the data sequences to be studied must be assumed to contain dc and harmonics, as well as the 50 Hz, if they are to resemble real fault data sequences.

5.2.1 The Half-Cycle Repetition Method

In this method the first N/2 samples of the sequence, covering half a cycle duration of the fundamental 50 Hz, are assumed known, and are repeated to form the last N/2. In Figure 5.4, it is seen that negative repetition correctly reproduces the second half of the sequence when the fundamental and odd harmonics only are present, with the dc and even harmonics requiring positive repetition in turn. In both cases, synchronised sampling is not necessary.

Negative repetition is to be employed, since the fundamental is of prime interest. The second half of the sequence is thus defined by Equation (5.2) as:

$$f(nT) = -f((n - \tfrac{N}{2})T), \qquad \tfrac{N}{2} \leqslant n \leqslant N-1$$

and remembering that the fundamental component in the DFT was given by Equation (4.1) as:

$$F(\Omega) = \sum_{n=0}^{N-1} f(nT).\exp(-j\Omega nT)$$

this component becomes:

$$* F_{hrn}(\Omega) = \sum_{n=0}^{\frac{N}{2}-1} f(nT).\exp(-j\Omega nT) + \sum_{n=\frac{N}{2}}^{N-1} -f((n-\tfrac{N}{2})T).\exp(-j\Omega nT)$$

which, by the change of variable $\ell = n - N/2$ and the substitution $\frac{\Omega NT}{2} = \pi$ in the second summation, reduces to:

$$F_{hrn}(\Omega) = 2.\sum_{n=0}^{\frac{N}{2}-1} f(nT).\exp(-j\Omega nT) \qquad (5.5)$$

It can readily be proved that negative repetition gives a DFT that is zero at the dc and all even harmonics. Similarly, positive repetition gives no spectral components at the fundamental and odd harmonics. Negative repetition thus forms a discontinuous completed sequence if dc and even harmonics are present, translating their presence to contributions to the fundamental and odd harmonics and thereby rendering the component of Equation (5.5) incorrect. However, what matters here is to recognise that negative repetition makes it

---

* See List of Abbreviations at the beginning of the thesis for explanation of the subscript notation.

possible to obtain a fundamental component from a data sequence that covers only half a cycle duration, with no specific need for synchronised sampling.

5.2.2 The Half-Cycle Replication Method

The knowledge of the $(\frac{N}{2}+1)^{th}$ sample of the sequence, as well as the first N/2 samples, makes its completion by replication possible. The rest of the sequence is now defined, as in Equations (5.3) and (5.4a), by:

$$f(nT) = \mp f((N-n)T), \qquad \frac{N}{2} < n \leqslant N-1$$

so that the fundamental component, as given by the DFT, becomes:

$$F_{ht}(\Omega) = \sum_{n=0}^{N/2} f(nT).\exp(-j\Omega nT) \pm \sum_{n=\frac{N}{2}+1}^{N-1} f((N-n)T).\exp(-j\Omega nT)$$

and the change of variable $\ell = N-n$ in the second summation above simplifies this component to:

$$F_{ht}(\Omega) = \sum_{n=0}^{N/2} f(nT).\exp(-j\Omega nT) \pm \sum_{n=1}^{\frac{N}{2}-1} f(nT).\exp(j\Omega nT)$$

$$= \left|f(nT).\exp(-j\Omega nT)\right|_{n=0} + \sum_{n=1}^{\frac{N}{2}-1} f(nT).\exp(-j\Omega nT)$$

$$+ \left|f(nT).\exp(-j\Omega nT)\right|_{n=\frac{N}{2}} \pm \sum_{n=1}^{\frac{N}{2}-1} f(nT).\exp(-j\Omega nT)$$

$$= \left[f(0)-f(\tfrac{N}{2}T)\right] + \sum_{n=1}^{\frac{N}{2}-1} f(nT).\left[\exp(-j\Omega nT) \pm \exp(j\Omega nT)\right]$$

which, for positive replication, is all real:

$$F_{htp}(\Omega) = \left[f(0)-f(\tfrac{N}{2}T)\right] + 2.\sum_{n=1}^{\frac{N}{2}-1} f(nT).\cos(\Omega nT) \qquad (5.6)$$

and, for negative replication, is complex:

$$F_{htn}(\Omega) = \left[f(0)-f(\tfrac{N}{2}T)\right] -2j.\sum_{n=1}^{\frac{N}{2}-1} f(nT).\sin(\Omega nT) \qquad (5.7a)$$

Positive replication thus gives a real fundamental component. This is expected, since the completed data sequence is now even, giving an all real transform as is known from basic DFT theory [34] . However, with negative replication, the completed sequence is odd only when the first and $(\frac{N}{2} + 1)^{th}$ samples are taken as zeros, as explained in Section 5.1. The fundamental component of Equation (5.7a) of the negatively replicated sequence then reduces to the imaginary value:

$$F_{htn}(\Omega) = -2j.\sum_{n=1}^{\frac{N}{2}-1} f(nT).\sin(\Omega nT) \qquad (5.7b)$$

While repetition was shown to correctly complete data sequences that contained one group of frequencies only: dc and even harmonics or the fundamental and odd harmonics, different restrictions apply to replication. As can be seen in Figure 5.5, replication forms a correct completed sequence that contains both the fundamental and dc, and this in fact applies to all odd and even harmonics too. However, each frequency present must have a phase that is either zero or an integer multiple of $\pi/2$, and this necessitates synchronised sampling in turn.

Positive replication should therefore be used for frequencies with a zero or π phase shift, while negative replication would

similarly cater for the fundamental and all harmonics when their phases are equal to $\pi/2$ or $3\pi/2$. However, it will not correctly complete a sequence containing dc, since the phase of the latter can only be taken as zero, when it is positive, or π when it is negative. This explains the use of the second harmonic in place of the dc for illustrating the cases of the $\pi/2$ phase in Figure 5.5.

5.2.3 The Quarter-Cycle Method

The sequence in this method is constructed from the knowledge of its first $(\frac{N}{4}+1)$ samples. These samples are replicated to form the second quarter of the sequence, since, for the fundamental and all harmonic cosinusoids with a phase of zero or a multiple of $\pi/2$, the first half of the sequence will either be even or odd about the $(\frac{N}{4}+1)^{th}$ sample. The first half is then replicated to form the second half, and this replication could be replaced by repetition because of the nature of construction of this first half itself.

The two replication signs that are now needed: s_1 in completing the first half; and s_2 in obtaining the whole sequence, yield four different sign combinations. These combinations are used in the four completion cases that are illustrated in Figure 5.6, where it is seen that all cases require synchronised sampling and phase synchronisation as with half-cycle replication. Also, each case allows the presence of one group of frequencies only: the fundamental and odd harmonics or the dc and even harmonics. Every case, in fact, imposes the combined requirements of half-cycle repetition, with a sign that is the product of s_1 and s_2, and half-cycle replication with a sign s_2. When such requirements are not met, the completed sequence

is incorrect, as is shown in Figure 5.7, which illustrates the use of all the sign combinations for completing a quarter-sequence that satisfies only case (a) of Figure 5.6.

As with half-cycle replication, the use of the first $(\frac{N}{2}+1)$ samples of the sequence for completely defining it simplifies the DFT fundamental coefficient to:

$$F_{qtt}(\Omega) = [f(0)-f(\tfrac{N}{2}T)] + \sum_{n=1}^{\frac{N}{2}-1} f(nT).\,[\exp(-j\Omega nT)+s_2.\exp(j\Omega nT)]$$

But since replication is also applied in forming the first half, the first and $(\frac{N}{2}+1)^{th}$ samples are thus related by:

$$f(\tfrac{N}{2}T) = s_1.f(0)$$

while $$f(nT) = s_1.f((\tfrac{N}{2}-n)T), \qquad \tfrac{N}{4} < n \leqslant \tfrac{N}{2}-1$$

making it possible to write the summation above as:

$$\sum_{n=1}^{\frac{N}{2}-1} f(nT).\,[\exp(-j\Omega nT)+s_2.\exp(j\Omega nT)] =$$

$$= \sum_{n=1}^{\frac{N}{4}-1} f(nT).\,[\exp(-j\Omega nT)+s_2.\exp(j\Omega nT)] +$$

$$+ \left| f(nT).\,[\exp(-j\Omega nT)+s_2.\exp(j\Omega nT)] \right|_{n=\frac{N}{4}}$$

$$+ s_1.\sum_{n=\frac{N}{4}+1}^{\frac{N}{2}-1} f((\tfrac{N}{2}-n)T).\,[\exp(-j\Omega nT)+s_2.\exp(j\Omega nT)]$$

and this, when simplified by the change of variable $\ell = \frac{N}{2} - n$ in its second summation term, and substituted back into the expression for the fundamental component, gives for that component:

$$F_{qtt}(\Omega) = f(0) - s_1.f(0) + \left[\exp(-j\frac{\pi}{2}) + s_2.\exp(j\frac{\pi}{2})\right].f(\frac{N}{4}T) + \sum_{n=1}^{\frac{N}{4}-1} f(nT).\left[\exp(-j\Omega nT) + s_2.\exp(j\Omega nT) - s_1.\exp(j\Omega nT) - s_1.s_2.\exp(-j\Omega nT)\right] \quad (5.8)$$

The DFT coefficient at the fundamental frequency, as given by Equation (5.8) above, is now evaluated for the four possible sign combinations.

(a) s_1 -ve, s_2 +ve:

This combination is suitable for correctly completing a sequence that contains the fundamental frequency and its odd harmonics, each with a phase shift that is either zero or π. The fundamental component is:

$$F_{qtt}(\Omega) = 2.f(0) + 4.\sum_{n=1}^{\frac{N}{4}-1} f(nT).\cos(\Omega nT) \quad (5.9a)$$

(b) s_1 +ve, s_2 -ve:

Correctly completes sequences that contain the fundamental and odd harmonics again, but having phases that are $\pi/2$ or $3\pi/2$. The fundamental component now is:

$$F_{qtt}(\Omega) = -2j.f(\frac{N}{4}T) - 4j.\sum_{n=1}^{\frac{N}{4}-1} f(nT).\sin(\Omega nT) \quad (5.9b)$$

(c) s_1 +ve, s_2 +ve:

To be used with positive and negative dc, and with even harmonics having phases that are zero or π. It gives a fundamental

component of:

$$F_{qtt}(\Omega) = 0 \qquad (5.9c)$$

(d) $\underline{s_1 \text{ -ve, } s_2 \text{ -ve:}}$

Suitable for use with even harmonics with phases of $\pi/2$ and $3\pi/2$. The fundamental component is again given by:

$$F_{qtt}(\Omega) = 0 \qquad (5.9d)$$

The negative replication applied to the first quarter in case (d) above compelled taking $f(\frac{N}{4}T)$ to be zero in obtaining Equation (5.9d). This is in accordance with Equation (5.4b) which is also applicable to the negative replication that is applied to the first half, making $f(\frac{N}{2}T)$ zero, which in turn sets $f(0)$ to zero. This last condition was also used in obtaining Equation (5.9d).

Of the four quarter-cycle completion cases discussed above, cases (a) and (b) only are useful since (c) and (d) do not cater for the fundamental and give zero DFT fundamental coefficients. However, the presence of dc and even harmonics would still be undesirable in cases (a) and (b), since it would then introduce errors in the fundamental component as given by Equations (5.9a) and (5.9b).

5.2.4 Implementation and Data Interpretation Considerations

The different phasor determination methods are now assessed in view of the restrictions they place on data, and by their interpretation of some data that would not lie within such restrictions. This will help in eliminating the unsuitable methods,

thereby making possible the determination of the method that is most compatible with the data sequences expected to be encountered.

A scheme that employs replication would require synchronised sampling of waveforms with specific phases, and it would give magnitude information only of the voltage and current signals. Such scheme would offer very little versatility, since synchronised sampling of both the voltage and current may be impossible. This is because the initial phase difference between the two signals is determined by the load impedance and line constants, and will not necessarily be an integer multiple of the phase increment between successive samples at the particular sampling rate being employed.

Assuming, however, that sampling and phase requirements could initially be met, then abrupt changes in the voltage and current phases that could be brought about by a fault would cause loss of synchronisation and would thus render the initial requirements unsatisfied. Replication would then give wrong magnitude information and no phase information at a time when this is vitally important for correct relaying.

It may be argued that the phase of a signal could always be obtained by employing both positive and negative replication simultaneously in the half-cycle method, for example. This would yield two components, one real and the other imaginary, that, according to Equations (5.6) and (5.7b), are given by:

$$F_{htp}(\Omega) = \left[f(0)-f(\tfrac{N}{2}T)\right] + 2.\sum_{n=1}^{\frac{N}{2}-1} f(nT).\cos(\Omega nT)$$

and

$$F_{htn}(\Omega) = -2j.\sum_{n=1}^{\frac{N}{2}-1} f(nT).\sin(\Omega nT)$$

However, these components are in fact almost identical to those which would be obtained from half-cycle negative repetition which, according to Equation (5.5), gives:

$$F_{hrn}(\Omega) = 2.\sum_{n=0}^{\frac{N}{2}-1} f(nT).\exp(-j\Omega nT)$$

$$= 2.f(0)+2.\sum_{n=1}^{\frac{N}{2}-1} f(nT).\cos(\Omega nT)-2j.\sum_{n=0}^{\frac{N}{2}-1} f(nT).\sin(\Omega nT)$$

This similarity is accounted for by the fact that the sequences formed by negative and positive replication add up to a sequence with samples that are twice those of the initial incomplete sequence over the defined first half, and that are zero over the second half, as is illustrated in Figure 5.8. The combined negative and positive replication components would therefore equal the fundamental component of the doubled first half of the sequence, which is mathematically identical to the fundamental component of the sequence when the latter is completed by negative repetition as is apparent from Equation (5.5). It appears, therefore, that the simultaneous use of both positive and negative replication is equivalent to negative repetition in the half-cycle methods.

The same requirements of synchronised sampling and phase apply to the quarter-cycle method also. Some phase information, after synchronisation is lost, could now be obtained by calculating both the real components of case (a) and the imaginary component of case (b) of the quarter-cycle method. Adding the sequence completed in accordance with the replication sign combinations of the two cases, however, would now give a negatively repeated discontinuous

sequence that is interspaced with intervals of zeros, as shown in Figure 5.9. The fundamental component of this can thus be found from its first half, in fact first quarter, and it can readily be proved to be equal to the fundamental component of the defined first quarter when this is quadrupled.

The above observation is consistent with the expressions that were obtained for the fundamental components of sequences that are completed by the quarter-cycle method. We have, from Equations (5.9a) and (5.9b), for cases (a) and (b):

$$F_{qtt}(\Omega) = 2.f(0) + 4.\sum_{n=1}^{\frac{N}{4}-1} f(nT).\cos(\Omega\, nT)$$

and

$$F_{qtt}(\Omega) = -2j.f(\tfrac{N}{4}T) - 4j.\sum_{n=1}^{\frac{N}{4}-1} f(nT).\sin(\Omega\, nT)$$

while the fundamental component of the quadrupled first quarter is almost identical, being:

$$4.\sum_{n=0}^{\frac{N}{4}-1} f(nT).\exp(-j\Omega nT) = 4.f(0) + 4.\sum_{n=1}^{\frac{N}{4}-1} f(nT).\cos(\Omega\, nT) - 4j.\sum_{n=1}^{\frac{N}{4}-1} f(nT).\sin(\Omega\, nT) \quad (5.10)$$

However, the sequence completion procedure that yields this component cannot correctly complete a sequence representing any frequency with any phase, and the use of the quarter-cycle method is thus ruled out.

5.3 PERFORMANCE OF PREDICTIVE SCHEME

The half-cycle negative repetition method emerged as the most easily implementable and meaningful of all the predictive methods presented. It is now adopted as the basis of a protection scheme that is basically the same as that described in Chapter 4, the main difference being in the use of N/2 samples only, rather than N samples, for the phasor determinations.

In the full cycle method of Chapter 4, the fundamental component-calculating equation, Equation (4.2a), was written in a non-recursive digital filter form as:

$$F_m(\Omega) = \sum_{p=0}^{N-1} f((m-p)T).\exp(j\Omega pT)$$

and the application of negative repetition now makes it possible to define the latest half of the data sequence from the earliest N/2 samples.

The underlying requirements of incorporating as much post-fault data as possible in the sequence, and as soon after fault incidence as possible, however, compel the use of the latest N/2 samples for defining the earlier half of the sequence. This gives a completed sequence that makes the fault appear older, and it results in a more accurate phasor estimation. Such switching in the completion procedure can be proved to be causing no change in the filtering performance of the method, as it simply results in a reduced transient delay of the corresponding digital filter.

Thus, defining the older half of the sequence by negatively repeating the latest half modifies the fundamental component to:

$$F_h(\Omega) = \sum_{p=0}^{\frac{N}{2}-1} f((m-p)T).\exp(j\Omega pT) - \sum_{n=\frac{N}{n}}^{N-1} f((m-p+\frac{N}{2})T).\exp(j\Omega nT)$$

which, by the change of variable $\ell = p - N/2$ in the second summation, reduces to:

$$F_h(\Omega) = 2.\sum_{p=0}^{\frac{N}{2}-1} f((m-p)T).\exp(j\Omega nT) \qquad (5.11)$$

and this can be implemented as two transversal digital filters [46] defined by:

$$A_h(mT) = 2.\sum_{p=0}^{\frac{N}{2}-1} f((m-p)T).\cos(\Omega nT) \qquad (5.12)$$

and

$$B_h(mT) = 2.\sum_{p=0}^{\frac{N}{2}-1} f((m-p)T).\sin(\Omega pT) \qquad (5.13)$$

These filters are similar to the cosine and sine filters of Equations (4.3) and (4.4) of the full cycle method, and are therefore to be referred to by the same nomenclature.

The sampling rates to be adopted in the predictive scheme are 4, 8, 16 and 32 s/c, as with the full cycle scheme, since considerations that determined these rates there also apply here. The corresponding processing cycle durations are now 1.01 msec., 1.13 msec., 1.37 msec. and 1.85 msec., and they thus differ very slightly from the processing cycle durations of the full cycle scheme. This is because simplifications in coefficient calculation resulting from phasor symmetry were explored to the full in the full cycle scheme, with the half-cycle data symmetry allowing relatively little further simplification.

5.3.1 Frequency Response

The frequency response of the scheme is found by forming the transfer functions of the linear time-invariant cosine and sine filters, and combining the respective responses in a manner similar to that used for the full cycle method. For the cosine filter, the transfer function is:

$$H_{hc}(z) = \frac{2(1 + z^{-\frac{N}{2}})(1 - z^{-1}.\cos x)}{1 - 2.z^{-1}.\cos x + z^{-2}} \qquad (5.14a)$$

$$= (1 + z^{-N/2}).\left(\frac{1}{1-z^{-1}.\exp(jx)} + \frac{1}{1 - z^{-1}.\exp(-jx)}\right) \qquad (5.14b)$$

where $x = \Omega T$ (5.14c)

while for the sine filter it is:

$$H_{hs}(z) = \frac{2(1+z^{-N/2})(z^{-1}.\sin x)}{1 - 2.z^{-1}.\cos x + z^{-2}} \qquad (5.15a)$$

$$= \frac{(1+z^{-N/2})}{j}\left(\frac{1}{1-z^{-1}.\exp(jx)} - \frac{1}{1-z^{-1}.\exp(-jx)}\right) \qquad (5.15b)$$

and the frequency responses are thus:

$$\left|H_{he}(e^{j\omega t})\right| = \frac{2.\left|\cos(\frac{\omega NT}{4})\right|}{\left|\cos(\omega T)-\cos x\right|} .\sqrt{1-2.\cos(\omega T).\cos x+\cos^2 x} \qquad (5.16a)$$

and $$\theta_{hc}(\omega) = -\omega T(\frac{N}{4} - 1)+\arctan(\frac{\sin(\omega T).\cos x}{1 - \cos(\omega T).\cos x}) \qquad (5.16b)$$

while $$\left|H_{hs}(e^{j\omega T})\right| = \frac{2.\left|\cos(\frac{\omega NT}{4})\right|}{\left|\cos(\omega T) - \cos x\right|} . \left|\sin x\right| \qquad (5.17a)$$

and $$\theta_{hs}(\omega) = -\frac{\omega NT}{4} \qquad (5.17b)$$

As with the full cycle methods, both transfer functions contain real resonators, but the comb filter $(1-z^{-N})$ of the full cycle method is now replaced by another filter $(1+z^{-N/2})$. This has N/2 zeros uniformly spaced along the unit circle in the z-plane, but none of these is real. Two of them are again cancelled by the poles of the real resonator, giving nonzero magnitudes at the corresponding frequencies.

The magnitudes of the frequency responses, normalised at 50 Hz, are shown in Figures 5.10 to 5.13 for the different sampling rates. The worst combined responses are obtained as in the full cycle method, and the combined filter involved is again time varying. However, at the fundamental and odd harmonics, the time-invariance disappears and the structure becomes linear. At the fundamental, for example, the frequency responses as from Equations (5.16) and (5.17) would be:

$$H_{hc}(e^{j\omega T}) = \frac{N}{2} \cdot \exp(j.0) \qquad (5.18a)$$

and

$$H_{hs}(e^{j\omega T}) = \frac{N}{2} \cdot \exp(-j.\frac{\pi}{2}) \qquad (5.18b)$$

giving a transmission of:

$$|H_{hcs}(e^{j\omega T})| = \frac{N}{2} \qquad (5.19)$$

and these are the same responses as those obtained in Equations (4.16) and (4.17) for the full cycle method at the fundamental.

The time running outputs of the cosine and sine filters of the full cycle method, and for a 50 Hz input, are thus identical to the corresponding outputs of the half-cycle negative repetition method.

Such outputs are shown in Figure 5.14, and they serve to demonstrate the limitations, relating to phase, that are imposed on half-cycle replication. Half-cycle positive and negative replications were associated with the cosine and sine filters respectively of the half-cycle negative repetition method. This means that positive replication, when used on its own, yields a fundamental component magnitude that is correct only when the input phase is zero or π, or at instants t_1 and t_3 in Figure 5.14. Equally, negative replication gives the correct fundamental magnitude only when the sine filter output is at a peak: instants t_2 and t_4, which now correspond to a $\pi/2$ or $3\pi/2$ phase of the input 50 Hz.

The worst combined responses depicted in Figures 5.10 to 5.13 all show appreciable transmissions at even harmonics. However, the analogue lowpass filter to be used will significantly suppress these frequencies, as well as nonharmonics, and this will be proved in Chapter 6. Alas, an analogue lowpass filter can offer no improvement in the undesirable dc transmission that characterises the cosine and sine responses and the combined responses. In the latter, this transmission is calculated to be 1.414, 1.305, 1.281 and 1.275 of the transmission at 50 Hz for 4, 8, 16 and 32 s/c respectively. It appears therefore that dc transmission approaches a value of 1.2 as the sampling rate increases, with sampling rates above 8 s/c offering no significant improvements in reducing such transmission.

5.3.2 Fault Detection Times

The detection time in the scheme of Chapter 4 was governed mainly by the transient delay of the digital filter. The same concept

is applicable here, since the same sampling rates are being employed, and since the processing cycle durations in the predictive method differ very little from those in the full cycle method.

The transient delay of the half-cycle method is a mere 5 msec., and fault detection times would therefore probably average just over this. For faults near the end of the line, however, detection times could be as long as 10 msec., with the presence of dc in the line voltage and current giving rise to inaccurate phasor estimates that could delay fault detection even further.

The capacity of the half-cycle method for increasing the proportion of postfault information in data sequences, during the 20 msec. that immediately follow fault incidence, is demonstrated in Figure 5.15. The figure illustrates how the method 'extrapolates' the little available postfault data for redefining some earlier data.

5.4 CONCLUSION

Predictive techniques for the completion of partly defined data sequences were devised. One such technique was then used in modifying the full cycle phasor determination method, and a protection scheme giving fault detection times not exceeding 10 msec. consequently evolved.

Investigations of the filtering performance of the scheme revealed, however, that it was characterised by large dc transmission, thereby severely restricting the scope of faults that it could successfully handle.

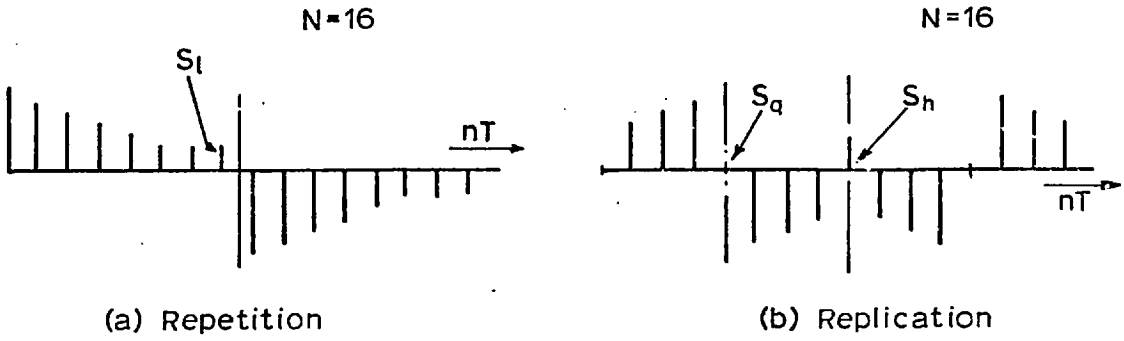

Fig. 5·1 Sequence completion by repetition and replication.

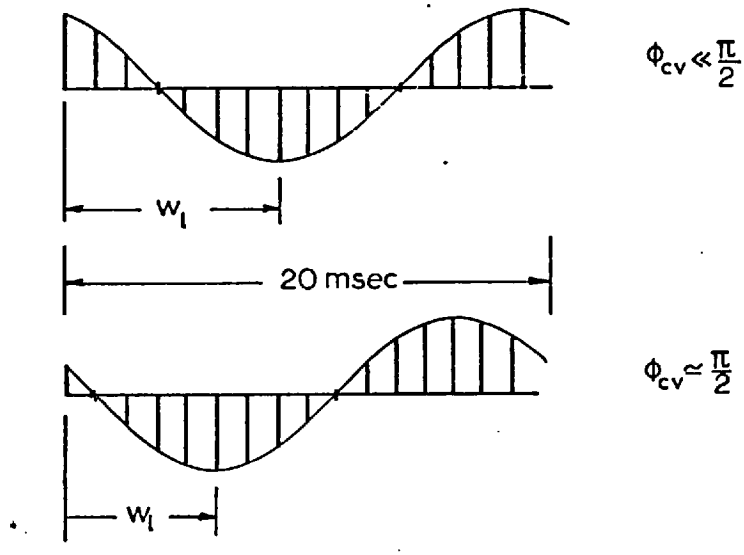

Fig. 5·2 Minimum defining window of the 50 Hz waveform.

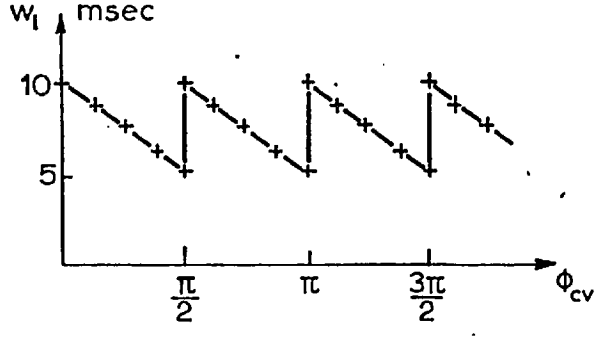

Fig. 5·3 Variation of the defining window duration with phase shift.

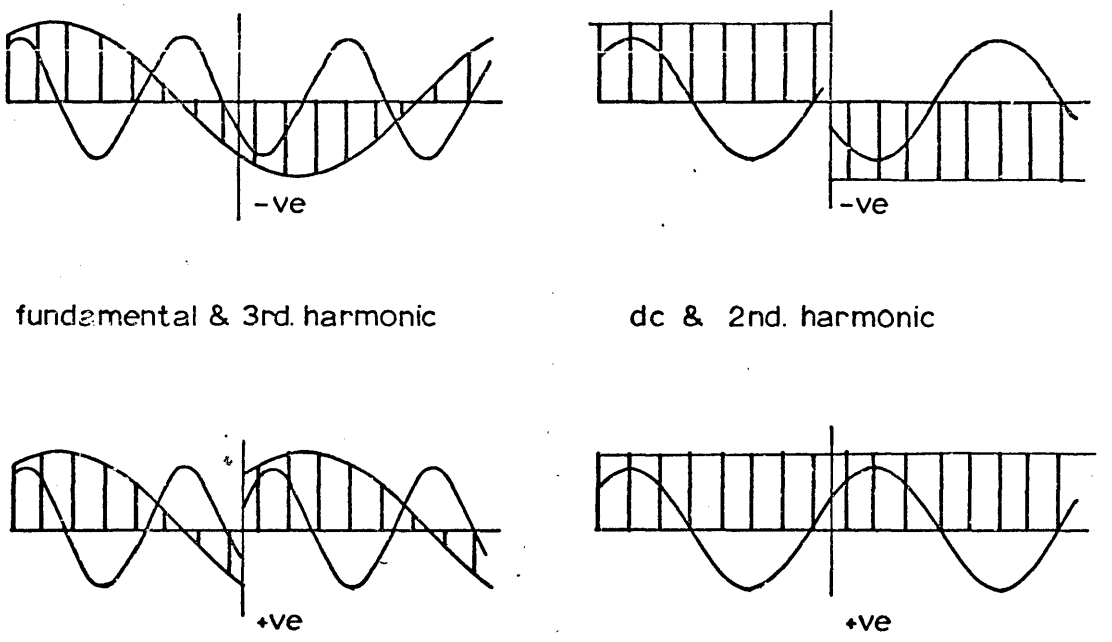

Fig. 5·4 Half-cycle repetition

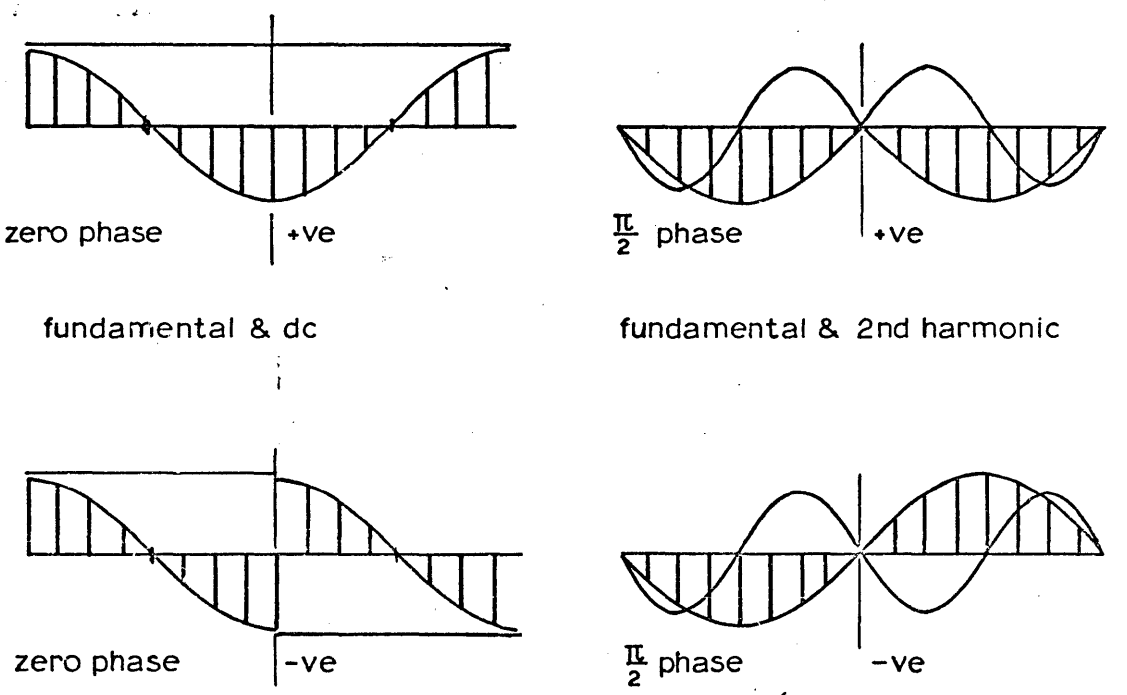

Fig. 5·5 Half-cycle replication

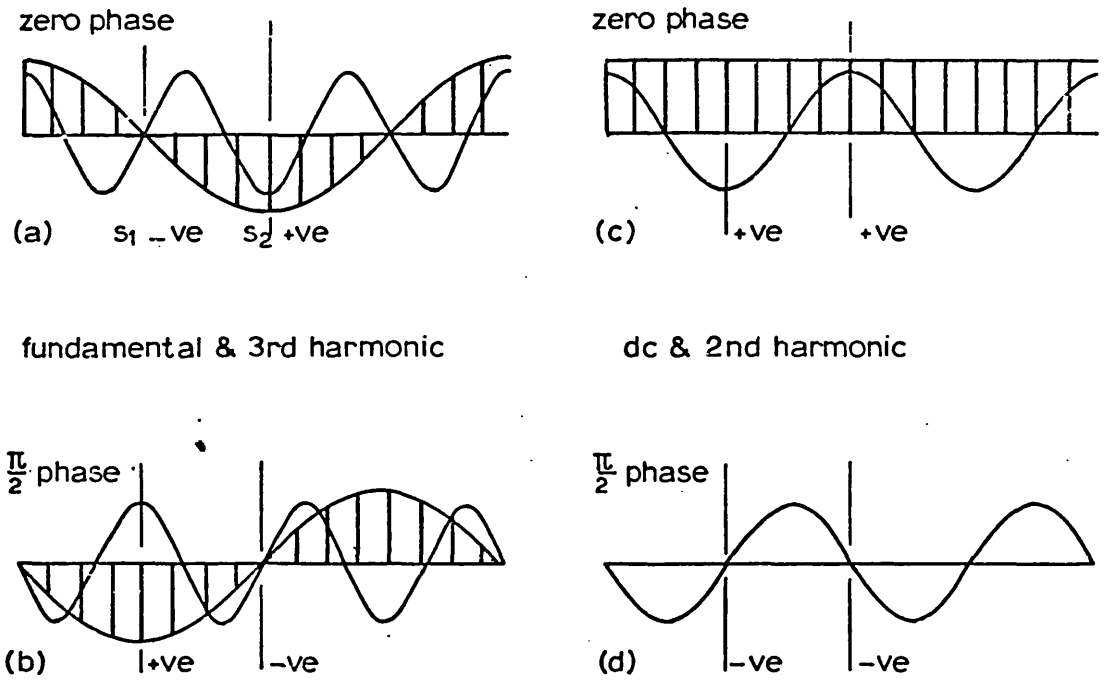

Fig. 5·6 Quarter-cycle sequence completion.

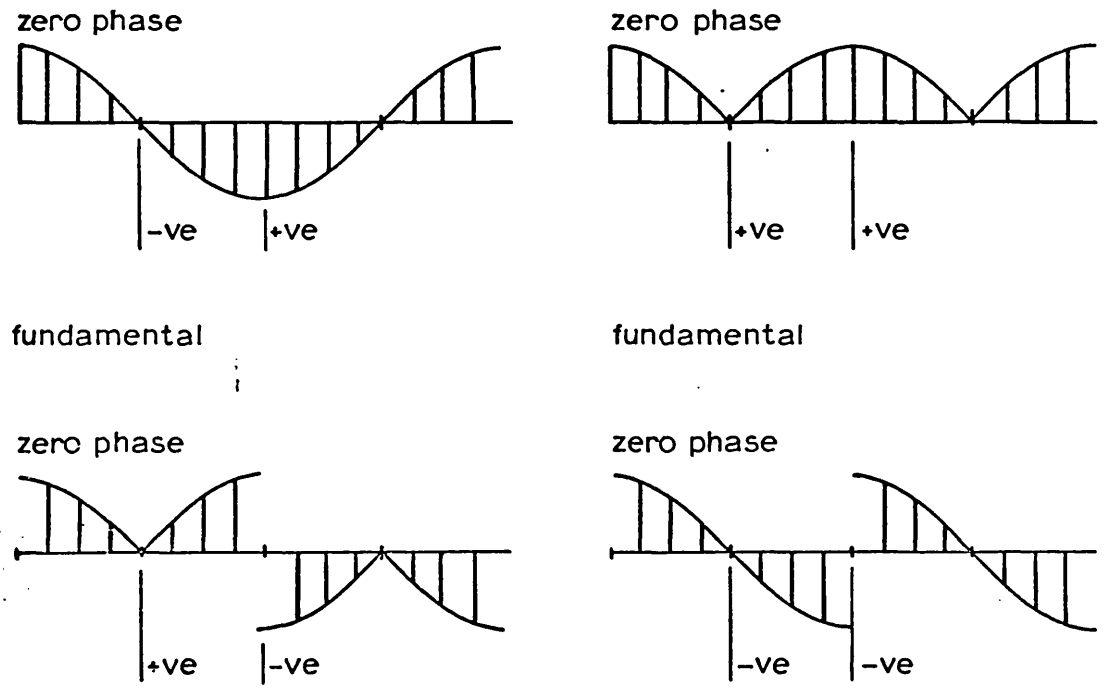

Fig. 5·7 Correct and incorrect completions by quarter-cycle method.

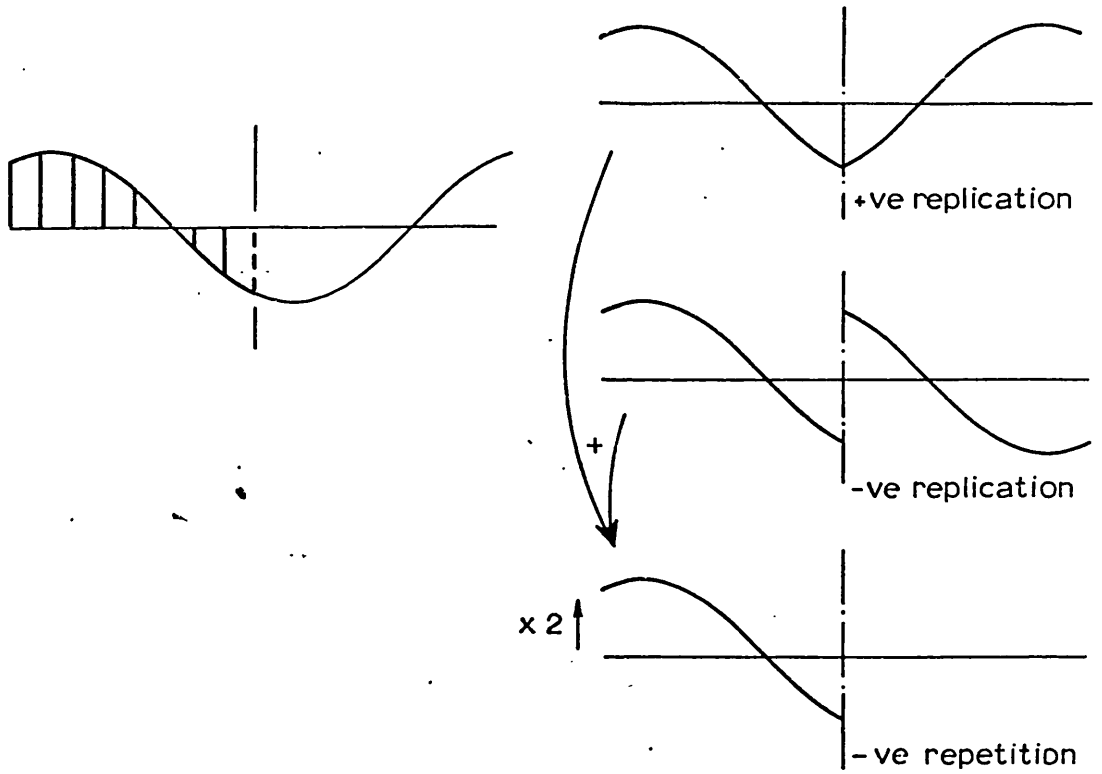

Fig. 5·8 Comparison of the half-cycle methods.

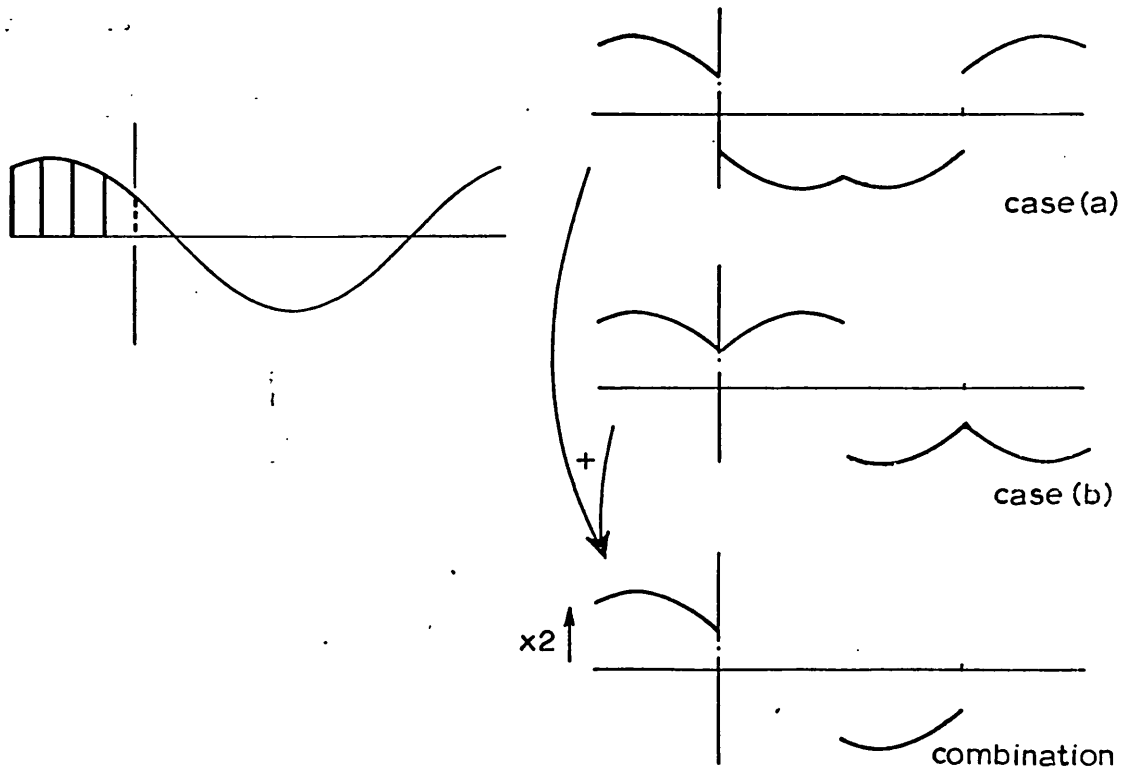

Fig. 5·9 Interpretation of the quarter-cycle method.

HALF CYCLE NEGATIVE REPETITION METHOD
4 SAMPLES PER CYCLE

AMPLITUDES OF FREQUENCY RESPONSES

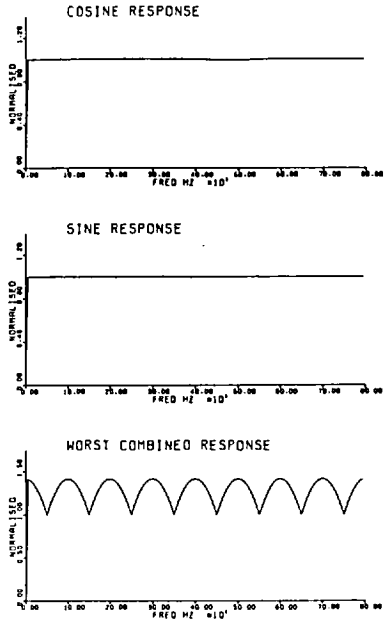

Fig. 5·10

HALF CYCLE NEGATIVE REPETITION METHOD
8 SAMPLES PER CYCLE

AMPLITUDES OF FREQUENCY RESPONSES

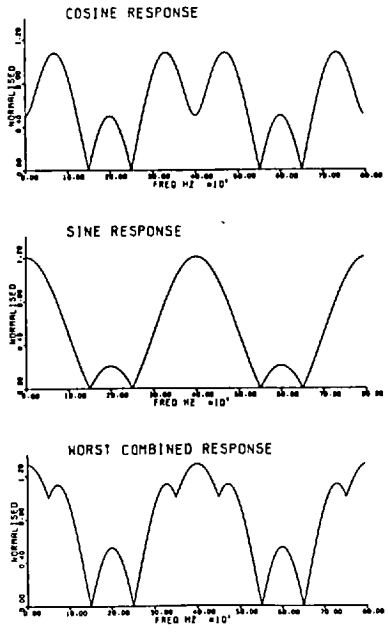

Fig. 5·11

HALF CYCLE NEGATIVE REPETITION METHOD
16 SAMPLES PER CYCLE

AMPLITUDES OF FREQUENCY RESPONSES

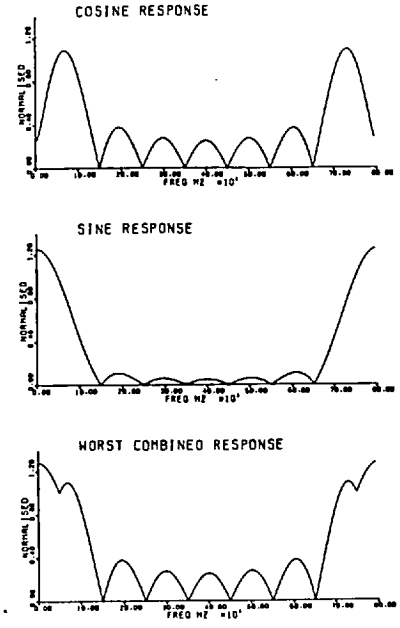

Fig. 5·12

HALF CYCLE NEGATIVE REPETITION METHOD
32 SAMPLES PER CYCLE

AMPLITUDES OF FREQUENCY RESPONSES

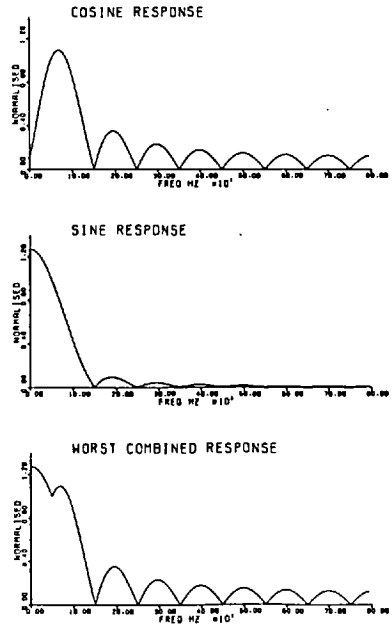

Fig. 5·13

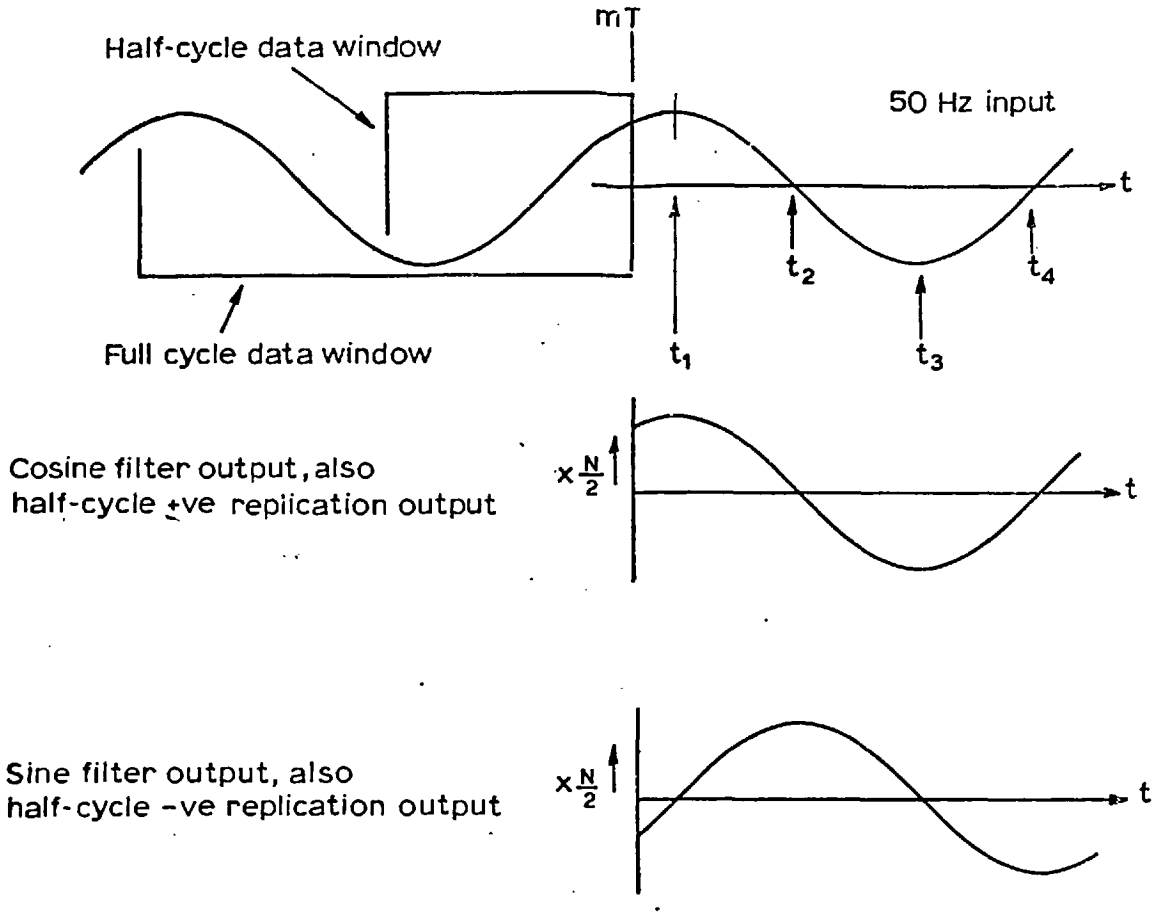

Fig. 5·14 Orthogonal outputs of the cosine and sine filters for a 50 Hz input.

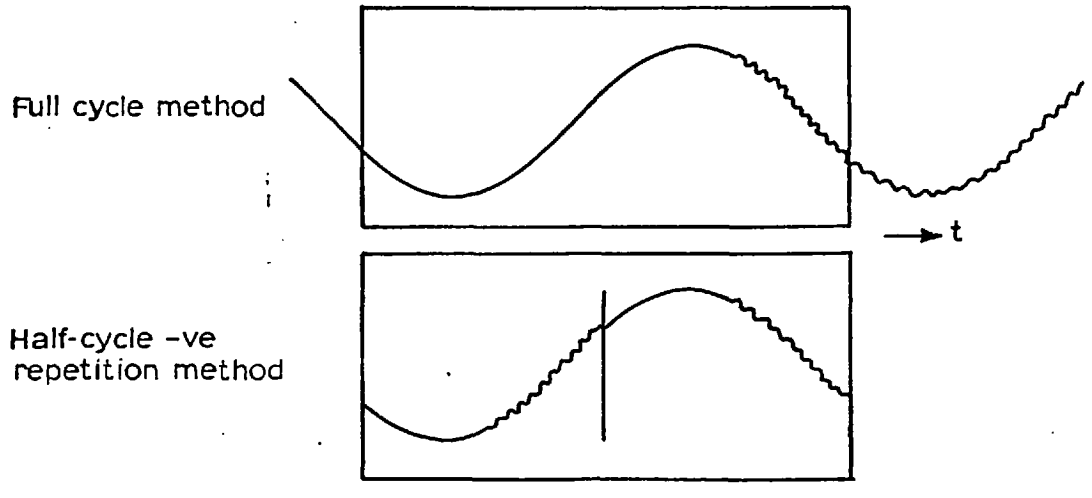

Post fault data shown zig zagged

Fig. 5·15 Original and completed data sequences shown 5 msec after fault incidence

CHAPTER 6

ANALOGUE FILTER CONSIDERATIONS

One interpretation of the Sampling Theorem [26,27,28] is that an analogue signal can only be correctly and retrievably represented by its samples if the sampling rate employed in obtaining these samples is at least twice the highest frequency present in the signal. The low sampling rates, proposed for the protection schemes described in Chapters 4 and 5, are therefore only possible if all high frequencies are first eliminated from the analogue signals by analogue lowpass filters, with each of the suggested rates dictating the use of a different filter.

The lowest of the sampling rates of interest may seem the most logical to adopt, since it involves the least computation time for the phasor determination, and is yet capable of correctly reproducing the 50 Hz component. However, the delay of the respective analogue filter must also be considered, and this modifies the optimum sampling rate, for a particular protection scheme, to that giving the least total time, which includes both the computations and the analogue filter delay. The delay of the digital filters, accounting for their transient behaviour as discussed in Chapter 4, is not to be included, since it is a constant in each of the two protection schemes with any sampling rate.

This chapter describes how a number of different analogue filters are initially chosen to match each of the sampling rates of 4, 8, 16 and 32 s/c. The chapter then gives a review of various definitions of analogue filter delay, and outlines the development of a theory for the simple estimation of this delay. Values obtained by

this theory are next used to reduce the choice of analogue filters to one filter per sampling rate, making the determination of an optimum sampling rate for each protection scheme possible. The frequency responses of the schemes at their optimum rates, and with the analogue filters, are finally derived.

6.1 THE ANALOGUE FILTER PARAMETERS: ALIASING CONSIDERATIONS

The analogue signal, it was stated above, should only be sampled after it has been band-limited by a lowpass analogue filter, as in the arrangement of Figure 6.1. However, practical realisable analogue filters can only approximate the ideal lowpass filters since they only attenuate, rather than eliminate, the high frequencies. Consequently, the least acceptable degree of suppression of the high frequencies must be specified, this depending in general upon the frequency composition of the analogue input signal.

A wideband input signal, having the most high frequency content possible, represents the worst case. The corresponding output of the analogue filter will have a frequency spectrum that is identical to the frequency response of the filter [47], as shown in Figure 6.2(a). When this output is sampled, an infinite number of shifted versions of its spectrum are introduced and superimposed, forming the periodic spectrum depicted in Figure 6.2(b). The magnitude of this spectrum at half the sampling frequency serves as an indication of the extent of aliasing. It must be limited to an arbitrary fraction of the gain at dc if a certain degree of fidelity in the samples representation of the signal is to be guaranteed. Constantinides [48] treated a similar problem in his lowpass digital filter design from analogue

filter characteristics, and here we present a theory developed on the same lines.

Remembering that the sampling frequency is defined in terms of the sampling interval as:

$$\Omega_s = \frac{2\pi}{T} \quad \text{radians/sec.} \tag{6.1}$$

then, from the Sampling Theorem [26,27,28], the magnitude of the frequency response of the sampled filtered wideband signal will be:

$$\left| H_{\ell p}(e^{j\omega T}) \right| \leq \frac{1}{T} \cdot \sum_{r=-\infty}^{\infty} \left| H_{\ell p}(j(\omega + \frac{2\pi}{T} \cdot r)) \right| \tag{6.2}$$

where, in the above, $H_{\ell p}(j\omega)$ is the frequency response of the analogue filter, and the inequality sign is used because of phase considerations. The magnitude of the response of Equation (6.2) at the folding frequency $\frac{\Omega_s}{2}$ is:

$$\left| H_{\ell p}(e^{j\omega T}) \right|_{\omega = \frac{\Omega_s}{2}} \leq \frac{1}{T} \cdot \sum_{r=-\infty}^{\infty} \left| H_{\ell p}(j\tfrac{\pi}{T}(1 + 2r)) \right|$$

$$< \frac{1}{T} \cdot \sum_{r=-\infty}^{-2} \left| H_{\ell p}(j\tfrac{\pi}{T}(1+2r)) \right| + \frac{1}{T} \cdot \left| H_{\ell p}(-j\tfrac{\pi}{T}) \right| + \frac{1}{T} \left| H_{\ell p}(j\tfrac{\pi}{T}) \right| + \frac{1}{T} \cdot \sum_{r=1}^{\infty} \left| H_{\ell p}(j\tfrac{\pi}{T}(1+2r)) \right|$$

which, because $\left| H_{\ell p}(j\omega) \right|$ is even, reduces to:

$$\left| H_{\ell p}(e^{j\omega T}) \right|_{\omega = \frac{\Omega_s}{2}} \leq \frac{2}{T} \cdot \sum_{r=0}^{\infty} \left| H_{\ell p}(j\tfrac{\pi}{T}(1 + 2r)) \right| \tag{6.3}$$

Ranjbar [9] finds that any analogue lowpass filter that is more complicated than the maximally flat response (Butterworth) filter can have no distinct advantage in protection schemes. We therefore

choose the simple Butterworth filter, the frequency response of which is given by [49] :

$$H_B(j\omega) = \left(\frac{\omega_c}{\omega}\right)^n \quad \text{for} \quad \omega \gg \omega_c \tag{6.4}$$

where ω_c is the cutoff frequency and n the order. Using this response in Equation (6.3) gives:

$$\left|H_B(e^{j\omega T})\right|_{\omega=\frac{\Omega_s}{2}} \leqslant \frac{2}{T} \cdot \sum_{r=0}^{\infty} \left(\frac{T.\omega_c}{\pi(1+2r)}\right)^n$$

or
$$A \leqslant \frac{2}{T} \cdot \sum_{r=0}^{\infty} \left(\frac{2W}{1+2r}\right)^n \tag{6.5}$$

where
$$W = \frac{\omega_c}{\Omega_s} = \frac{T.\omega_c}{2\pi} \tag{6.6}$$

The ratio of the magnitude A to the gain at dc is now found as:

$$\begin{aligned} G = \frac{A}{1/T} &= AT \\ &\leqslant 2.(2W)^n . \sum_{r=0}^{\infty} \frac{1}{(1+2r)^n} \\ &\leqslant 2.(2W)^n . S_n \end{aligned} \tag{6.7}$$

and the sum, S_n, of the series is, for even values of n [50] :

$$S_{2m} = \frac{\pi^{2m}.\alpha_m}{4.(2m)!} \tag{6.8}$$

where tabulated values of α_m are as follows:

m	1	2	3	4	5	...
α_m	1	1	3	17	155	...

so that $S_2 = \frac{\pi^2}{8} \simeq 1.23$,

$S_4 \simeq 1.01$,

$S_6 \simeq 1.00$, and so on.

It follows from the above that S_n may be approximated to 1 for $n \geqslant 2$, reducing the expression for G in Equation (6.7) to:

$$G \leqslant 2.(2W)^n \tag{6.9}$$

and consequently limiting the order of the filter to:

$$n \geqslant \frac{\log G - \log 2}{\log 2 + \log W} \tag{6.10}$$

Negative values of n, corresponding to unrealisable filters, are therefore avoided only when W is less than 0.5. This means that the cutoff frequency ω_c of the filter must be less than the folding frequency $\frac{\Omega_s}{2}$ of the spectrum, as is expected from considerations relating to the Sampling Theorem.

Evaluating W for different cutoff frequencies ω_c and different sampling frequencies Ω_s, and restricting the ratio G to 0.1, yields the least allowed orders, n, of the filter that are given in Table (6.1) below. The sampling rates in samples per cycle are used in place of the sampling frequencies Ω_s.

Cutoff Frequency f_c Hz	Least Integer Order, n			
	4 s/c	8	16	32
50	5	3	2	2
60	6	3	2	2
70	9	3	2	2
80	14	4	2	2
90	29	4	3	2
100	∞	5	3	2

TABLE (6.1): Least allowed orders of the analogue filter.

It becomes apparent that a number of analogue filters, which guard against aliasing, are possible for each sampling rate. However, filter delay is now used as a criterion to narrow down the choice to one optimum filter per sampling rate.

6.2 FILTER DELAY

The elemental pure delay filter defined by the system function [47] :

$$H_{pd}(s) = \exp(-sT) \tag{6.11}$$

constitutes the core around which the various recognised definitions of delay are formulated. It has a frequency response given by:

$$H_{pd}(j\omega) = \exp(-j\omega T) \tag{6.12}$$

while its impulse response is:

$$h_{pd}(t) = \delta(t - T) \tag{6.13}$$

There exist, therefore, two domains, frequency and time, from which delay parameters could be obtained. These two domains are now separately examined, and the delay that is most meaningful in relation to the performance of the protection schemes is adopted.

6.2.1 The Frequency Domain Considerations

The phase of the transfer function $H_{pd}(j\omega)$ of the pure delay, together with its derivative with respect to ω, are shown in Figure 6.3. Two delay parameters, first the phase delay:

$$T_p = -\frac{\phi}{\omega} \tag{6.14}$$

and secondly the group delay:

$$T_g = -\frac{d\phi}{d\omega} \tag{6.15}$$

could be defined [47] . Both happen to be T, but have different physical interpretations. Phase delay is the shift in the phase of a particular frequency as apparent from the difference between the phases of an input and the output cosinusoidal signals. Group delay is an indication of the distortion effect of the filter on an envelope comprising a band of frequencies.

Group delay is usually adopted as a measure of performance in network theory [47,51] . But as Kuo [47] points out, it is meaningless when the phase does not go through the origin, as then the phase shift component that appears in addition to the delay is hard to account for in the case of wideband signals.

The above definitions of delay give no direct indication of its interpretation in the time domain. They both happen to be equal to the actual delay, T, in the case of the pure delay, but will not necessarily be so for other realisable filters. In fact, linear phase, constant group delay analogue filters are non-existent in practice. What is required here is a measure of how long a change at the input takes to manifest itself as a corresponding change at the output, since the transmission through the filter of transients in the input is desired in as short a time as possible.

6.2.2 The Time Domain Considerations

The impulse and step responses of the pure delay filter are shown in Figure 6.4. From these, the familiar definitions [52] of

the impulse and step delays, T_i and T_s respectively, are derived. Input signals, however, appear distorted at the outputs of lowpass filters in general, with impulses appearing smeared out, and steps becoming gradual rises to the steady-state values. In such cases, the positions of the peaks of the smeared out impulses, and the midpoints of the slowly rising steps, determine the delays.

The impulse response, however, is the time derivative of the step response. Its peak value, therefore, occurs at the instant of maximum rate of rise of the step response. This is roughly when the step response is transcribing the midpoint of its steady-state value, and the two delays are thus approximately equal. Hence the study of the step delay only will suffice.

The step response of an analogue filter is found by forming the inverse Laplace transform of the quotient of its system function and the transform variable s [47] :

$$e_{\ell p}(t) = \mathcal{L}^{-1}\left(\frac{H_{\ell p}(s)}{s}\right) \tag{6.16}$$

from which the step delay T_s is defined as:

$$e_{\ell p}(T_s) = 0.5.\left|e_{\ell p}(t)\right|_{t \longrightarrow \infty} \tag{6.17}$$

The evaluation of T_s will thus involve numerical methods, as the step response of a Butterworth lowpass filter will contain exponentially decaying cosinusoids [52] . In the interest of avoiding elaborate solutions, a considerably simpler method is used for calculating the step delays. It is due to Elmore and Sands [53] , who define the delay as the first moment or centroid of the impulse response:

$$T_s = \int_0^{\infty} t.h_{\ell p}(t)\, dt \tag{6.18}$$

and prove that it is given by:

$$T_s = b_1 - a_1 \tag{6.19}$$

where b_1 and a_1 are coefficients appearing in the expansion of $H_{lp}(s)$ in the form:

$$H_{lp}(s) = \frac{1 + a_1 s + \ldots + a_n s^n}{1 + b_1 s + \ldots + b_n s^n} \tag{6.20}$$

Delay times obtained by the Elmore and Sands method reportedly differ very little from those obtained by conventional definitions [53] , for filters with monotonic step responses. This last condition is assumed satisfied by the low order Butterworth filters under consideration, since their transient responses contain only small overshoots [52] .

Thus, step delays of Butterworth filters of orders 1 to 6 are calculated from Equation (6.19) using the well-tabulated [49] coefficients of the normalised polynomials that appear in Equation (6.20). Each of these normalised delay values is then divided by the cutoff frequencies ω_c to give the delays of a particular filter order at those frequencies. Final delays are given in Table (6.2) below.

Cutoff Frequency	Step Delay, T_s, msec.					
f_c Hz	1st order	2	3	4	5	6
50	3.18	4.50	6.37	8.32	10.30	12.30
60	2.65	3.75	5.30	6.93	8.58	10.25
70	2.27	3.21	4.55	5.94	7.36	8.78
80	1.99	2.81	3.98	5.20	6.44	7.69
90	1.77	2.50	3.54	4.62	5.72	6.83
100	1.59	2.25	3.18	4.16	5.15	6.15

TABLE (6.2): Delays of Butterworth Filters.

It was earlier postulated that step delays, as opposed to the phase and group delays, represent the transient behaviour. A comparison of the various delays is given in Table (6.3) for filters with cutoff frequencies at 50 Hz and 100 Hz, and with the phase and group delays computed at 50 Hz. Group delays for both cutoff frequencies are seen to vary most with the order, while step delays vary least. In fact, the differences are appreciable, and the initial reservations about using the readily obtainable group and phase delays were thus justified.

Cutoff Frequency f_c	Order	1st	2nd	3rd	4th	5th	6th
50 Hz	Step Delay T_s msec.	3.18	4.50	6.37	8.32	10.30	12.30
	Phase Delay T_p msec.	2.50	5.00	7.50	10.00	12.50	15.00
	Group Delay T_g msec.	1.59	4.50	7.96	11.76	15.83	20.10
100 Hz	Step Delay T_s msec.	1.59	2.25	3.18	4.16	5.15	6.15
	Phase Delay T_p msec.	1.48	2.41	3.35	4.33	5.34	6.36
	Group Delay T_g msec.	1.27	2.65	3.72	4.74	5.79	6.85

TABLE (6.3): Comparison of step, phase and group delays.

6.3 THE OPTIMUM FILTERS

The aliasing requirements at each sampling rate were shown to be met by a number of analogue filters with different cutoff frequencies and orders. Of these filters, the one giving least delay is now chosen.

At the sampling rate of 4 s/c, the least order filters allowed, as from Table (6.1), are a 5^{th} order with a cutoff at 50 Hz and a 6^{th} order with a cutoff at 60 Hz. The delay of the second of these, obtained from Table (6.2) as 10.25 msec., is less than the delay of the

first, this being 10.30 msec. The other possible higher order filters with higher cutoffs, that appear in Table (6.1), are not considered as their corresponding delays, which are not tabulated here, are in fact too large. The 6^{th} order, 50 Hz cutoff frequency, filter is thus chosen as optimum for the sampling rate of 4 s/c.

The above procedure is repeated for 8, 16 and 32 s/c, and the resulting optimum filters for these sampling rates are defined in Table (6.4) below.

Sampling Rate s/c	Optimum Filter		
	Order	Cutoff Frequency, Hz	Delay msec.
4	6^{th}	60	10.25
8	3^{rd}	70	4.55
16	2^{nd}	80	2.81
32	2^{nd}	100	2.25

TABLE (6.4): Optimum filters for the different sampling rates.

6.4 THE OPTIMUM SAMPLING RATE

The initial problem of finding the optimum sampling rate, as discussed at the beginning of this chapter, is now examined. We require the sampling rate which gives the least total time due to both the analogue filter delay and the time for computations. For the latter, we use the processing cycle concept as introduced and defined in Chapter 4, that being the time required for the multiplications and additions involved in the phasor determinations plus a margin for impedance calculation and other logical operations needed in the protection algorithm. The total times so obtained for the full cycle method are given in Table (6.5) following.

Sampling Rate s/c	Optimum Filter Delay msec.	Processing Cycle Duration msec.	Total Time msec.
4	10.25	1.01	11.26
8	4.55	1.15	5.70
16	2.81	1.43	4.24
32	2.25	1.99	4.24

TABLE (6.5): Total times for the different sampling rates for the full cycle method.

While the sampling rate of 16 s/c seems to be giving the least total time, 8 s/c is chosen as the optimum rate. This makes continuous processing possible, thereby avoiding the complexity of fault-initiated processing that is needed with 16 s/c. The difference between the total times for the two rates amounts to just over one millisecond, and may conceivably be compensated for by possible savings in the 0.5 msec. estimate that was allocated to the relaying logic in the processing cycle.

The half-cycle method requires optimum analogue filters that are identical to those of the full cycle method at their respective sampling rates. Thus, 8 s/c is taken as the optimum rate for the half-cycle method, too, since its processing cycle durations differ very slightly from those of the full cycle method, being 1.01 msec., 1.13 msec., 1.37 msec. and 1.85 msec. for 4, 8, 16 and 32 s/c respectively.

The total times obtained for the full cycle and half-cycle methods, though almost equal, are not to be interpreted as indicating that the fault detection times of the two methods are nearly the same. As was pointed out in Chapter 5, the digital filter transient delay associated with the half-cycle method is considerably less than that of

the full cycle method. However, this delay is a constant for each method at all sampling rates, and it therefore has no influence on the choice of the optimum rate.

6.5 FREQUENCY RESPONSE OF THE ANALOGUE-DIGITAL FILTER COMBINATION

The frequency responses of the full cycle and half-cycle methods, at their optimum sampling rate and with the corresponding optimum analogue filter, are now derived. Spectral descriptions without the analogue filter were obtained in Chapters 4 and 5, and were termed worst combined responses. However, the introduction of the analogue filter now forms a hybrid system that is considerably more complicated to analyse.

Conventionally, the frequency response of a hybrid system is taken as the periodic response of the digital filter defined over its baseband only. This assumes the analogue filter to be an ideal lowpass, with brickwall frequency characteristics, and is thus hardly applicable for realisable filters. Recognising such fact, direct multiplication of the analogue and digital filter responses over the entire frequency range was proposed as an alternative [9].

Both of the above procedures lacked sound justification. The second, in fact, is fundamentally incorrect since it implies a linear overall model for the hybrid system, which is obviously inconsistent with the non-linearity introduced by the sampling of a non-bandlimited signal. Also, its account of the attenuated high frequencies is arbitrary. These high frequencies appear as low frequencies in the baseband because of sampling, and although this may be overlooked as

the digital filters are giving amplitude information only, and for no other frequency than the 50 Hz, it would still be desirable to arrive at some simpler frequency description.

An approach that employs the spectral considerations criteria of standard speech processing is here adopted. Frequencies higher than half the sampling rate are assumed negligible in speech processing if guardbands are employed, and when a 40 db loss is specified for these frequencies [25] . This is comparable to the approximate 30 db loss which corresponds to the 0.1 foldover gain used in specifying the analogue filters, and it thus suffices to multiply the response of the analogue with that of the digital filter over the baseband of the latter, taking the response of the hybrid system over the rest of the frequency range to be zero. The resulting response should now be interpreted in the same manner as that used for the worst combined response of Chapters 4 and 5.

Figures 6.5 and 6.6 show the multiplied responses defined over the baseband for the full cycle and half-cycle methods respectively, and with 8 s/c. The very small magnitudes in the immediate vicinity of the 200 Hz folding frequency illustrate that aliasing is, in fact, small enough to be neglected.

In an attempt at examining the feasibility of employing the lowest sampling rate of 4 s/c, the responses of the methods at this rate are obtained. However, because of the prohibitive delay of 10.25 msec. that the optimum filter for this rate incurs, the optimum filter for 8 s/c is used instead. This results in appreciable aliasing distortion in the vicinity of the folding frequency of 100 Hz, as is apparent from the sudden truncation there of the plots of Figures 6.7

and 6.8. The rate of 4 s/c is thus ruled out, while the significance of the correct choice of the analogue filter to match a sampling rate is emphasised.

It is to be noted that a comparison of the frequency responses of any of the two methods at different sampling rates could not have been used as an alternative criterion for determining the optimum sampling rate. The only visible difference between the frequency responses of any one method without the analogue filter was in the slightly different levels of non-harmonic suppression that the different sampling rates gave rise to. It was considered that such difference would be further reduced by the analogue filters, thus making all responses almost identical for each method.

6.6 CONCLUSION

The use of analogue lowpass filters for bandlimiting signals before sampling them is mandatory. Designs of such filters that matched the sampling rates being investigated were drawn, and the rate of 8 s/c consequently emerged as optimum in that it gave the least filter delay plus processing time that were consistent with simple implementation.

The frequency responses of the full cycle and half-cycle methods at 8 s/c, and with the analogue filter, were finally obtained. Both responses were favourably characterised by appreciable non-harmonic suppression, and low aliasing distortion, but the unacceptably large dc transmission in the response of the half-cycle method still remained.

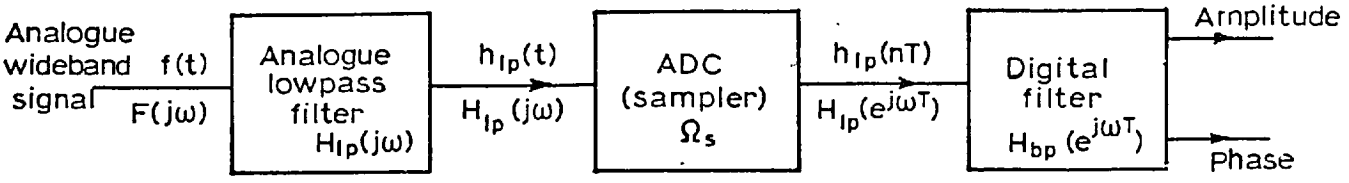

Fig. 6·1 Block diagram of system with analogue lowpass filter.

(a) Frequency response of the analogue filter.

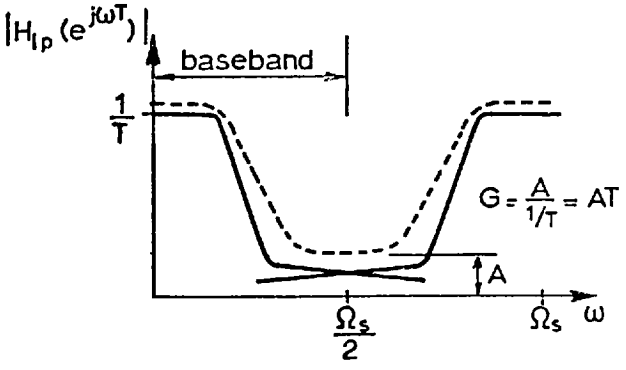

(b) Spectrum of the lowpass-filtered sampled wideband signal.

Fig. 6·2 Aliasing in spectrum of the sampled signal.

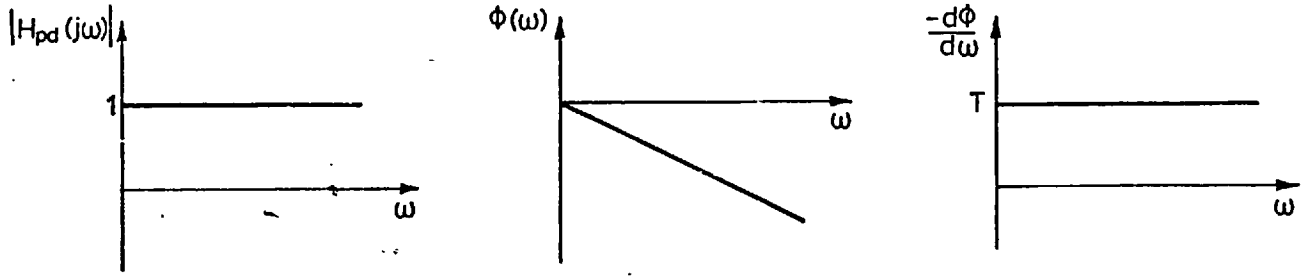

(a) transmission (b) phase (c) group delay

Fig. 6·3 Frequency domain characterisation of the pure delay.

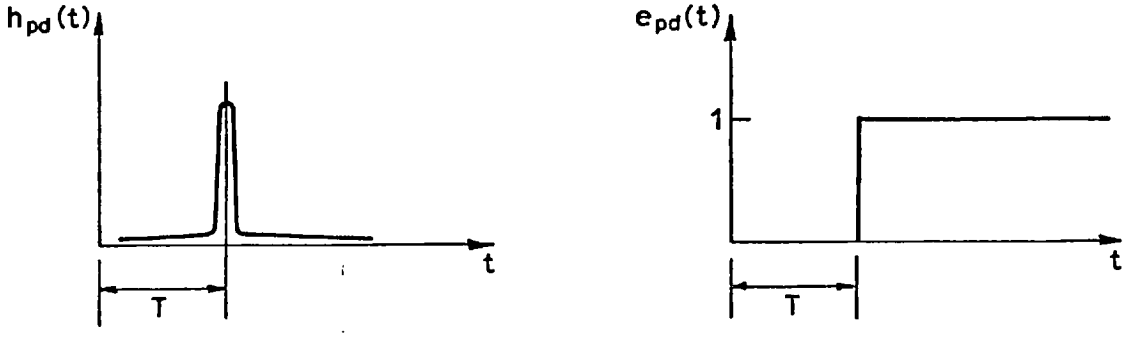

(a) impulse response (b) step response

Fig. 6·4 Time responses of the pure delay.

FULL CYCLE METHOD 8 SAMPLES PER CYCLE

WORST COMBINED RESPONSE WITH OPTIMUM ANALOGUE FILTER

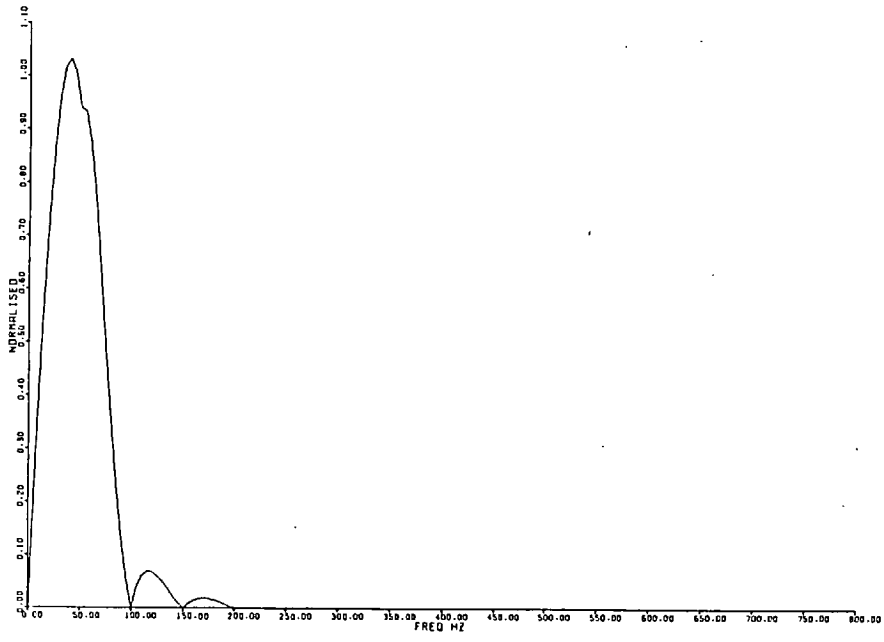

Fig. 6·5

HALF CYCLE NEGATIVE REPETITION METHOD 8 SAMPLES PER CYCLE

WORST COMBINED RESPONSE WITH OPTIMUM ANALOGUE FILTER

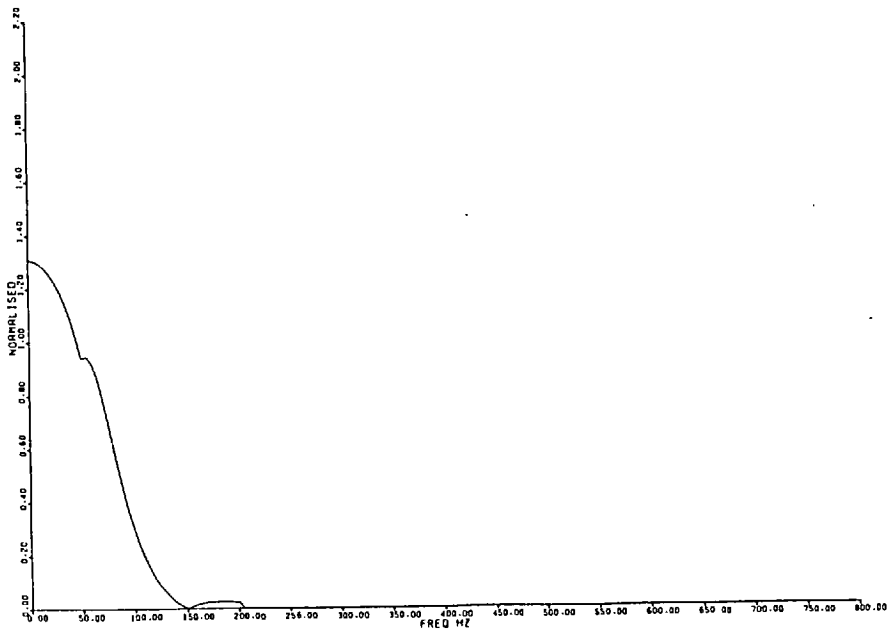

Fig. 6·6

FULL CYCLE METHOD 4 SAMPLES PER CYCLE

WORST COMBINED RESPONSE WITH OPTIMUM ANALOGUE FILTER

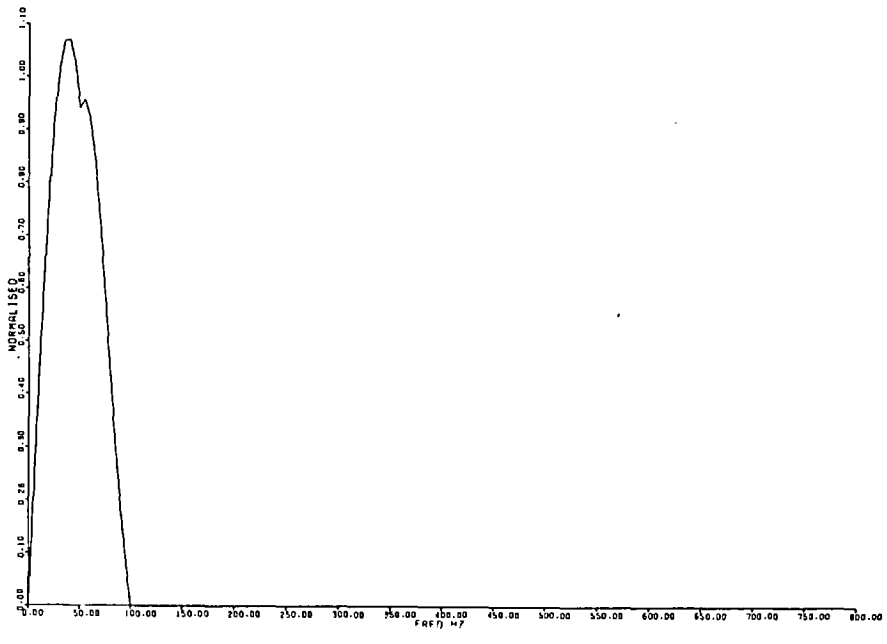

Fig. 6·7

HALF CYCLE NEGATIVE REPETITION METHOD 4 SAMPLES PER CYCLE

WORST COMBINED RESPONSE WITH OPTIMUM ANALOGUE FILTER

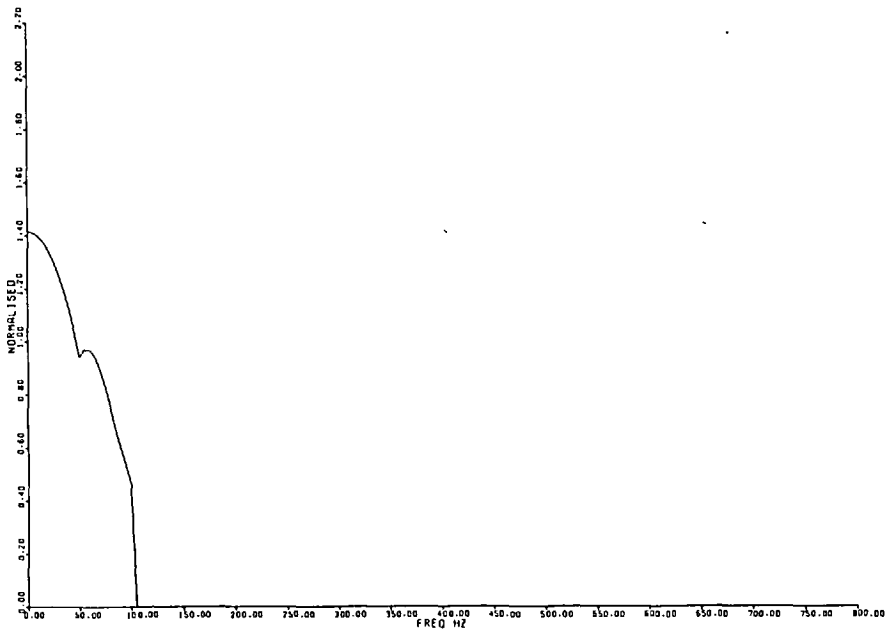

Fig. 6·8

CHAPTER 7

PREDICTIVE SCHEME MODIFICATION

The predictive scheme developed in Chapter 5 was shown to offer satisfactory nonharmonic suppression when used with the analogue lowpass filter, and it is thus comparable with the full cycle method in this respect. However, it is also characterised by large dc transmission, and this renders it unacceptable.

This chapter discusses the reduction of the dc transmission by employing additional filters. The chapter first justifies opting for digital filters for this task, and then suggests a number of highpass filters that could be used. The resulting frequency responses of the scheme are then obtained, and a few criteria devised and applied to these responses to assist in the determination of the most suitable highpass filter. Finally, some refinements on this filter are briefly investigated.

7.1 USING AN ANALOGUE BANDPASS FILTER: DELAY CONSIDERATIONS

The dc signal can be attenuated by an analogue highpass filter immediately following the analogue lowpass filter that precedes the ADC. Such highpass filter must have a cutoff frequency of about 50 Hz if it is not to accentuate high frequencies, as it would otherwise disturb the aliasing specifications that were discussed in Chapter 6. It must also be of a second, or preferably third, order for it to appreciably attenuate subharmonics too.

The above suggests that the analogue highpass filter being sought could be incorporated in a bandpass filter that will both reduce the level of dc signals, and meet the high frequency attenuation

requirements designed to ensure against aliasing. The frequency response of an elemental bandpass filter [49], with the roll-off rate of 6 db/octave, is sketched in Figure 7.1.

However, aliasing considerations require attenuation at the foldover frequency, which is 200 Hz for a sampling rate of 8 s/c, to be 30 db or more. Therefore, with the bandpass filter centre frequency being 50 Hz, an attenuation rate of 15 db/octave is needed. This can only be met with three cascaded elemental filters at least, giving a sixth order filter. The delay of such filter, judging from the analogue filter delays calculated in Chapter 6, will be prohibitive: possibly as large as 10 msec. An analogue bandpass filter is thus ruled out, and the optimum analogue lowpass filter that is also compatible with the full cycle method is left unchanged.

7.2 THE DIGITAL HIGHPASS FILTER

The elimination of dc signals could be carried out by a simple digital highpass filter. This is now investigated in the hope that any resulting improvements in the frequency response of the predictive scheme will not be at the expense of excessive extra delay. No complications are expected in the implementation of a digital highpass filter, since it can readily be incorporated in the main phasor determination algorithm of the scheme.

A number of factors influence the adoption of a digital filter in a protection scheme. As was discussed in Chapter 4, recursive structures are generally undesirable because of their infinite impulse responses. The impulse response associated with a non-recursive structure, on the other hand, is finite. In the case

of the DFT filter, such response manifests itself in the output as a component that is much smaller than the output to a sampled cosinusoidal input having the same magnitude as the impulse.

The transient delay of a digital filter should be kept as low as possible, if long detection times are to be avoided. Also, the possibility of the protection scheme supplying information for steady-state monitoring makes it desirable to have the digital filter phase delay at 50 Hz kept to a minimum, but this is by no means critical for fast protection since the same filter operates on both the voltage and current signals, yielding correct impedance angles.

7.2.1 Possible Digital Highpass Filters

The simplest three possible choices of the digital highpass filters are given below. Orders are restricted to first or second because transient delays exceeding 5 msec. are unacceptable.

Prototype I: This is described by the transfer function:

$$H_{hpl}(z) = 1 - a_1.z^{-1} \qquad (7.1a)$$

which, when $a_1 = 1$, gives the frequency response:

$$H_{hpl}(e^{j\omega T}) = 2j.\exp(\frac{-j\omega T}{2}).\sin(\frac{\omega T}{2}) \qquad (7.1b)$$

with amplitude and phase variations that are sketched in Figure 7.2. A value of a_1 that is less than 1 is initially considered because it results in a reduction in the phase delay at 50 Hz. However, such reduction will be relatively small, and will also be accompanied by the flattening of the amplitude spectrum and the loss of total dc elimination, as shown in Figure 7.2. The multiplication factor a_1 is

thus taken as 1, with the impulse response reducing to an anti-symmetric sequence of length 2 which gives a linear phase with constant group delay [25] .

Prototype II: This has a transfer function that is given by:

$$H_{hp2}(z) = (1 - a_2.z^{-1})^2 \qquad (7.2a)$$

Its impulse response becomes symmetric when a_2 is taken to be equal to 1, giving a linear phase with constant phase delay for the frequency response which is now given by:

$$H_{hp2}(e^{j\omega T}) = 2.\exp(-j\omega T).(\cos(\omega T) - 1) \qquad (7.2b)$$

and is shown in Figure 7.3. The filter is thus a special case of the general form $1-2\cos(\omega_o T).z^{-1}+z^{-2}$, with $\omega_o = 0$.

Prototype III: This is a second order filter defined by:

$$H_{hp3}(z) = 1 - a_3.z^{-2} \qquad (7.3a)$$

Investigations of the frequency response reveal that any choice of a_3 other than 1 offers no overall advantage. We therefore take a_3 as 1, and this gives a frequency response of:

$$H_{hp3}(e^{j\omega T}) = 2j.\exp(-j\omega T).\sin(\omega T) \qquad (7.3b)$$

which has an amplitude response that varies twice as fast with frequency as the response of the first prototype. Examination of the response shown in Figure 7.4 over its baseband reveals that this prototype is in fact a bandpass filter.

The third prototype above would probably be the most suitable because its gain decreases for frequencies above 100 Hz,

reaching zero at the folding frequency. It therefore seems to be least upsetting the aliasing considerations of the analogue lowpass filter. A final decision on its adoption , however, must be based on some more definite criteria.

7.2.2 The Frequency Response Criteria

The frequency responses of the half-cycle negative repetition method at 8 s/c, and with the prototype digital highpass filters, are now obtained. The digital highpass filter is to immediately precede the DFT filter, and the frequency responses of both the cosine and sine filters of the latter must therefore be multiplied by the highpass filter frequency response. The multiplied cosine and sine responses are shown in Figure 7.6 when the first prototype is used, and the worst combined response is formed from these in a manner identical to that adopted in Chapters 4 and 5. This combined response is then multiplied over its baseband by the analogue filter response, giving the scheme response shown in Figure 7.7. The responses with the second and third prototypes are shown in Figures 7.8 and 7.9 respectively.

All of the scheme responses are seen to have zero dc transmission. However, they differ in their suppression of nonharmonics and the second harmonic in relation to their transmission of the 50 Hz. We therefore devise a few criteria for determining the most satisfactory scheme response.

a) The Relative Energy Index

This is a measure of the fraction of the energy of the output contained in the 50 Hz when the intput is a wideband signal. It should

be as large as possible, and is in fact determinable from the frequency response of the scheme since the energy in a time signal is known to be equal to the integral of the square of its amplitude spectrum [23] . The index can thus be defined as:

$$M1 = \frac{\Delta f.|H(f_0)|^2}{\sum_k \Delta f.|H(k.\Delta f)|^2} \qquad (7.4)$$

where the frequency increment Δf can be arbitrarily chosen, with the summation carried out over the whole of the baseband. In the computations that will follow, Δf is taken equal to 5 Hz, this being the interval used in the frequency plots.

b) The 50 to 100 Ratio

This ratio of the gain at 50 Hz to that at 100 Hz should be as large as possible. It is an indication of the Q factor of the scheme, and is given by:

$$M_2 = \frac{|H(f_0)|}{|H(2f_0)|} \qquad (7.5)$$

c) The Peak Difference Criterion

This applies to the responses being considered because their peak gains do not occur at 50 Hz as desired. The peak gain should be as near to the gain at 50 Hz in value as possible, so that the relative difference defined by:

$$M3 = \frac{\hat{H} - |H(f_0)|}{\hat{H}} \qquad (7.6)$$

is to be kept to a minimum.

The above criteria are illustrated in the sketch of the scheme frequency response shown in Figure 7.5. They were computed for each of the responses of Figure 7.7 to 7.9, and are given in Table (7.1) below.

Digital Highpass	Frequency Response Criteria		
	M1	M2	M3
Prototype I	0.064	1.696	0.151
Prototype II	0.039	0.918	0.368
Prototype III	0.072	2.216	0.107

TABLE 7.1 Scheme frequency response criteria with the three highpass filter prototypes.

The third prototype clearly emerges as the best highpass filter, since it offers the largest relative energy index M1 and largest gain ratio M2, as well as the smallest peak difference M3. In fact, it is evident from the plots of Figures 7.7 to 7.9 that this prototype is the only one that will not give rise to aliasing distortion, as the first, and more so the second, prototypes both give scheme responses with appreciable magnitudes in the vicinity of the 200 Hz folding frequency.

The only shortcoming of the scheme response with the third prototype, however, is the occurrence of the peak at around 70 Hz instead of at 50 Hz. It is now attempted to rectify this by employing a peak shifting network.

7.2.3 Peak Shifting

The peak in the magnitude response of the third prototype highpass filter was shown to be occurring at 100 Hz. To shift this to a lower frequency, the peak shifting network defined by Equation (7.7) below is examined.

$$H_{ps}(z) = \frac{1}{1 + b.z^{-1}} \tag{7.7}$$

This network, when cascaded with the third prorotype highpass filter, gives the transfer function:

$$H_{hp3}(z) = \frac{1 - z^{-2}}{1 + b.z^{-1}} \tag{7.8a}$$

so that the magnitude of the frequency response becomes:

$$|H_{hp3}(e^{j\omega T})| = \frac{2.|\sin(\omega T)|}{\sqrt{1 + 2b.\cos(\omega T) + b^2}} \tag{7.8b}$$

and this has a maximum of 2 that occurs at $\omega = \frac{\cos^{-1}(-b)}{T}$ for $|b| < 1$. Values of b outside this range are not considered since they result in a pole lying outside the unit circle in the z-plane, which gives rise to instability.

Negative values of b will thus shift the peak towards 50 Hz, as is shown in Figure 7.10(a). The peak will actually occur at 50 Hz with b set to $-\frac{1}{\sqrt{2}}$.

However, the infinite impulse response of the recursive peak shifting network is also to be considered. The time needed for this impulse response to reach 10 per cent of its initial value is an unacceptably high 15 msec. The network is thus not to be used after all, and the system is left with the third prototype highpass filter as the only modification, as shown in Figure 7.11.

7.3 CONCLUSION

The reduction of the dc transmission that characterised the frequency response of the predictive scheme was attempted. A few simple non-recursive digital highpass filters were therefore suggested as possible additions to the scheme, and the most suitable of these was determined.

The predictive scheme was thus made immume to dc noise signals, and at the expense of the little extra transient delay of the highpass filter.

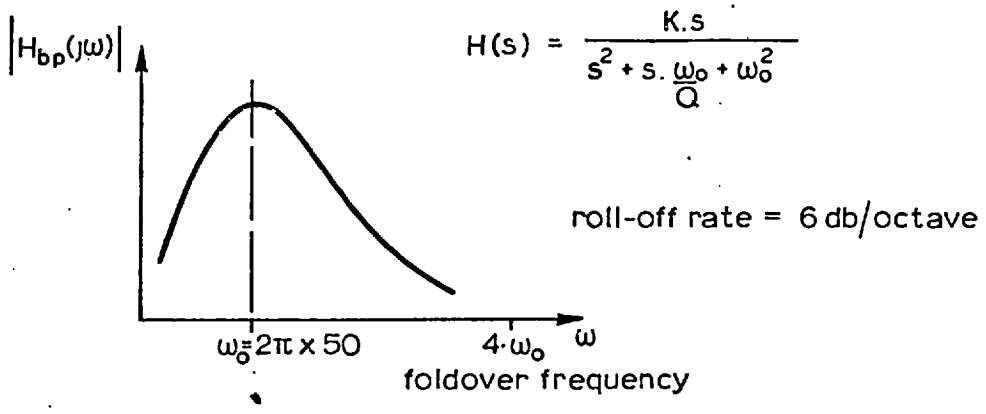

Fig. 7·1 Frequency response of the elemental analogue bandpass filter.

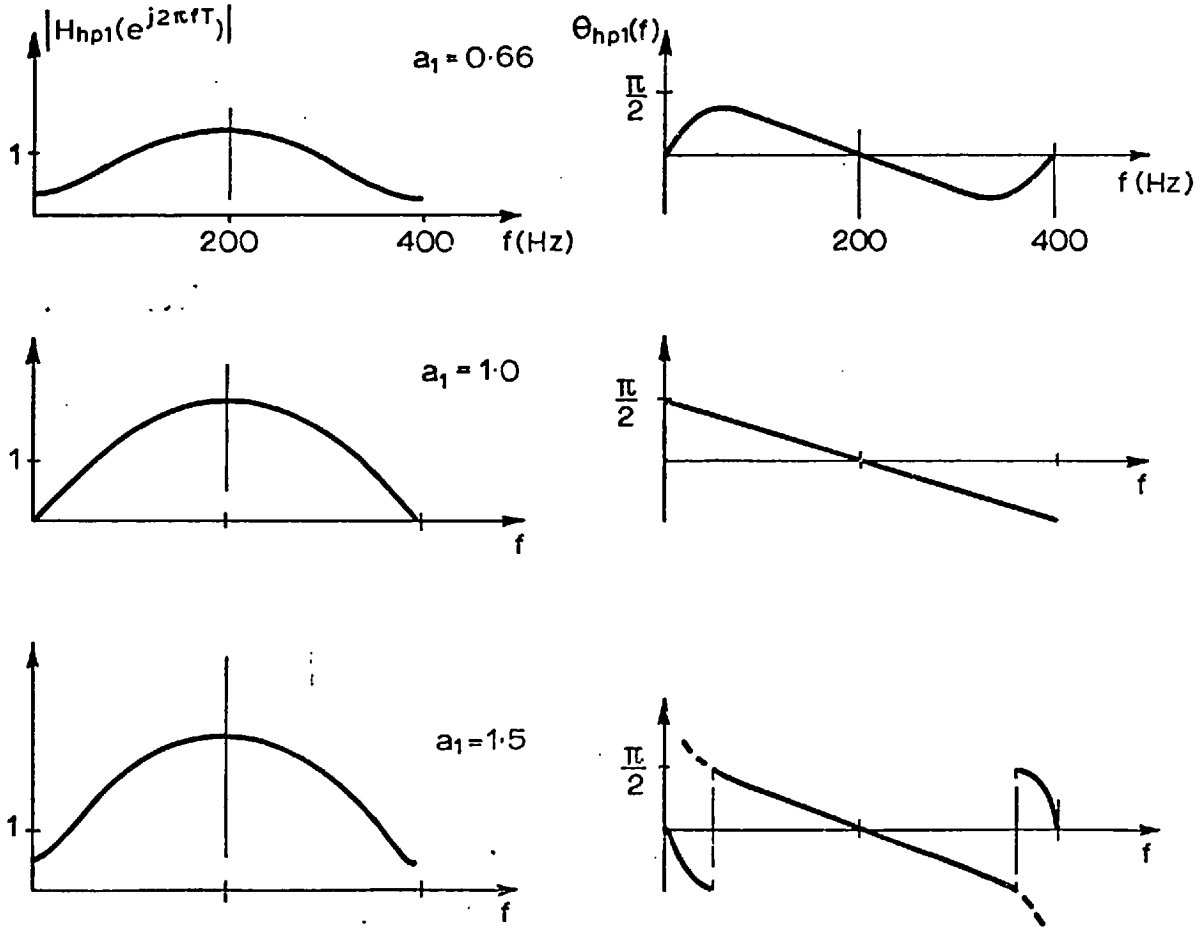

Fig. 7·2 The magnitude and phase responses of the first digital highpass filter with different values of the coefficient a.

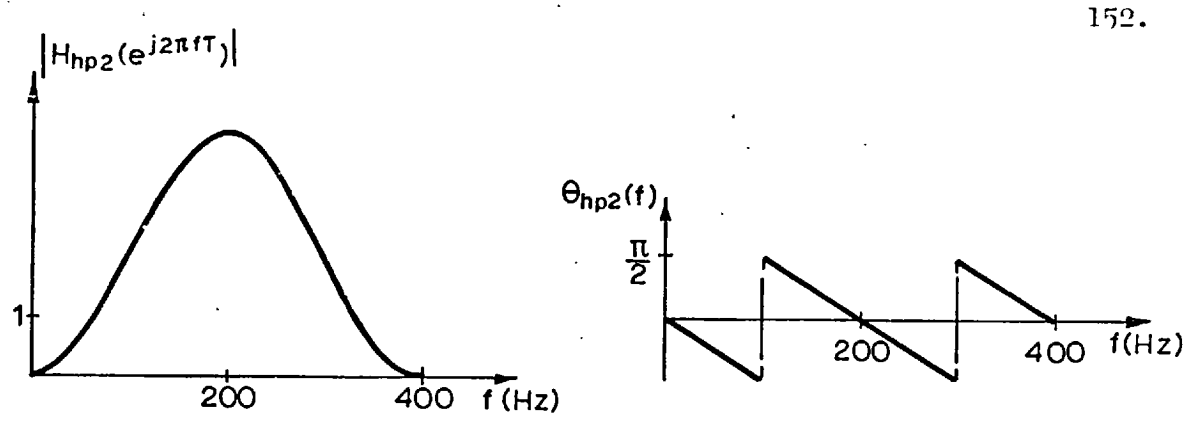

Fig. 7.3 Frequency response of the second digital highpass filter

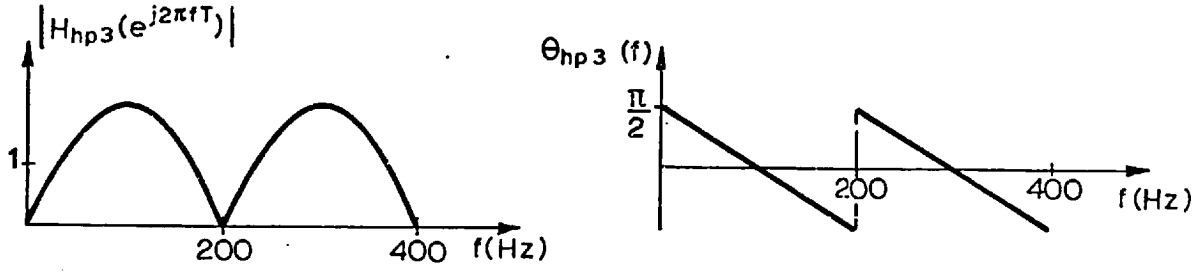

Fig. 7.4 Frequency response of the third digital highpass filter

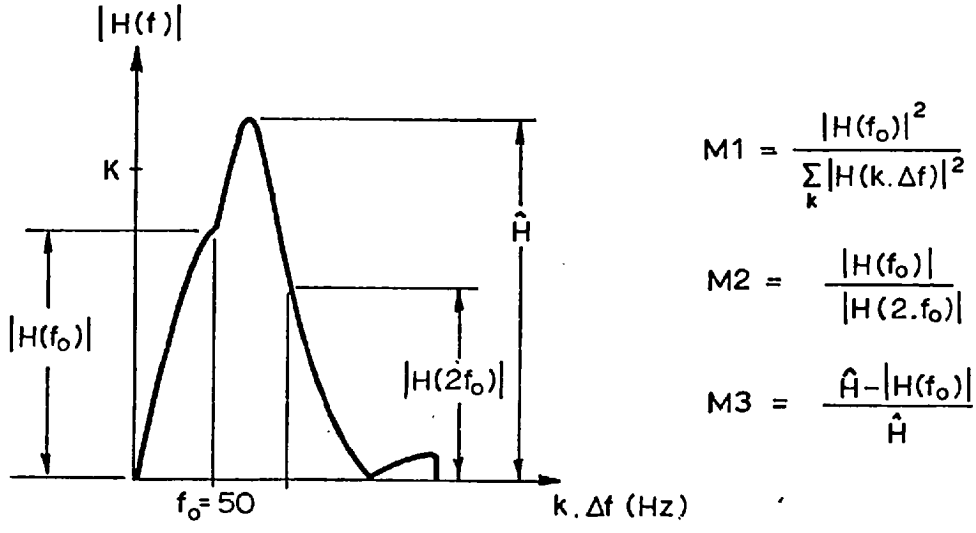

Fig. 7.5 Criteria for the frequency response

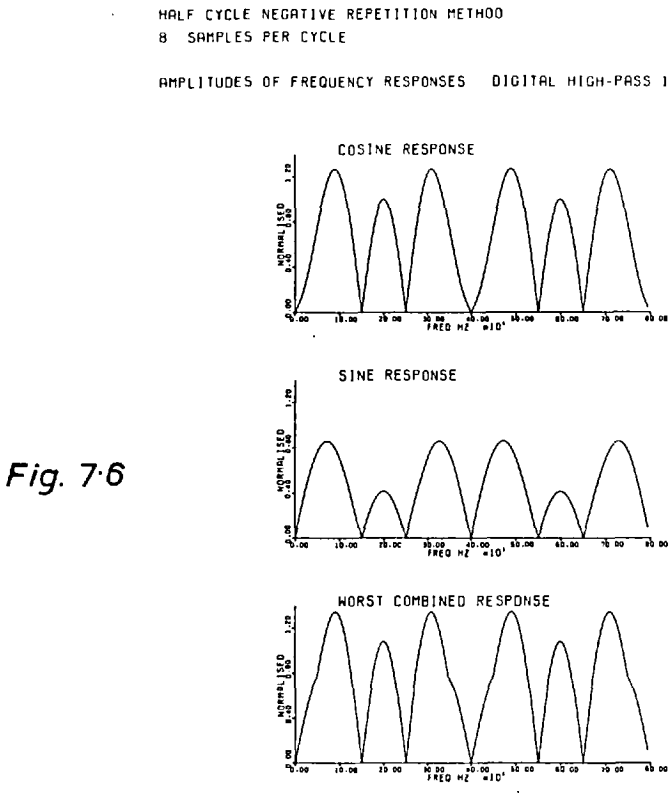
HALF CYCLE NEGATIVE REPETITION METHOD
8 SAMPLES PER CYCLE
AMPLITUDES OF FREQUENCY RESPONSES DIGITAL HIGH-PASS 1
COSINE RESPONSE
SINE RESPONSE
WORST COMBINED RESPONSE
NORMALISED
FREQ HZ

Fig. 7·6

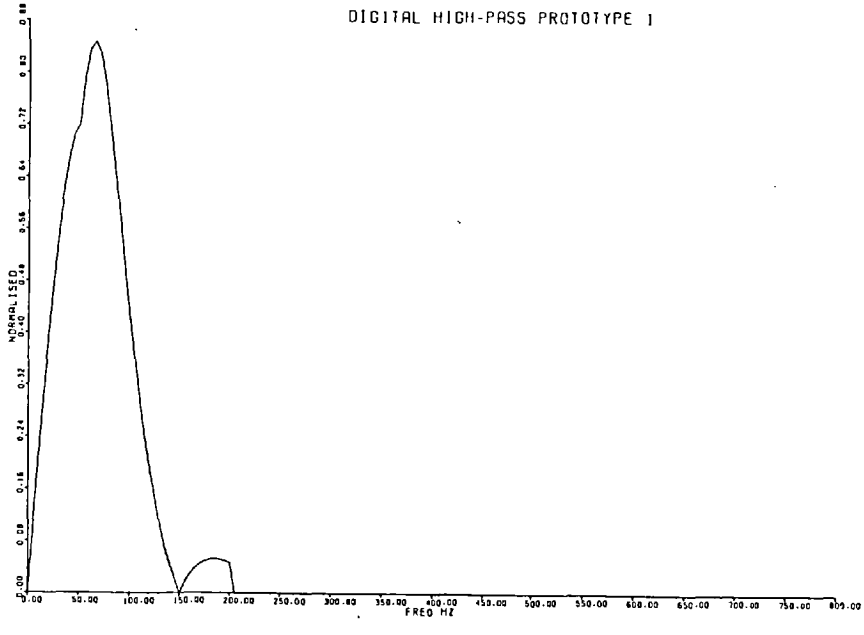
HALF CYCLE NEGATIVE REPETITION METHOD 8 SAMPLES PER CYCLE
WORST COMBINED RESPONSE WITH OPTIMUM ANALOGUE FILTER
DIGITAL HIGH-PASS PROTOTYPE 1
NORMALISED
FREQ HZ

Fig. 7·7

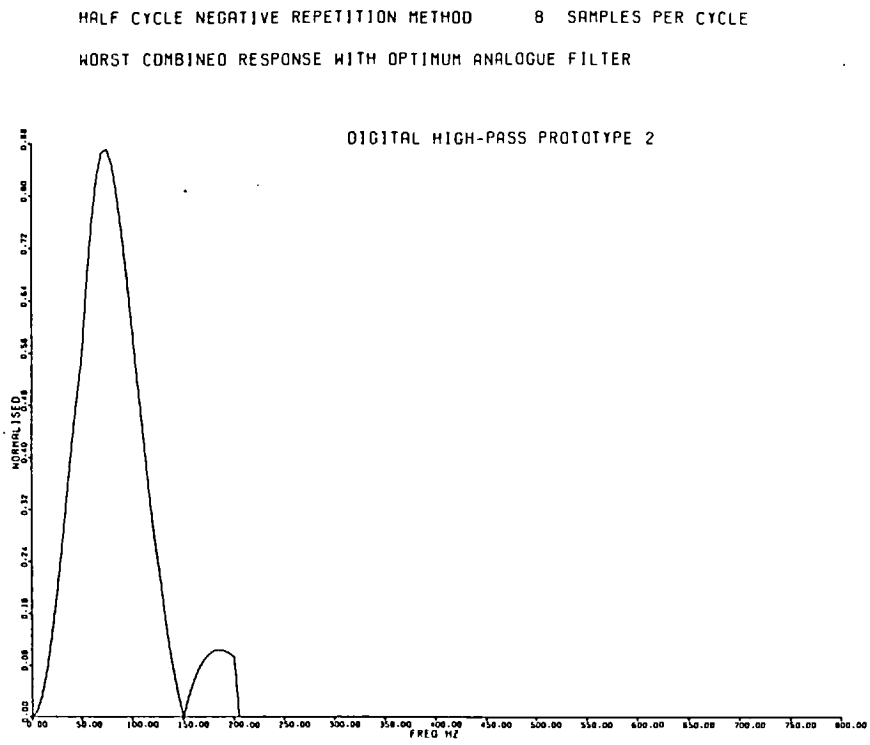
HALF CYCLE NEGATIVE REPETITION METHOD 8 SAMPLES PER CYCLE
WORST COMBINED RESPONSE WITH OPTIMUM ANALOGUE FILTER
DIGITAL HIGH-PASS PROTOTYPE 2
NORMALISED
FREQ HZ

Fig. 7·8

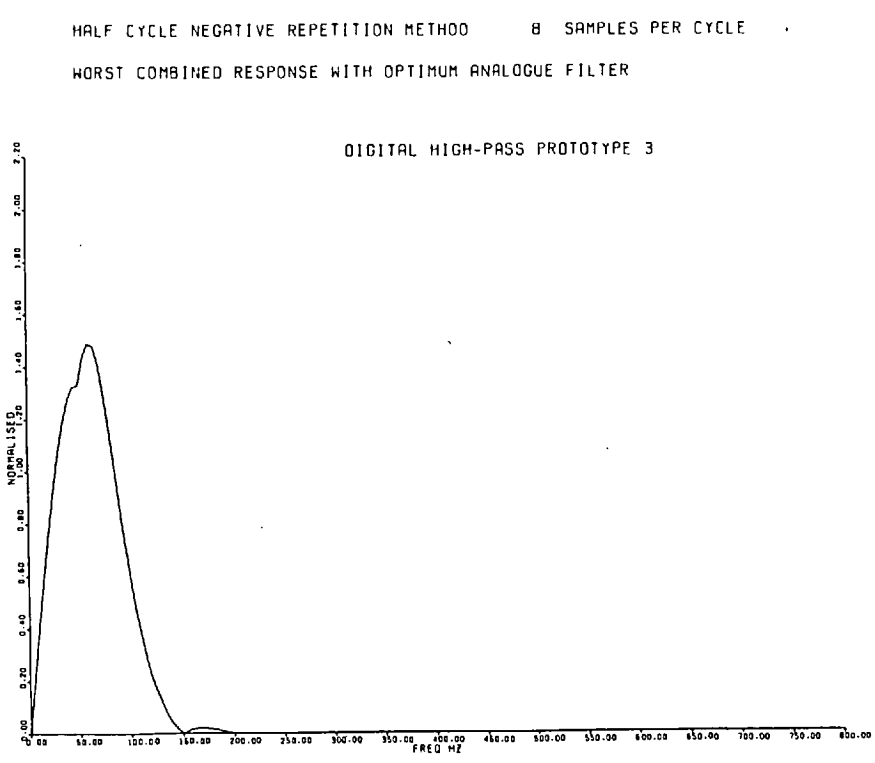
HALF CYCLE NEGATIVE REPETITION METHOD 8 SAMPLES PER CYCLE
WORST COMBINED RESPONSE WITH OPTIMUM ANALOGUE FILTER
DIGITAL HIGH-PASS PROTOTYPE 3
NORMALISED
FREQ HZ

Fig. 7·9

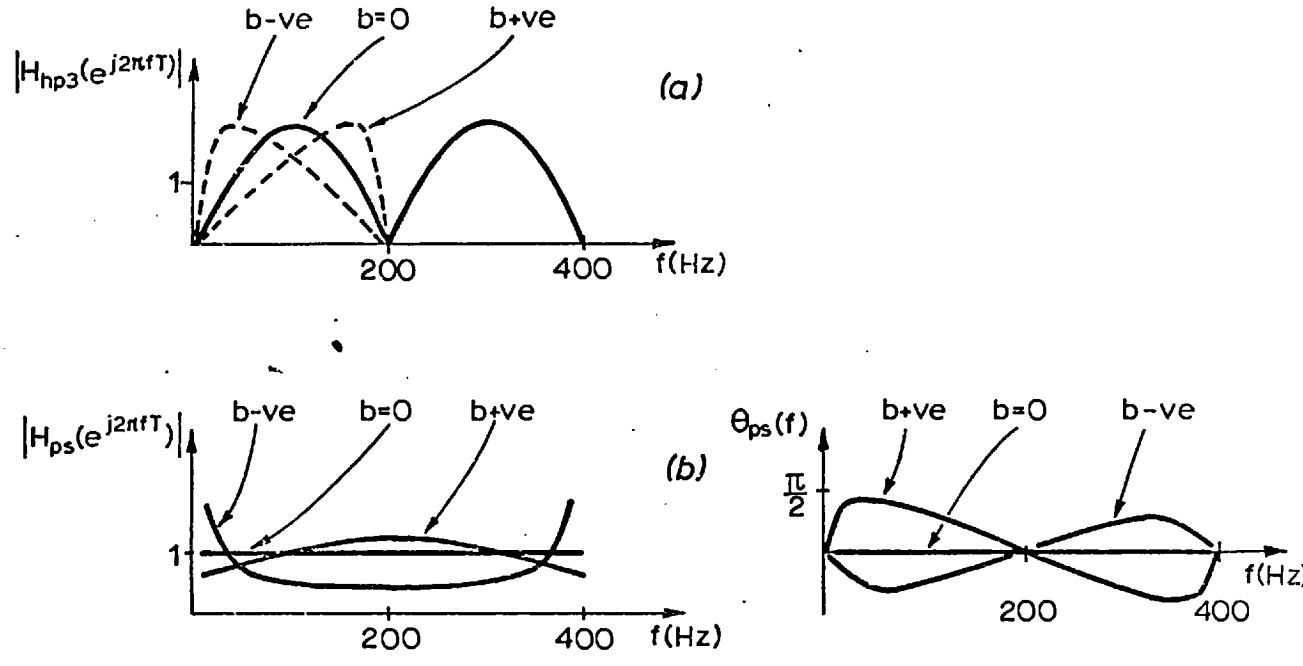

Fig. 7·10 Effect of the peak shifting network

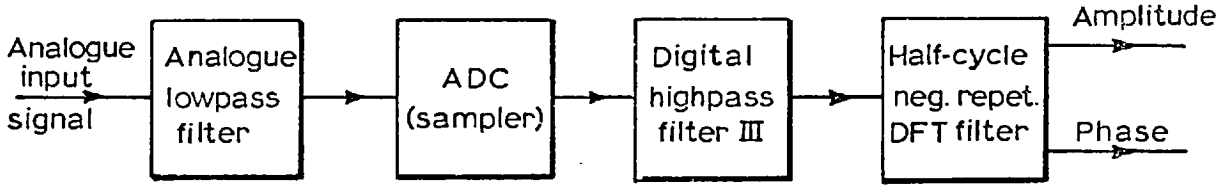

Fig. 7·11 Block diagram of system with digital highpass filter

CHAPTER 8

OFF-LINE TESTS

Initial theoretical assessment of the full cycle and half-cycle protection schemes discussed in Chapters 4 to 7 was favourable. The schemes were shown capable of satisfactorily filtering signals having the compositions of fault transients. However, further tests that would approximate real operating conditions remain necessary for an indication of the fault detection speeds of the schemes.

This chapter describes some off-line tests that were designed to explore various aspects of the performance of the schemes in general, and to highlight a few of the more interesting of these aspects in particular. The tests were kept as thorough as is consistent with simplifications that resulted from the adoption of a one-phase model for the line, since such model could not accommodate a few factors and phenomena that are usually encountered with three-phase lines.

The chapter begins by describing the system chosen for the tests, and by outlining a procedure for tailoring a relaying characteristic that best suits such system. Simulated fault voltages and currents are then discussed, and modifications to these to account for factors that were not considered in the study of Chapter 3 are derived. The protection schemes are finally tested with various fault locations and resistances, and for differing system loading conditions.

8.1 TEST SYSTEM

The system used was similar to the radial feeder studied in Chapter 3. It consists of four 500 MVA turbo-alternators

connected in parallel, and supplying 300 MW through one phase of a 400 kV line that is 100 miles long. The line was operating at about its natural load rating, and its parameters were those of a typical 400 kV line [42]. A line diagram of the system is shown in Figure 8.1.

The steady-state voltage and current at the relaying point, which immediately follows the step-up transformer, were calculated from the equivalent circuit of Figure 8.2. The phase voltage was 399 kV peak, and the phase current 2296 A peak at 48^{o} lag.

8.2 RELAYING CHARACTERISTIC

When assessing protection performance, it is necessary to consider the impedance presented to the measuring unit together with the operating characteristic of that unit. The impedance as seen by the relay under steady-state conditions is given in terms of the line surge impedance Z_o and the load impedance Z_R by the impedance transformation formula:

$$Z_L = Z_o \cdot \frac{Z_R + Z_o.\tanh(\gamma \ell)}{Z_o + Z_R.\tanh(\gamma \ell)} \qquad (8.1)$$

which, because of the very small values of the propagation constant γ, reduces for a line that is only 100 miles long to:

$$Z_L \simeq Z_R \qquad (8.2)$$

After a short-circuit, which is equivalent to the application of a load with zero impedance at the end of a fraction of the line, the apparent impedance becomes:

$$Z_L = Z_o.\ \tanh(\gamma \ell) \qquad (8.3a)$$

which can be approximated to:

$$Z_L = (R + j\omega_o L).\ell = Z.\ell \qquad (8.3b)$$

for small values of the argument $\gamma\ell$. Thus the relay now sees the series impedance of the fraction of the line up to the fault point, which is inductive.

The presence of a fault resistance R_f modifies the apparent impedance to:

$$Z_L = Z.\ell + k_r.R_f \qquad (8.3c)$$

where the factor k_r, which depends, among other things, on the load to line impedance ratio [54] , is approximately equal to 1 for the system under consideration.

The relaying characteristic should both include apparent faulted line impedances and provide wide discriminating margins for the extremes of circuit loading and power swing conditions. The mho type characteristic is the most widely used in present relaying practice, but it is known [54] that, in terms of its discriminative properties, the characteristic having the widest application potential is the quadrilateral. This is because such characteristic can be made to possess a restricted reach along the real axis, which in turn permits high load transfers, while retaining in its measurement the ability to accommodate increased fault resistance values.

Conveniently, the quadrilateral characteristic lends itself more easily to implementation in a digital relay than does the mho characteristic , since computations involved in the definition of straight lines in the X/R plane are simpler than those necessary for

defining a circle. Thus, the quadrilateral characteristic offers the additional advantage of simplicity of implementation that is not achieved at the expense of a degradation in the speed of operation of the protection scheme.

A quadrilateral characteristic suitable for the test system of Figure 8.1 is defined in Figure 8.3. The tripping area is chosen to include fault conditions within 85% of the feeder length as in normal practice because protection is expected to be unable to discriminate for faults adjacent to the remote busbar. The 85% setting also allows for errors in transformation that may occur in current transformers as a consequence of dc offset and remanent flux, and that would otherwise cause overreaching.

A fault resistance that is one-third of the series impedance of the full length of the line is allowed for faults at any point on the line. Overall, the zone 1 reach setting [2] only is considered, since it is this setting that controls the instantaneous tripping that is of interest here.

The relaying characteristic of Figure 8.3 provides a wide margin for normal circuit loading conditions. The apparent impedance of the load considered in Section 8.1, for example, has resistive and reactive components that are both larger than 100 ohms. Even with the highest load current, which corresponds to the largest load transfer that the line is capable of, these components drop to just under 100 ohms, thereby still leaving a comfortable margin since encroachments into the maximum load impedance area will then only occur when the forward reach setting of the characteristic approaches 200 miles.

It may be argued that the wide margins that the relaying characteristic offers should allow the inclusion of a considerably larger fault resistance in the tripping area. This would make the detection of faults with larger resistances possible, as well as speed up the detection of faults that the tripping area already covers. However, encroachments upon the protection characteristic due to power swing conditions are not to be overlooked. It has been established [54] that considerations relating to these are important for 400 kV circuits. Thus, operations for sudden load changes, and particularly for sudden load additions from no load at an initiation angle of 0^{o} [1], must first be considered, and the relay must be guarded against tripping on swings from which the system would be likely to recover. Elaboration on such factors is, however, outside the scope of this thesis, and the maximum allowed fault resistance is thus left at just under 15 ohms.

8.3 FAULT SIMULATION

The solution of the transmission line equations for fault conditions, as was treated in detail in Chapter 3, gave a description of fault transients. Figures 8.4 and 8.5 depict the line voltage and current formed according to that description for two faults, each at a different point on the line. The high frequency component, or eigenfrequency, is seen in the voltage of fault I, where the fault inception angle (f.i.a.) is 90^{o}, while in fault II the current is characterised by a large exponentially decaying dc component because of the 0^{o} fault inception angle. A damped 235 Hz component was added to the voltage of both faults, as the possible existence of such component became apparent from the waveform analysis carried out in Chapter 3.

Figures 8.4 and 8.5 also show the filtered voltages and currents. These are obtained by using a third order Butterworth digital lowpass filter having a frequency response similar to that of the optimum analogue filter specified in Chapter 6. The digital filter, described by the difference equation:

$$v_m = 0.0000018(u_m + 3.u_{m-1} + 3.u_{m-2} + u_{m-3}) + 2.9511320.v_{m-1} - 2.9034507.v_{m-2} + 0.9523046.v_{m-3} \quad (8.4)$$

where v_m and u_m are its current output and input respectively, in fact has a cutoff frequency at just under 70 Hz, while its gain at the 200 Hz foldover frequency is low enough to satisfy the aliasing requirements. It was designed by the bilinear transformation method, and details of this are of no particular significance here and can be found elsewhere [25,34,46].

8.3.1 Fault Resistance and Source Reactance Compensation

It is to be recalled that the transient solution of the transmission line equations, obtained in Chapter 3, assumed both the fault resistance and source reactance to be zero. In the fault waveforms shown in Figures 8.4 and 8.5, therefore, no indication of the fault resistance is to be expected. In fact, the fault resistance was only used for modifying the time constants of the exponentially decaying high frequency components in the voltage, and the dc offset in the current. This is obviously not sufficient, since the resulting steady-state component in the transient current solution is now too large, giving a total postfault current that is wrong in both magnitude and phase. This effect is more marked in faults that are close to the source, as fault II is, since then the short length of the faulted line gives some very high postfault currents.

The reactance and resistance as obtained from the line voltage and current for fault II are shown in Figure 8.6, with the voltage and current phasors determined by the full cycle method. It is seen that both components level off to values that are smaller than their apparent postfault values as calculated from Equation (8.3c), and that they eventually become negative. This is because the large postfault current now induces a voltage in the source reactance that almost cancels the prefault voltage, giving a small overall voltage V_L having the wrong phase, as shown in the phasor diagram of Figure 8.7(a).

Compensation for the fault resistance and source reactance is thus included by reducing the steady-state transient current component. This is consistent with introducing the fault resistance and source reactance as series components in the faulted circuit, and it results in a larger overall postfault voltage, as is shown in Figure 8.7(b). The total postfault current I_L is additionally forwarded in phase to account for the small power factor that now results from the inclusion of the fault resistance in the faulted circuit.

The compensation described above is independent of the fault inception angle. The corrected voltage and current waveforms it results in, for fault II, give a resistance and a reactance variation that are shown in Figure 8.8. It can be seen that these quantities now closely follow their actual values after fault incidence. In fact, the postfault current was slightly undercompensated to leave it at slightly larger than its true value, thereby simulating a similar effect that is introduced by current transformers in practice, and that results in smaller apparent impedances.

Corrected voltage and current waveforms for faults I and II are shown in Figure 8.9. Differences from Figures 8.4 and 8.5 are more obvious for fault II, where the postfault current is now reduced, which in turn lessens the drop in the postfault voltage. The sudden change in the current at fault incidence will have no serious effects, as it would be smoothed out by the lowpass filter. More importantly, the correct phases of the voltage and current are now obtained, and positive values for the resistance and reactance thus result.

The compensation discussed here will be applied to all the tests that are to follow. Further waveform modifications to account for nonlinear and time-varying fault resistances, and capacitor voltage transformers and current transforms distortion effects, are not considered.

8.4 EVALUATION OF SCHEMES

The full cycle and half-cycle protection schemes are now tested. The digital highpass filter of Chapter 7 is used with the half-cycle scheme.

The fault detection times reported below were those needed for the impedance trajectory to enter the relaying characteristic. The transient delay of the digital lowpass filter used was measured to be about 1 msec. longer than that of the recommended analogue lowpass filter, and this difference, together with the processing cycle duration, was allowed for in the detection times.

Plots of the impedance trajectories for faults I and II, obtained by the full cycle and half-cycle methods, are given in

Figure 8.10. It is seen that for both faults the half-cycle trajectories describe shorter paths to the postfault impedance points, giving faster fault detection as a result.

Fault I was detected by both schemes although the 15 ohms fault resistance lay just outside the relaying characteristic resistive reach setting. This was because the current compensation described in Section 8.3 above meant that the fault resistance appeared slightly smaller than its actual value.

8.4.1 Accuracy of Methods

Three faults with different resistances, and at different points on the line, were simulated. The first had a 5 ohms resistance 90 miles along the line, and the second had a 2 ohms resistance and was 20 miles away from the relaying point, while the third, which was at the midpoint of the line, had a 15 ohms resistance.

The reactance and resistance, as obtained from the full cycle and half-cycle methods, are plotted against time after fault incidence in Figures 8.11 to 8.13. It is seen that about 15 msec. after fault incidence both methods give almost correct resistances and reactances, and that in general values obtained by the half-cycle method converge faster.

8.4.2 Effect of the Sampling Angle

It was stated in Section 4.3 that fault detection can be delayed by as much as a sampling interval if the fault occurs immediately after a sampling instant. To investigate this, a 5 ohms

fault 40 miles along the line was considered. Detection times for such fault were obtained for different sampling angles, and with fault inception angles of 0^{o} and 90^{o}.

The detection times are plotted in Figure 8.14(a) and (b), where it is seen that over the 45^{o} range of variation of the sampling angle, corresponding to the sampling interval of 2.5 msec., these times vary by a maximum of about 3 msec. It is therefore to be understood that in some of the tests that follow, and where the sampling angle is taken as zero, the obtained detection times could vary by 1 or 2 msec. for different sampling angles.

8.4.3 Fault Distance

The variation of the fault detection time with the position of the fault on the line is shown in Figures 8.15 and 8.16 for two faults, one with a 1 ohm resistance and the other with a 3 ohms resistance.

Detection times by both the full cycle and half-cycle methods generally increase with the distance to fault, since the impedance trajectories for faults near the relaying point on the line would enter the relaying characteristic sooner than trajectories of faults near the far end of the line. This in itself is explained by the fact that it takes all trajectories roughly the same length of time to arrive at their final destinations in the X/R plane for a particular type of fault, irrespective of the fault position.

Figure 8.15 also shows a typical time characteristic of an analogue relay. It is well known [2] that there exists a minimum to

the length of a line that an analogue distance relay can effectively protect. This is determined by the limit of relaying signal below which the comparator will no longer measure accurately, and is in fact dependent on both the distance to fault and on the ratio of the source impedance to the line series impedance. Such limitation is much less obvious in a digital relay, where a typical dynamic range of the signals allowed makes the detection of faults that are very close to the relaying point possible.

Detection times of analogue relays are also characterised by large increases before the reach point of the relay, as zone 2 is approached. This again poses no problems in digital relays, where detection times are fairly consistent for all faults up to the reach point. The detection of faults occurring beyond this point, as is indicated in Figures 8.15 and 8.16, is a result of the fault current compensation that was expected to cause overreaching.

8.4.4 General Tests

Fault detection times for various faults covering differing conditions are given in Table (8.1) overleaf. In all cases, the sampling angle was adjusted to give a sampling instant immediately after fault incidence, thereby producing detection times that do not include the effects of the sampling angles.

Detection by the half-cycle method, it appears from Table (8.1), is on average about 2.5 msec. faster than by the full cycle method. The speed of both methods deteriorates for larger fault resistances and for increases in the distances to the faults, while, for faults with a 10 ohms resistance at least, detection times

x_f miles	R_f ohms	f.i.a. degrees	Fault Detection Times, msec.	
			full cycle	half-cycle
25	0	0	12.20	9.68
		45	12.20	9.68
		90	12.20	17.18
	10	0	22.20	19.68
		45	19.70	14.68
		90	17.20	12.18
75	0	0	17.20	14.68
		45	14.70	12.18
		90	19.70	17.18
	10	0	24.70	22.18
		45	22.20	17.18
		90	19.70	17.18

TABLE 8.1 Fault detection times for the full cycle and half-cycle methods.

improve for large fault inception angles. This is significant in view of the fact that in practice over 95% of faults occur within 40° of a voltage maximum [4], since insulation breakage is more likely when the voltage is at about its peak value. Detection of zero resistance faults, however, is slower for 90° fault inception angles, and this is probably because the measured resistance in such cases momentarily becomes negative. This warrants no further consideration here, since it is known that true short-circuit conditions seldom arise in practice.

Detection times given in Table (8.1) above can be taken as an indication of the performance of the protection schemes for single-shunt faults. Extensions to other fault conditions involving more than one phase are not obvious. It was reported [55] that flashover faults to earth, cross-country earth faults and open-conductor plus earth faults on double-circuit lines [2] are not always correctly

cleared by phase-fault measuring elements employing the polarised mho characteristic. While it remains true that such faults can be catered for by techniques other than fault location discriminative protection, they are nonetheless expected to create some confusing conditions for digital distance protection that, under cross-country earth faults at least, could lead to tripping of a healthy phase.

8.5 HEAVY SYSTEM LOADING

The performance of the full cycle and half-cycle schemes with almost maximum load transfer conditions was next investigated. A one-phase load of 500 MW at 0.8 p.f. was used, requiring a total power of nearly 90% of the maximum cold weather thermal rating of 2200 MVA [42] for the three-phase line.

x_f miles	R_f ohms	f.i.a. degrees	Fault Detection Times, msec.	
			full cycle	half-cycle
25	0	0	12.20	9.68
		45	12.20	9.68
		90	9.70	7.18
	10	0	22.20	19.68
		45	19.70	14.68
		90	17.20	7.18
75	0	0	17.20	12.18
		45	14.70	12.18
		90	17.20	17.18
	10	0	24.70	19.68
		45	22.20	14.68
		90	19.70	14.68

TABLE 8.2 Fault detection times with line operated almost at maximum rating.

Table (8.2) gives the detection times for the same faults as those considered in the general tests of Section 8.4. Thus, comparing these detection times to those given in Table (8.1), it is seen that the half-cycle method is now faster by a sampling interval for nearly all the faults. This is explained by the location in the X/R plane of the prefault impedance, which is now closer to the relaying characteristic than it was in the case of the natural load. However, as has already been discussed in Section 8.2, this condition of maximum load transfer still leaves an adequate margin between the tripping area and the impedance location, and stability for power swings is thus not significantly degraded.

8.6 THE HALF-CYCLE METHOD WITHOUT THE HIGHPASS FILTER

The effect of the highpass filter on the half-cycle method was next studied. A 4 ohms fault 60 miles along the line and a 1 ohm fault 20 miles along the line were simulated. Different fault inception angles were used, and in each case the sampling angle was chosen so as to allow fault occurrence to immediately precede a sampling instant, as was done in the general tests of Sections 8.4 and 8.5.

Table (8.3) gives the detection times obtained for the two faults with the different fault inception angles, and with and without the inclusion of the digital highpass filter in the half-cycle algorithm. The current for the 4 ohms fault was not very large, and its dc offset was expected to be insignificant. Consequently, fault detection times were equal for small fault inception angles, decreasing for the algorithm without the highpass filter as the fault

Fault Inception Angle, degrees	Fault Detection Times, msec.			
	4 ohms, 60 miles		1 ohm, 20 miles	
	Highpass	No Highpass	Highpass	No Highpass
0	14.68	14.68	9.68	14.68
10	14.68	12.18	9.68	12.18
20	12.18	12.18	9.68	12.18
30	12.18	12.18	9.68	12.18
40	12.18	12.18	9.68	9.68
50	9.68	12.18	9.68	9.68
60	9.68	12.18	7.18	9.68
70	14.68	12.18	7.18	9.68
80	14.68	12.18	7.18	9.68
90	14.68	9.68	7.18	9.68

TABLE 8.3 Detection times of faults by the half-cycle method with and without the digital highpass filter.

inception angle approached 90^{o} and the dc offset diminished. The improvement is in fact attributed to the disappearance of the transient delay that the highpass filter introduced.

Detection speeds for the 1 ohm fault, and by the algorithm employing no highpass filter, again improved as the fault inception angle increased. However, the relatively large current in this fault resulted in an overall deterioration of the detection speed by this algorithm in relation to the algorithm with the highpass filter, as the effect of the dc current offset was now more marked.

The above suggests that the exclusion of the highpass filter from the half-cycle algorithm can result in some improved performance for large fault inception angles. However, a degradation in performance is to be expected for faults with large currents and with small inception angles, where errors due to the dc offset in the current

would probably be giving rise to large oscillations in the impedance trajectory. It is therefore concluded that the highpass filter is, after all, necessary.

8.7 CONCLUSION

The full cycle and half-cycle algorithms both proved to be offering satisfactory detection of faults of varying types and locations. In particular, faults close to the relaying point, and faults near the remote busbar, were all successfully detected under differing conditions. The digital relaying algorithms therefore appear to be giving excellent fault location discrimination.

Fault detection times by the half-cycle method were better throughout, being less than 10 msec. for many faults. Furthermore, the method's sensitivity to dc offset was successfully dealt with by the use of a highpass filter.

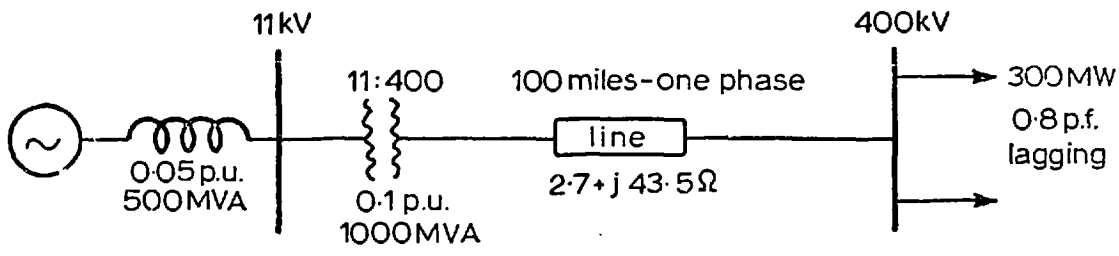

Fig. 8·1 Schematic diagram of system used in off-line studies

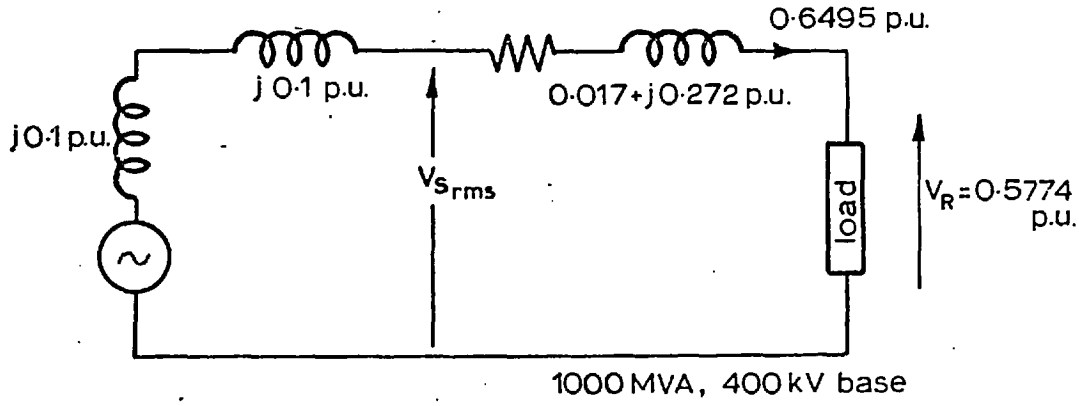

Fig. 8·2 Equivalent circuit of system

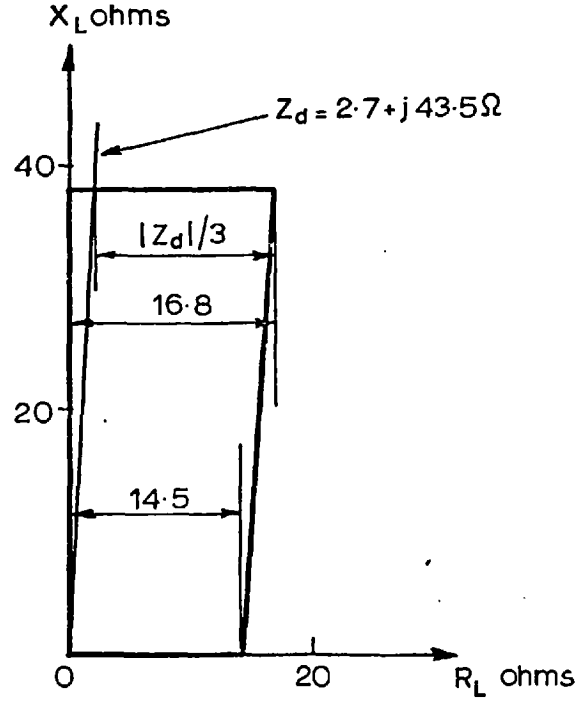

Fig. 8·3 Quadrilateral relaying characteristic

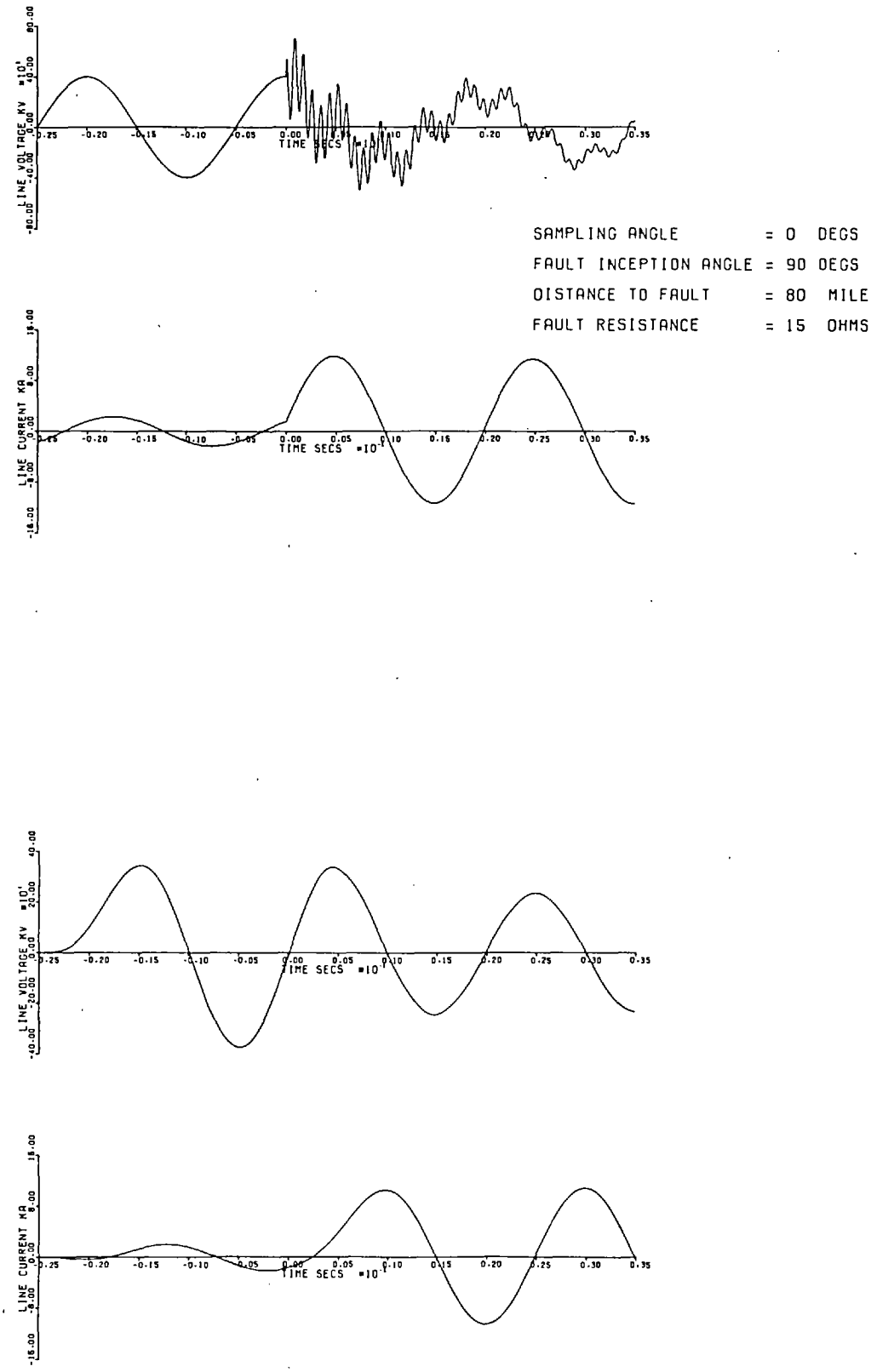

Fig. 8·4 Unfiltered and filtered voltages and currents for fault I.

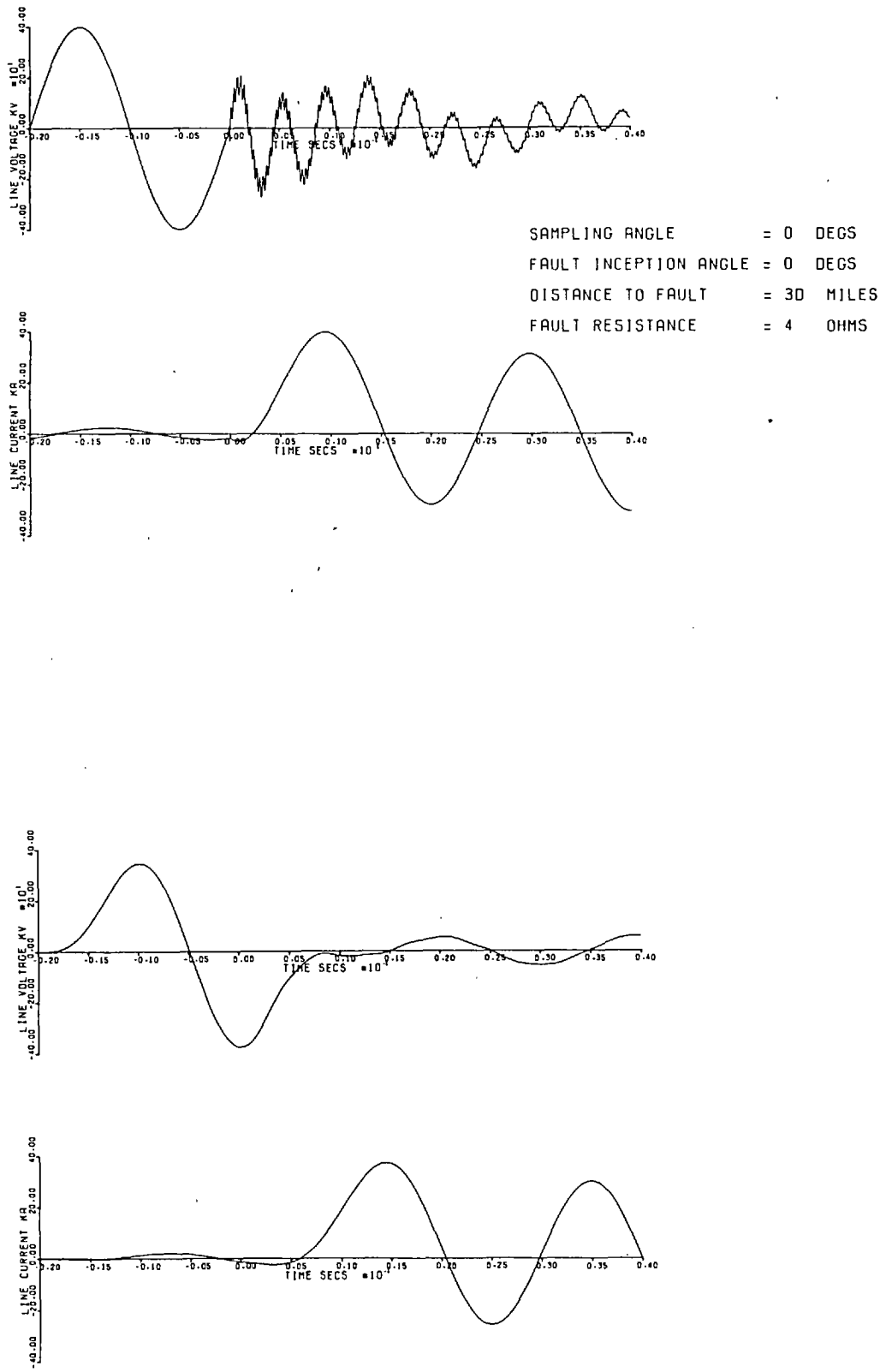

Fig. 8·5 Unfiltered and filtered voltages and currents for fault II.

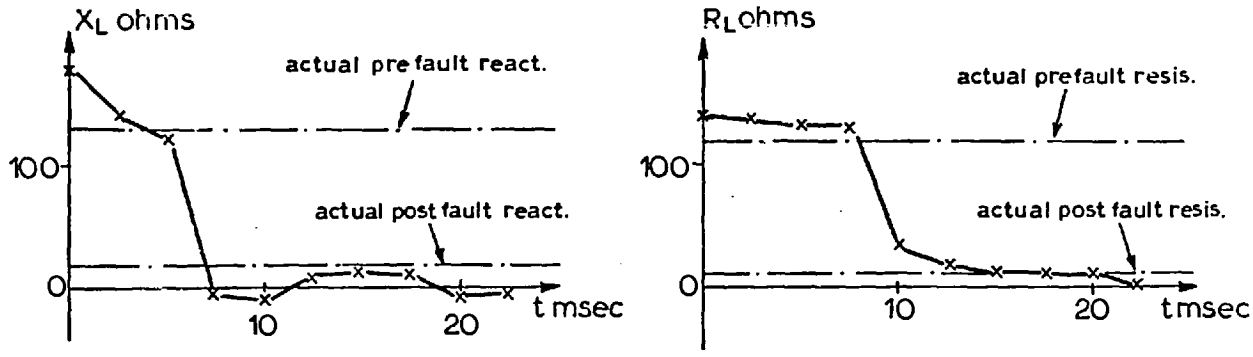

Fig. 8·6 Reactance and resistance variations for fault II, calculated from uncorrected voltages and currents

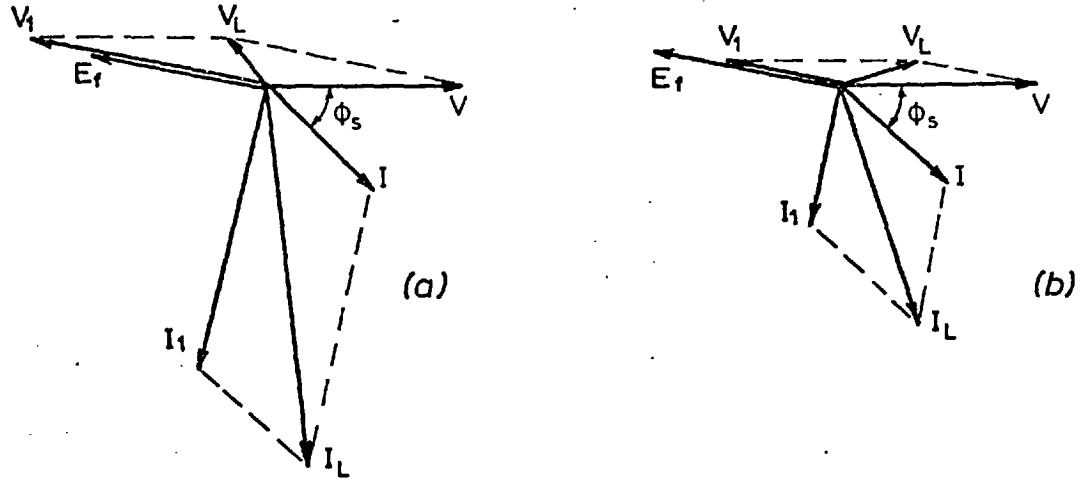

Fig. 8·7 Fault resistance and source reactance compensation

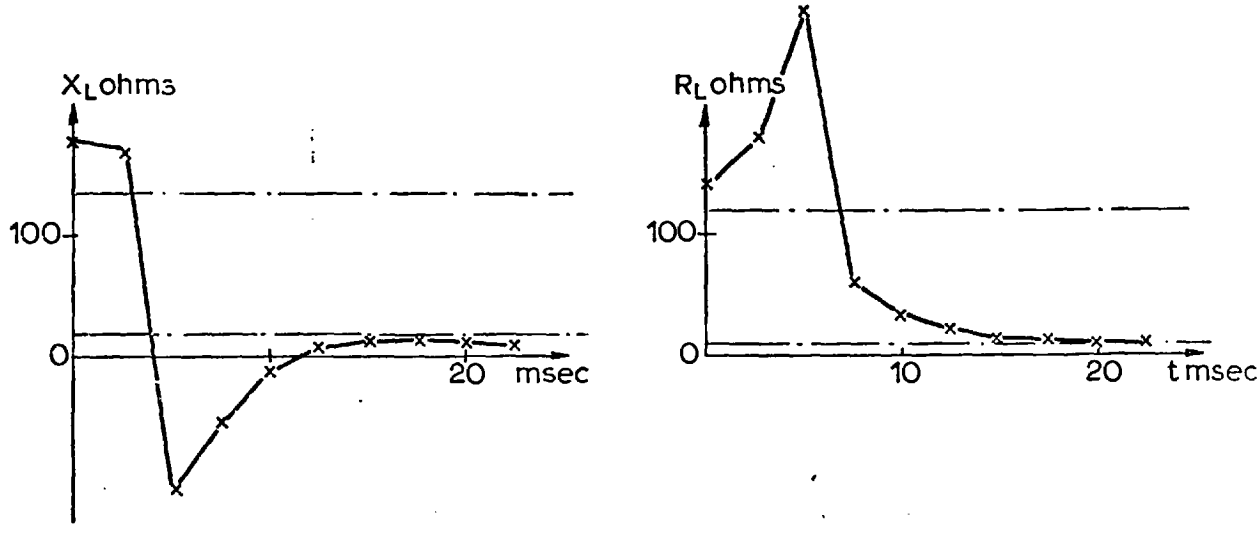

Fig. 8·8 Reactance and resistance as calculated from corrected voltage and current for fault II

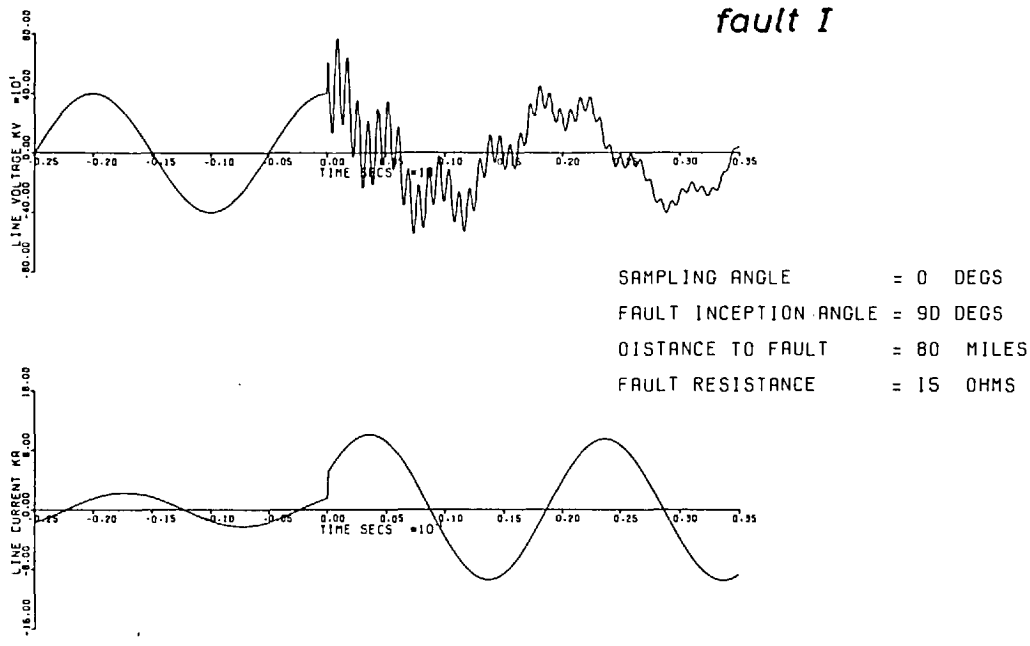

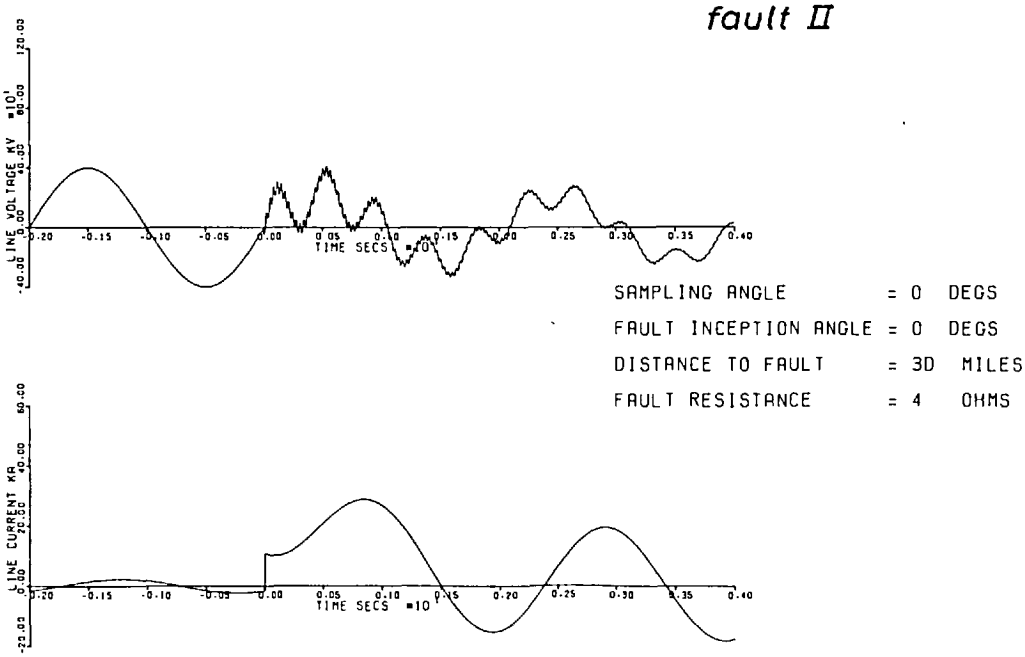

Fig. 8·9 Corrected voltages and currents for faults I and II

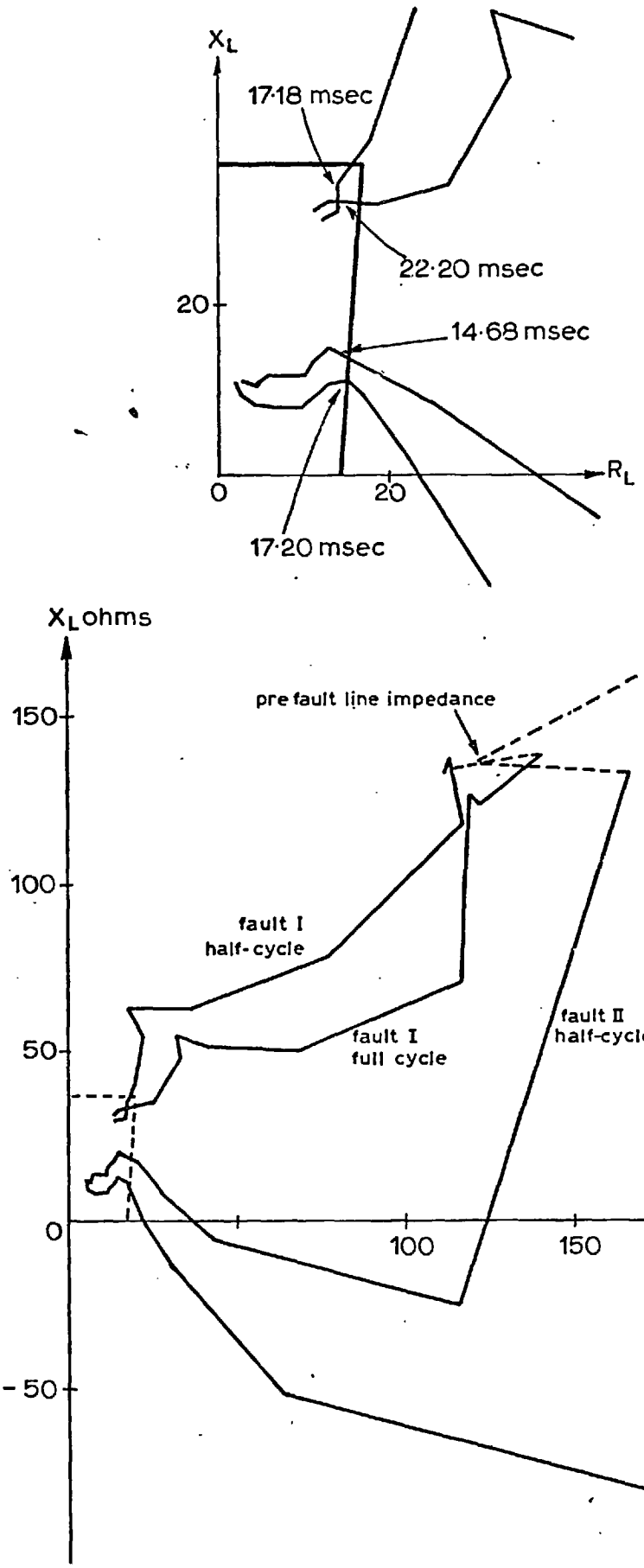

Fig. 8·10 Impedance loci by the full cycle and half-cycle methods for faults I and II

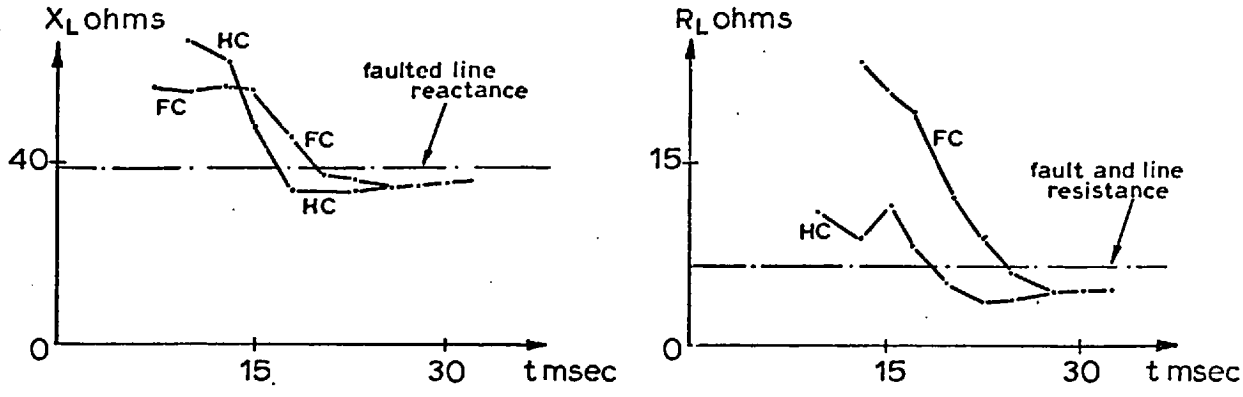

Fig. 8·11 Line reactance and resistance after fault incidence for a 5 Ω fault 90 miles away from source with an f.i.a. of 90°

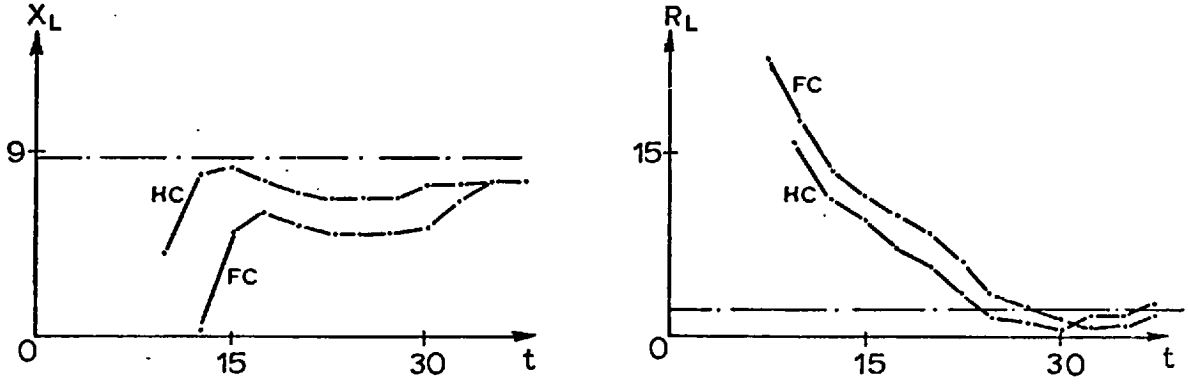

Fig. 8·12 Reactance and resistance for a 2 Ω fault 20 miles along the line, zero f.i.a.

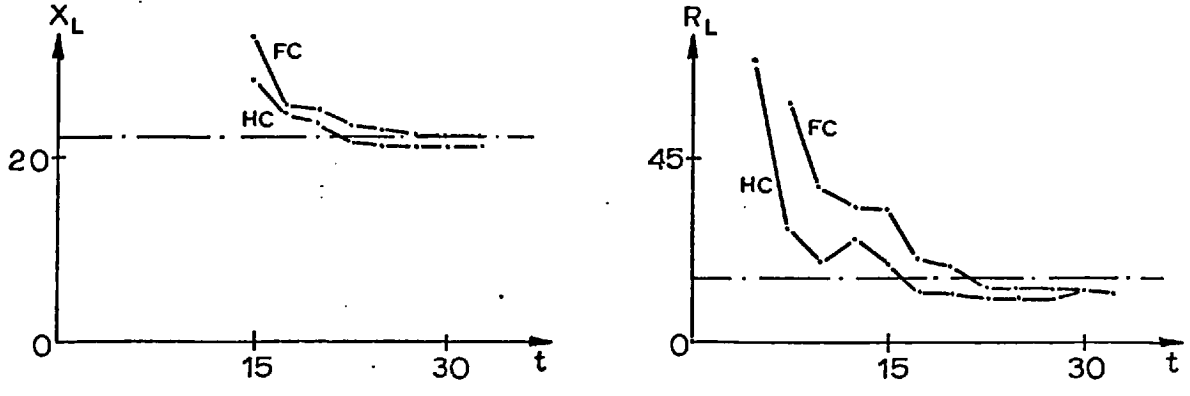

Fig. 8·13 Reactance and resistance for a 15 Ω fault 50 miles down the line, 90° f.i.a.

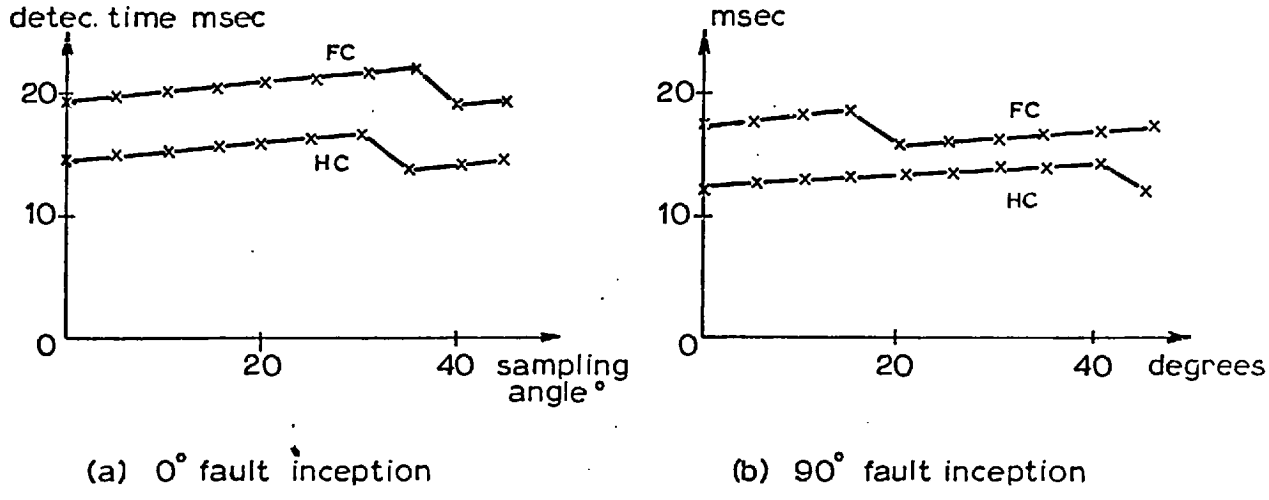

(a) 0° fault inception (b) 90° fault inception

Fig. 8·14 Detection time variations with the sampling angle for a 5Ω fault 40 miles along the line

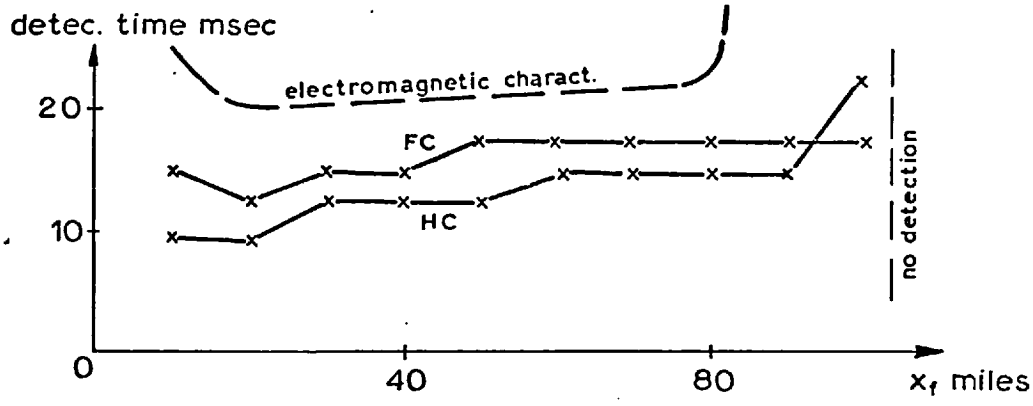

Fig. 8·15 Variation of detection time with fault distance for a 1Ω fault

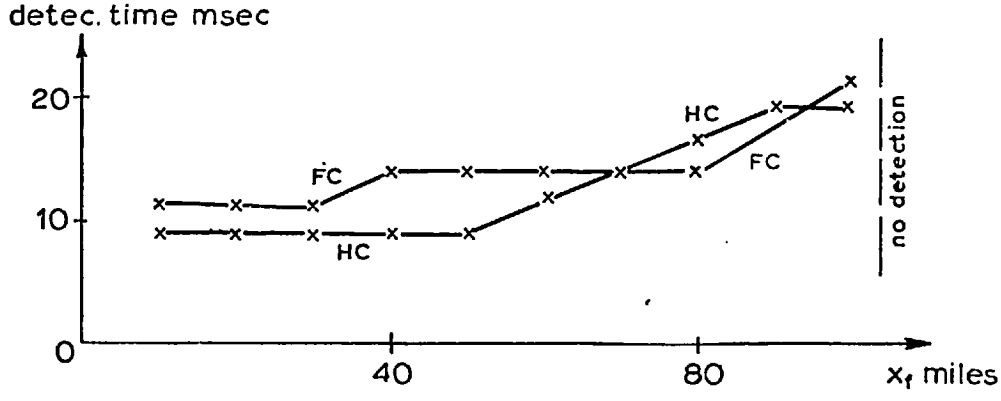

Fig. 8·16 Variation of detection time with distance for a 3Ω fault with a 60° inception angle

CHAPTER 9

CONCLUSIONS

The aim of the work presented in this thesis was to develop a digital relaying algorithm capable of providing more reliable and faster line protection than is currently obtainable from analogue relays. Consequently, digital harmonic filtering was fundamentally examined, and a new filtering method was devised and used for the phasor determination involved in impedance relaying. The method was then supplemented by appropriate analogue lowpass and digital highpass filters, thereby forming a complete digital distance relaying scheme that gave both fast detection and improved discrimination. The initial aim of the study was thus achieved.

The original contributions that have emerged through the course of this work in the field of transmission line protection are as follows:

1. The formulation of a description of the composition of fault transients that systematically accounted for both the line natural frequencies and the parasitic ringing components.

2. The complete analysis of the nonlinear time-varying filter that resulted from the amalgamation of the orthogonal filters appearing in the Discrete Fourier Transform.

3. The derivation of a number of modified Discrete Fourier Transforms that are applicable to signals with specific compositions.

4. The adoption of one such modified transform as the basis of a distance protection scheme, and the further

modification of its algorithm for acquiring immunity against dc offset.

5. The application of sigital signal processing criteria for the determination of suitable analogue lowpass filters, and through an optimisation procedure that was set to take protection requirements into consideration.

Few possibilities can be suggested for future work. It is thought that the adoption of the quarter-cycle method could result in slight further improvements in fault detection speed. This was not examined in detail during the course of this work because preliminary investigations of the frequency response of the quarter-cycle method revealed the need for some appreciable modifications to this response, and it was felt that the extra complexity that this involved would make the scheme unsuitable. However, increased complexity can be justified if significantly improved performance were to result.

The performance of digital distance relaying schemes, it appears, is approaching its limits. Over the past decade, numerous computer methods for the determination of the line impedance have been suggested, and some of these, as with the improved method introduced in this thesis, do provide excellent discrimination and fast detection. The algorithm's simplicity, and the low sampling rate used, make real-time implementation on a small processor possible. This, in turn, is lending itself conveniently to the trend of contemplating modular digital electronic relaying units for the replacement of conventional analogue relays.

However, attention has been drawn recently to a new class of relaying methods based on a different phenomenon. It has been suggested [56] that the limitation of the response time, that is fundamental to all the impedance determination methods, can be bypassed by employing fault discriminants derived from the analysis of travelling wave transients. This principle has so far been implemented in a form that requires a signalling channel linking both ends of the line, and the development of a nonunit system employing a low sampling rate thus remains to be seen.

REFERENCES

[1] Slemon, G.R., Robertson, S.D.T. and Ramamoorty, M., High Speed Protection of Power Systems Based on Improved Power System Models, CIGRE Paper 31-09, Paris, June 1968.

[2] Electricity Council, Edited by The, Power System Protection, Vols. I, II and III, Macdonald, London, 1969.

[3] Westinghouse Electric Corporation, Electrical Transmission and Distribution Reference Book, Westinghouse, East Pittsburgh, Pa., U.S.A., 1950.

[4] Warrington, A.R. Van C., Protective Relays: Their Theory and Practice, Vols. I and II, Chapman and Hall, London, 1962/69.

[5] Mathews, P. and Nellist, B.D., Generalised Circle Diagrams and Their Application to Protective Gear, IEEE Trans. PAS, Vol. 83, pp. 165-173, February 1964.

[6] Cory, B.J., Dromey, G. and Murray, B., Digital Systems for Protection, CIGRE Paper 34-08, Paris, August 1976.

[7] Mann, B.J. and Morrison, I.F., Digital Calculation of Impedance for Transmission Line Protection, IEEE Trans. PAS, Vol. 90, pp. 270-276, January/February 1971.

[8] Mann, B.J. Real Time Computer Calculation of the Impedance of a Faulted Single-Phase Line, I.E. Aust., Elec. Engg. Trans., Vol. EE5, pp. 26-28, March 1969.

[9] Ranjbar, A.M., Computer Protection of High Voltage Transmission Lines, Ph.D. Thesis, Imperial College of Science and Technology, University of London, 1975.

[10] Wright, A., Current Transformers: Their Transient and Steady-State Performance, Chapman and Hall, London, 1968.

[11] Mann, B.J. and Morrison, I.F., Relaying a Three-Phase Transmission Line with a Digital Computer, IEEE Trans. PAS, Vol. 90, pp. 742-749, March/April 1971.

[12] Gilcrest, G.B., Rockefeller, G.D. and Udren, E.A., High-Speed Distance Relaying using a Digital Computer, Parts I and II, IEEE Trans. PAS, Vol. 91, pp. 1235-1258, May/June 1972.

[13] McLaren, P.G. and Redfern, M.A., Fourier-Series Techniques Applied to Distance Protection, Proc. IEE, Vol. 122, pp. 1301-1305, November 1975.

[14] Hope, G.S. and Umamaheswaran, V.S., Sampling for Computer Protection of Transmission Lines, IEEE Paper T 74 034-5, PES Winter Power Meeting, New York, N.Y., January 1974.

[15] McInnes, A.D. and Morrison, I.F., Real Time Calculation of Resistance and Reactance for Transmission Line Protection by Digital Computer, I.E. Aust., Elec. Engg. Trans., Vol. EE7, pp. 16-23, March 1971.

[16] Ranjbar, A.M. and Cory, B.J., An Improved Method for the Digital Protection of High Voltage Transmission Lines, IEEE Trans. PAS, Vol. 94, pp. 544-548, March/April 1975.

[17] Luckett, R.G., Munday, P.J. and Murray, B.E., A Substation-based Computer for Control and Protection, IEE Conference on Developments in Power System Protection, London, 11-13 March 1975.

[18] Phadke, A.G., Hlibka, T. and Ibrahim, M., A Digital Computer System for EHV Substations: Analysis and Field Tests, IEEE Trans. PAS, Vol. 95, pp. 291-297, January/February 1976.

[19] Odgen, A.D., Walker, L.N., Ott, G.E. and Tudor, J.R., Implementation of a Fault Detector and Locator Utilizing the High Frequency Transient, IEEE Paper 70 CP 140-PWR, PES Winter Power Meeting, New York, N.Y., January 1970.

[20] Thorp, J.S., Phadke, A.G., Horowitz, S.H. and Bechler, J.E., Limits to Impedance Relaying, IEEE Paper F 78-219-8, PES Winter Power Meeting, New York, N.Y., January 1978.

[21] Laycock, G.K., Digital Signal Processing Techniques applied to Power System Protection, Ph.D. Thesis, University of Cambridge, 1972.

[22] McLaren, P.G. and Redfern, M.A., Hybrid Phase Comparator applied to Distance Protection, Proc. IEE, Vol. 122, pp. 1295-1300, November 1975.

[23] Bracewell, R.M., The Fourier Transform and its Applications, McGraw-Hill, Inc., New York, N.Y., 1965.

[24] Kharkevich, A.A., Spectra and Analysis (Translated from the Russian), Consultants Bureau Enterprises, Inc., New York, N.Y., 1960.

[25] Rabiner, L.R. and Gold, B., Theory and Application of Digital Signal Processing, Prentice-Hall, Inc., Englewood Cliffs, N.J., U.S.A., 1975.

[26] Goldman, S., Information Theory, Prentice-Hall, Inc., New York, N.Y., 1953.

[27] Black, H.S., Modulation Theory, D. Van Nostrand Company, Inc., N.J., U.S.A., 1966.

[28] Lathi, B.P., Communication Systems, John Wiley & Sons, Inc., New York, N.Y., 1968.

[29] Cochran, W.T. et al., What is the Fast Fourier Transform? IEEE Trans. AU, Vol. 15, pp. 45-55, June 1967.

[30] Cochran, W.T. et al., Burst Measurements in the Frequency Domain, Proc. IEEE, Vol. 54, pp. 830-841, June 1966.

[31] Conolly, B.W., Some Intrinsic Properties of the Discrete Fourier Transform, Notes issued at Chelsea College, University of London, May 1976.

[32] Papoulis, A., The Fourier Integral and its Applications, McGraw-Hill, Inc., New York, N.Y., 1962.

[33] Otnes, R.K. and Enochson, L., Digital Time Series Analysis, John Wiley & Sons, Inc., New York, N.Y., 1972.

[34] Gold, B. and Rader, C.M., Digital Processing of Signals, McGraw-Hill, Inc., New York, N.Y., 1969.

[35] Bendat, J.S. and Piersol, A.G., Random Data, Analysis and Measurement Procedures, John Wiley & Sons, Inc., New York, N.Y., 1971.

[36] Potter, J.L. and Fich, S.J., Theory of Networks and Lines, Prentice-Hall, Inc., Englewood Cliffs, N.J., U.S.A., 1963.

[37] Greenwood, A., Electrical Transients on Power Systems, John Wiley & Sons, Inc., New York, N.Y., 1971.

[38] Clarke, E., Circuit Analysis of A-C Power Systems, Vol. I, John Wiley & Sons, Inc., New York, N.Y., 1943.

[39] Bickford, J.P. and Doepel, P.S., Calculation of Switching Transients with Particular Reference to Line Energisation, Proc. IEE, Vol. 114, pp. 465-477, April 1967.

[40] Uram, R. and Miller, R.W., Mathematical Analysis and Solution of Transmission Line Transients, Part I: Theory, Vol. 83, pp. 116-123, November 1964.

[41] Battisson, M.J., Day, S.J., Mullineux, N., Parton, K.C. and Reed, J.R., Calculation of Switching Phenomena in Power Systems, Proc. IEE, Vol. 114, pp. 478-486, April 1967.

[42] Weedy, B.M., Electric Power Systems, John Wiley & Sons, Ltd., London, 1967.

[43] Westlin, S.E., Computational Methods for Fault Location on Electric Power Transmission Lines, Thesis, Department of Electric Power Systems Engineering, The Royal Institute of Technology, Stockholm, 1976.

[44] Starkey, B.J., Laplace Transforms for Electrical Engineers, Iliffe & Sons Ltd., London, 1954.

[45] Hughes, M.A., Distance Relay Performance as Affected by Capacitor Voltage Transformers, Proc. IEE, Vol. 121, pp. 1557-1566, December 1974.

[46] Bogner, R.E. and Constantinides, A.G., Editors, Introduction to Digital Filtering, John Wiley & Sons Ltd., London, 1975.

[47] Kuo, F.F., Network Analysis and Synthesis, John Wiley & Sons, Inc., New York, N.Y., 1962.

[48] Constantinides, A.G., Synthesis of Recursive Digital Filters from Prescribed Amplitude Characteristics, Ph.D. Thesis, University of London, 1968.

[49] Van Valkenburg, M.E., Introduction to Modern Network Synthesis, John Wiley & Sons, Inc., New York, N.Y., 1966.

[50] Jolley, L.B.W., Summation of Series, Dover Publications, Inc., New York, N.Y., 1961.

[51] Weinberg, L., Network Analysis and Synthesis, McGraw-Hill, Inc., New York, N.Y., 1962.

[52] Zverev, A.I., Handbook of Filter Synthesis, John Wiley & Sons, Inc., New York, N.Y., 1967.

[53] Elmore, W.C. and Sands, M., Electronics, National Nuclear Energy Series, McGraw-Hill, New York, N.Y., 1949.

[54] Rushton, J. and Humpage, W.D., Power-system Studies for the Determination of Distance-Protection Performance, Proc. IEE, Vol. 119, pp. 677-688, June 1972.

[55] Cook, V., Distance Protection Performance during Simultaneous Faults, Proc. IEE, Vol. 124, pp. 141-146, February 1977.

[56] Demmel, H.W. and Michels, J.M., High Speed Relaying using Travelling Wave Transient Analysis, IEEE Paper A 78 214-9, PES Winter Power Meeting, New York, N.Y., January 1978.